# Development of nano Ni-Zn catalysts supported on carbon onions for the production of bio-jet fuel from castor oil.

*Submitted by*

**Sharron Ratshoshi (562274)**

A Dissertation Submitted to the Faculty of Engineering and the Built Environment, University of the Witwatersrand, Johannesburg, South Africa, in fulfilment for the degree of Master of Science.

**Supervisor: Prof. Diakanua Nkazi**

**Co- supervisor: Dr. Manoko Maubane-Nkadimeng**

Johannesburg, 2021

# DECLARATION

I declare that this thesis titled *"Development of nano Ni-Zn catalyst supported on carbon onions for the production of bio-jet from castor oil"* is the result of my own unaided research work, except as cited and acknowledged in the references. This thesis has not been submitted for any degree.

Name: Sharron Ratshoshi

Student Number: 562274

Signature: …… 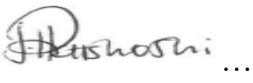 …

Date: …14 OCTOBER 2021

# DEDICATION

This Dissertation is dedicated to my parents:

Mr N.L Ratshoshi

and

Mrs M.M Ratshoshi

# ACKNOWLEDGMENTS

First of all, I would like to thank all mighty God, for his protection, guidance and for giving me strength throughout this journey.

I would like to express my sincere gratitude to the following individuals who contributed greatly to the successful completion of this work.

Thanks to my supervisor Prof. Diakanua Nkazi for his invaluable guidance and for giving me a chance to learn under his mentorship.

Thanks to my co-supervisor Dr. Manoko Maubane-Nkadimeng for her consistent guidance with catalyst synthesis and for introducing me to the great individuals from the school of chemistry.

Thanks to Dr. Hembe Mukaya for thoroughly assisting in editing my journal article. Your calmness and patience are much appreciated.

A special thank you to my loved ones (My parents Mr. N.L Ratshoshi and Mrs. M.M Ratshoshi, and my siblings Audrey, Grace, Judith, and Danny Ratshoshi) for their prayers, encouragement, and continued support.

Thanks to the following staff and postgraduate students from:

- The School of Chemical and Metallurgical Engineering
  To Mr. Motlatsi Phali for his assistance with GC-Ms.
  To Petra Dinham for her assistance with SEM analysis
  To Letta Ntuli for her teachings in using TGA and FTIR.
  To Tholakele Ntombela for her advice throughout this research**.**

- The Microscopic and Microanalysis Unit (MMU) and the school of chemistry.
  Dr. Manoko Maubane-Nkadimeng and Dr. Zikhona Tetana from the Microscopic and Microanalysis Unit for their assistance with TEM and XRD analysis.
  Prof. N.J Convile and Thuli Buthelezi a postgraduate student for their assisting me with BET analysis.
  Dr Thomas Mongwe for always willing to assist me with characterization.

# ABSTRACT

High demand for biofuels by emerging economies as well as environmental issues has resulted in more indebt research in petroleum fuel production. The edible oil feedstocks are currently the main resources for biofuel production but lately, the switch to non-edible oil is considered. The non-edible oils are a leading option considering that they do not clash with food security policy. From extensive research, it was found that transesterification is not sufficient alone for biofuels production. Hydrocracking is the ideal solution as it can at once produce different biofuels (bio-jet and bio-gasoline) with high quality and higher yields of the desired product.

Castor oil as an alternative and re-usable source of liquid fuel was used in this research to study the production of bio-jet fuel. The project focused on differently prepared hydrocracking catalysts that may be used to produce bio-jet as the desired biofuel and the parameters that would give the optimal production yields of bio-jet. The co-impregnation and sequential impregnation methods were used for the synthesis of the Ni-Zn/CNO catalysts with varied Ni: Zn metal loading ratios of 1:2, 1:3, 1:1, 2:1, and 3:1 wt% calcined at 500°C. The catalysts were characterized using the TGA, BET, SEM, TEM, XRD, and FTIR, characterization techniques that revealed different properties. When the catalysts were analysed with SEM, it was revealed that they have agglomerates, while BET revealed that all the catalysts have pores in the mesoporous regions.

Castor oil was hydrocracked using the 2:1 and 1:3 catalysts ratios prepared by the co-impregnation and sequential impregnation methods respectively. The catalysts were used to study the effects that temperature, time, and catalyst loading have on the bio-jet selectivity. The results revealed that when the temperature was increased the bio-jet selectivity increased up to 250 °C then decreased. When the time was varied the increase in time increased the bio-jet selectivity throughout until 2.5 hours and when the catalyst loading effect was studied it was observed that the increase in catalyst loading drastically decreased the bio-jet fuel production. At high catalysts loadings, the catalysts favoured mostly biodiesel and long hydrocarbons production. From the hydrocracking runs, the 2:1 and 1:3 catalyst ratio produced maximum yields of 65.33 and 72.33% respectively. The catalyst preparation method, the metal used, and process temperature should be considered for the prediction and catalyst activity assessment.

The 1:3 catalyst was further used for the optimization of process parameters (Temperature, time, and catalyst loadings) that were carried out using the response surface methodology

(RSM) of the design expert software. The experimental design was carried out by the RSM in order to evaluate the interactive effects. A higher regression coefficient of 82% was obtained which indicated a good evaluation of the experimental data by the obtained 2FI model. The RSM revealed a temperature of 280 ˚C, a reaction time of 3 hours and catalyst loading of 160 mg as the optimal reaction conditions. Bio-jet fuel was successfully produced with a maximum production yield of 55.62% obtained from the optimum conditions.

# DRAFT MANUSCRIPT UNDER REVIEW

Sharron Ratshoshi, Hembe Elie Mukaya and Diakanua Nkazi, *Hydrocracking Of Non-Edible And Waste Cooking Oils For The Production Of light Hydrocarbon Fuels:* A Review (under review with the Energy Technology Journal)

# NOMENCLATURE

| | |
|---|---|
| BET: | Brunauer-Emmet-Teller |
| CCD | Central Composite Design) |
| CHMT: | School of Chemical and Metallurgical Engineering |
| CNO | Carbon Nano Onions |
| EDS | Energy-dispersive X-ray spectroscopy |
| FFA: | Free Fatty Acid(s) |
| FTIR: | Fourier Transform Infrared Spectra |
| GC-MS: | Gas Chromatography and Mass Spectrometry |
| HDM: | Hydrodemetallization |
| HDN: | Hydrodenitrogenation |
| HDO: | Hydrodeoxygenation |
| HDS: | Hydrodesulphurization |
| OLP: | Organic Liquid Products |
| RON | Research Octane Number |
| RSM: | Response Surface Method |
| SEM: | Scanning Electron Microscopy |
| TEM: | Transmission Electron Microscopy |
| TGA: | Thermogravimetric analysis |
| USA: | United States of America |
| wt. %: | Weight Percentage |
| XRD: | X-Ray Diffraction |

# Table of contents

# List of Figures and Tables

**List of Figures**

**List of Tables**

# Outline of the Dissertation

The dissertation is outlined as follows:

**CHAPTER 1**: Introduction- This chapter gives an introductory insight into the research work that this project was focused on. The motivation, aim, and objectives of the study are included in this chapter.

**CHAPTER 2**: Literature Review- This chapter gives further insight and feedback from literature studies on work that have been done on the same or similar scope of the study. The focus was on different feedstocks that can be used, biofuels production routes, and catalysts as well as different parameters that can be used.

**CHAPTER 3**: Catalyst Synthesis-The experimental procedures followed for the synthesis of the Ni-Zn/CNO's catalyst are outlined in this chapter. The characterization methods used in this study are outlined and described in this chapter. The results are discussed and interpreted as far as possible.

**CHAPTER 4**: Biofuel's production using the synthesized catalyst- This chapter outlines the experimental procedures followed for hydrocracking of castor oil using the best selected synthesized catalysts. The results are discussed and interpreted as far as possible.

**CHAPTER 5**: Optimization of Bio-jet production process variables: -This chapter outlines the optimization of bio-jet production carried out using the RSM experimental design.

**CHAPTER 6**: Conclusions and Recommendations- This chapter concludes on the outcomes of this study based on the overall results obtained. Recommendations for future works relating to the same or similar study field are given.

# CHAPTER 1: Introduction

## 1.1 Background

Petroleum fuels are acknowledged to be unsustainable due to their exhausted supplies, economic uncertainty, and environmental issues. Renewable biofuels sources are promising alternatives to petroleum because they improve air quality and are environmentally beneficial (Usomboon, Santikunaporn and Butnar, 2012). Currently, edible oils are the main resources for biofuel production worldwide, (Taufiqurrahmi and Bhatia, 2011) but lately, the use of non-edible oils are considered for biofuel production because the non-edible oils do not clash with the food security policy (Prajitno *et al.*, 2017). These oils are vegetable oils also known as triglycerides. The triglycerides agricultural fats can be divided into various types which include: 1) Crude vegetable oils (Canola), 2) Used vegetable oils (Waste cooking oil), 3) Animal fats (Lard) and 4), Non-edible oil (Castor oil, Karanja) (Taufiqurrahmi and Bhatia, 2011).

The selection of feedstock that is cheaper, abundantly available, and economically feasible is important for biofuel production as this will reduce production costs. Of all the non-edible oils, castor oil is one of the most cost-effective feedstocks. It does not compete with food security policy, has a higher oil content of about 50%, and can grow on marginal soils (Meller *et al.*, 2014). The disadvantage of using castor beans is in their cost, especially in the South African context due to the import costs involved. Locally produced castor oil is a possible solution to reduce costs as importing is eliminated and the price may be reduced. Castor oil is known to produce biofuels with a high viscosity which is caused by the secondary hydroxyl group (-OH) that is contained in the ricinoleic acid (Meller *et al.*, 2014) and is known to be poisonous as they contain ricin. Proficient oil processing methods need to be employed to ensure the safety and feasibility of extracting and using castor oil.

Vegetable oils since are high-energy liquids that contain minimal oxygen are advantageously easy of conversion from triglycerides to liquids transportation fuels. The triglyceride-based feedstock can be converted to biofuels by implementing different methods based on the desired products. The production process that may be employed for biofuel production includes, transesterification/Esterification, pyrolysis (catalytic cracking), and hydrocracking these are the current techniques. Transesterification is a chemical conversion process of triglycerides with alcohol (methanol or ethanol) into alkyl esters with an assistance of a catalyst. This process produces only biodiesel, with low oxidative and storage stability (Zhao *et al.*, 2017). Pyrolysis

(thermal or catalytic) is the thermal decomposition of triglycerides and produces biofuel typically made of gasoline, kerosene, and diesel fraction (Ong and Bhatia, 2010), While hydrocracking is a catalytic process in which hefty feedstocks are transformed into saturated lighter products under hydrogen-rich conditions and a suitable catalyst. The hydrocracking technique has proven to produce products or biofuel with better quality (Al-Sabawi and Chen, 2012; Zaher *et al.*, 2015; El Khatib *et al.*, 2017) and higher yields (Zhao *et al.*, 2017) particularly biodiesel, with minimal modifications in the refineries existing conditions to make the process financially appealing (Rana *et al.*, 2013) than other conventional processes.

Catalysts have an important role in ensuring the triglyceride's high conversion and high yield for the desired product. Nickel (Ni) is considered as a cheap metal when compared to noble metals. The Ni's catalytic activity can be enhanced by the addition of the second metal to form a bimetallic catalyst. It was suggested that the Ni-Zn catalyst interaction of their acid and basic side respectively as a bimetallic catalyst can promote greater catalytic stability and enhance the deoxygenation activity. The catalyst support is also found to promote the catalyst life.

This study's purpose was to develop a method to produce bio-jet from castor oil. The challenge was to synthesize a catalyst that was going to be able to produce bio-jet fuel with the desired properties. The catalyst was successfully synthesized this can provide a way forward to upscale the process for pre-commercialization with castor oil being a primary feedstock.

### 1.2. Problem statement and research motivation

Petroleum consumption has been on the increase worldwide during the past decades due to the population and industrialization increase, which has resulted in the increased depletion of fossil fuels and petroleum prices. Research has shifted to focus on biofuel production which can be utilized to supplement petroleum-based fuels. Biofuels can be produced from a range of organic and renewable raw materials such as fresh vegetable oil or waste, oilseed plant, and animal fats.

Lately, biofuel production is from edible vegetable oils of which produce more than 95% of biofuels. However, the use of edible oils has recently posed an increased food competition (Sembiring and Saka, 2019). This realization has forced the industry to consider using non-edible oils because they are not suitable for human intake due to the presence of toxic components in the oil. Of all the non-edible oils, castor oil is one of the least used biofuel feedstocks due to its unique fatty acid composition, poisonous ricin content, and its use for many other applications which results in high costs. In order to decrease the biofuel production

cost, it is advisable to locally produce castor oil so that the economy can be improved and increase supply. The project's aim was to use a hydrocracking reactor to convert castor oil into bio-jet fuel which was catalysed with Zn-Ni/CNO’s catalyst.

### 1.3. Aim and objectives.

The project's aim was to produce bio-jet fuel successfully from locally produced castor oil using a suitable catalyst under hydrocracking conditions. For the achievement of the project's aim, the following objectives were investigated:

a. To synthesize bi-functional hydrocracking catalysts Ni-Zn/CNO’s using two impregnation methods (Co-impregnation and sequential impregnation)
b. To characterize the synthesized catalysts based on the preparation methods.
c. To investigate hydrocracking reaction parameters such as reaction temperature, time, and catalyst loading with the prepared catalysts.

## 1.4 References


Al-Sabawi M and Chen J, (2012), Hydroprocessing of biomass-derived oils and their blends with petroleum feedstocks: A review, *Energy and Fuels*, 26(9), 5373–5399.

El Khatib A. S, Hanafi A. S, Arief M, and Al-Amrousi F. E,(2017), Production of Petroleum-like Fractions from Waste Cooking Oil, 60, (1), 147–160.

Meller E, Green U, Aizenshtat Z, and Sasson Y, (2014), Catalytic deoxygenation of castor oil over Pd/C for the production of cost effective biofuel, *Fuel*, 133, 89–95.

Ong Y. K and Bhatia S, (2010),The current status and perspectives of biofuel production via catalytic cracking of edible and non-edible oils, *Energy*, 35( 1), 111–119.

Prajitno D.H, Roesyadi A, Al-muttaqii M, and Marlinda L, (2017), Hydrocracking of Non-edible Vegetable Oils with Co-Ni / HZSM-5 Catalyst to Gasoil Containing Aromatics, 12(3) 318–328

Sembiring K.C and Saka, ( 2019), Renewable hydrocarbons fuels from plant oils for diesel and gasoline, *Journal of the Japan petroleum institude*,62(4),157-172.

Taufiqurrahmi N and S. Bhatia, (2011),Catalytic cracking of edible and non-edible oils for the production of biofuels, *Energy Environ. Sci.*, 4,( 4), 1087–1112.

Usomboon N, Santikunaporn M, and Butnar S, (2012), Bio-Gasoline Production from Bio-Diesel via Catalytic Cracking Reaction on Platinum Zeolite Catalyst, 6, 17–22

Zaher F. A, El Sayed H. A, Heakal B. H, and Hamed S. F, (2015), Potential of Castor Oil as a Feedstock for the Production of Bio-fuel via Catalytic Hydro- Cracking, 443–449.

Zhao X,Wei L, Cheng S, and Julson J, (2017), Review of heterogeneous catalysts for catalytically upgrading vegetable oils into hydrocarbon biofuels, *Catalysts*, 7(3), 1-25.

# Chapter 2: Literature Review:

## 2.1 Hydrocracking feedstock material

The biomass-derived feedstock is classified into three categories :1) cellulosic biomass, 2) starch and sugar-derived biomass, and 3) triglyceride-based biomass, also known as vegetable oils. This biomass derived feedstocks are the current trend in biofuel technology (Ong and Bhatia, 2010). Biofuels are generally liquids, solid or gaseous fuels produced from the conversion of renewable resources using several methods for the production of the desired product depending on the used feedstock (Molefe *et al*., 2019). The selection of feedstock that is cheaper, easily available, and economically feasible is important for biofuel production as this will reduce production costs (Khan *et al.*, 2019). Advantageous ease of conversion of the triglycerides to liquid transportation fuels has made them the most priority in biofuel technology than other biomass since they are high energy liquid's that possess minimum oxygen (Taufiqurrahmi and Bhatia, 2011; Ong and Bhatia, 2010). Figure 1 depicts biomass feedstocks and conversion technologies for biofuel production.

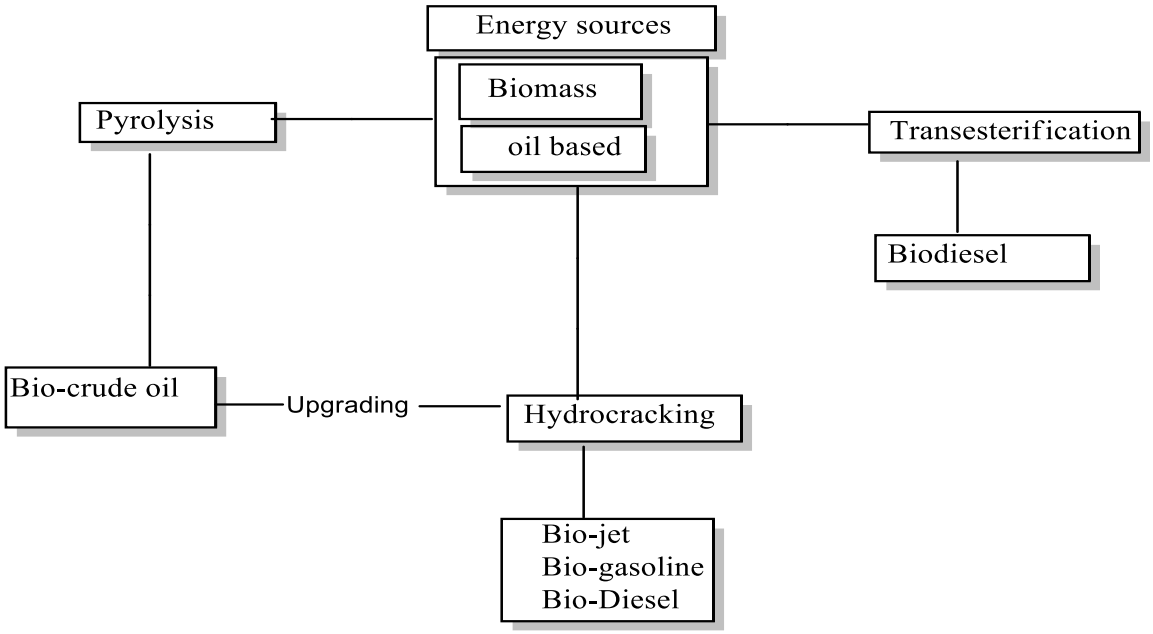


**Figure 1:Biofuel production feedstocks and routes (Ong and Bhatia, 2010; Atabani *et al*., 2013; Ameen *et al*., 2017)**

### 2.1.1 Solid waste

Solid waste can be regarded as garbage obtained from industrial, mining, domestic (unsorted residual/municipal waste), and agricultural activities (Elwan, 2014; Littlejohns *et al*., 2018). It is considered to be a potential feedstock for liquid transportation biofuels and chemicals production since it is readily available or free and can be a sustainable solution for energy needs while environmental landfill impacts are minimized (Klemetsrud *et al.*, 2016). Hydrocracking has been utilized in municipal solid waste conversion. Solid waste as a heterogeneous matter that contains materials of all sorts of different shapes sizes as well as composition, of which most comes from food leftovers and plastic, (Matsakas, 2017; Adhikari *et al.*, 2018) it is expected that its size must be reduced to 1mm and be sorted for it to be a suitable feedstock. The smaller particle sizes of the solid waste increase the fuel production combustion rate (Fodor and Klemeš, 2011). It was suggested that the solid municipal waste be converted into useful products like crude oil via pyrolysis, due to environmental concerns related to landfills or combustion of such waste (Saab *et al.*, 2020). Since the produced crude oil cannot be refined directly to petroleum fuels which can be used in combustion engines, so further processing or upgrading will be required and hydrocracking is the supported method to refine the oil into lighter biofuels (Li *et al.*, 2016).

### 2.2.2 Liquid waste

Wastewater, fats, oils or grease (FOG), gases, and sludges are considered to be liquid waste (Morais *et al.*, 2010). Used oil from cooking oil has an outstanding prospective as sustainable residual biomass that does not take part in food sources, while its recycling can prevent environmental problems caused by their disposal (De and Luque, 2014). WCO is the most economical choice of feedstock to produce biodiesel, (Zhang *et al.*, 2003; Morais *et al.*, 2010; Lee *et al.*, 2019) and its utilization lowers biodiesel production costs by 60-90% (Lee *et al.*, 2019). The oil can be collected from restaurants, cafeterias, and other large institutional kitchens, and it's 2-3 times cheaper compared to the vegetable oil (Zhang *et al.*, 2017; Khan *et al.*, 2019). The WCO contains a high level of free fatty acids of which reduces its application for biodiesel generation (Mohammad *et al.*, 2013). The liquid waste oils are converted into transportation fuels by different catalyst technologies, (Neuling and Kaltschmitt, 2017) and the WCO can undergo hydrocracking after the remaining impurities from cooking are removed through filtration, (Rana *et al.*, 2013) to produce biogasoline and bio-jet, (Bezergianni *et al.*, 2009) since the free fatty acids (FFA) content does not interfere with the process. FOG with its

high lipid content can be regarded as a blend component feedstock in order to boost other feedstock's conversion efficiency (Skaggs *et al.*, 2018). At the household level waste fat is usually discarded down the drain resulting in a sludge consisting of about 30% (by weight) lipid fraction, the sludge can also be used as a cheap and readily available feedstock for the production of biodiesel (Capodaglio and Callegari, 2018).

### 2.2.3. Vegetable oil

Vegetable oils are produced mainly from parts of the plants containing oil, which can be kernel or seeds from oil palms, jatropha, sunflower as well as fruits or seeds from olives (Neuling and Kaltschmitt, 2017). Vegetable oils are the most familiar ideal feedstock candidate to be transformed into liquid fuel as a result of their high energy density, liquid nature, and accessibility as a sustainable feedstock (Taufiqurrahmi and Bhatia, 2011). The vegetable oil's liquid nature makes them easily processable and transportable. Hydrocracking of vegetable oils produces paraffin in $C_{12}$ and $C_{18}$ range. Various oil types have been studied in the context of hydrocracking based on the countries the oil is mainly produced (Table 1).

**Table 1:Different vegetable oils used in Hydrocracking**

| Vegetable oils | Edibility | Country | References |
|---|---|---|---|
| canola | yes | Canada | (Al-Sabawi and Chen, 2012) |
| coconut | yes | Philippians | (Al-Sabawi and Chen, 2012) |
| Cottonseed | No | Greece/Turkey | (Moodley, 2015) |
| Soybean | yes | The U.S. A | (Atabani *et al.*, 2013) |
| Sunflower | yes | Europe | (Zheljazkov *et al.*, 2008) |
| Palm | yes | Southeast Asia | (Keera, El Sabagh and Taman, 2018) |

The sunflower and rapeseed have been widely studied as biofuel potential sources, while palm oil is stated to be easily processable due to their less content of linoleic acid (Table 2). The selection of vegetable oils relies mostly on its accessibility, cost, and weather conditions in that country (Taufiqurrahmi and Bhatia, 2011). This might be the reason why most non-edible oils have not been intensively studied for hydrocracking technology. Utilization of non-edible plant oils as feedstocks can mostly be considered the best option since they don't participate as a food source, (Al-Sabawi and Chen, 2012; Biswas and Sharma, 2014; Ameen, 2017) but the challenge with their use is that they might require high costs for harvesting or extraction of oil when compared to edible oils. Biodiesel derived from non-edible oil results in reduced costs,

(Al-Sabawi and Chen, 2012) and gives an environmental benefit since the feedstocks are renewable biomass sources. Also, it was observed that the non-edible oil has a higher product yield than the edible oil so the production costs can be reduced (Prajitno *et al.*, 2017).

## 2.2. Potential feedstock material

### 2.2.1 Castor

Castor is regarded to be amongst the most favourable non-edible oil crops and is mostly cultivated for their seed to produce castor oil and it makes up to only 0.15% of the vegetable oil produced (Patel *et al.*, 2016). Castor oil is extracted from castor beans using different methods that can be easily used (Dasari and Goud, 2013). Castor oil is a yellow-brown, non-volatile, and non-drying oil that possess a bland odour (Nekhavhambe et al., 2019). Castor oil is nonedible due to its toxicity and has a high oil yield of about 44-55% and requires less water. Castor oils FAME (Fatty acid methyl ester) is highly viscous which makes it have technological challenges due to fatty acid composition. The oil contains up to 90% ricinoleic acid (RA) which is the main fatty acid as observed in Table 2 (Liu *et al.*, 2015a). The high content of the ricinoleic acid makes the castor oil a versatile or valuable feedstock as the acid possesses 3 functional groups. The presence of hydroxyl group in the oil makes the oil have a high viscosity of which can be resolved by deoxygenation and hydrogenation of the castor oil FAME under partial hydrogen pressure. Thus the hydroxyl group will be extracted, double bonds saturated and the carboxylic group will be decarboxylated and a viable hydrocarbon diesel-like fuel will be generated (Meller *et al.*, 2014).

**Table 2:Various fatty acid composition (wt%) of the edible and non-edible oils**

| Fatty acid | Sunflower oil | Palm oil | Soybean oil | Rapeseed oil | Jatropha oil | Castor oil | Polanga oil | Rubber seed oil | Waste cooking oil |
|---|---|---|---|---|---|---|---|---|---|
| Palmic 16:0 $C_{16}H_{32}O_2$ | 8.03 | 43.3 | 13.9-14 | 3.5-4.8 | 15.9 | 1-1.1 | 12 | 10.2 | 9.28 |
| Stearic 18:0 $C_{18}H_{36}O_2$ | 3.26 | 4.52 | 2.1-4 | 0.9-1.5 | 6.9 | 1-3.1 | 13 | 8.7 | 3.95 |
| Oleic 18:1 $C_{18}H_{34}O_2$ | 29.27 | 40.61 | 23.2-24 | 60.7-64.1 | 41.1 | 3-4.9 | 34 | 24.6 | 54.55 |
| Linoleic 18:2 $C_{18}H_{32}O_2$ | 59.32 | 9.22 | 52-56.2 | 21.2-22.3 | 34.7 | 1.3-5 | 38 | 39.6 | 29.67 |
| Linoleic 18:3 $C_{18}H_{30}O_2$ | _ | 0.17 | 4.3-6 | 8.2-11.8 | 0.3 | _ | 0.3 | 16.3 | 0.25 |
| Ricinoleic 18:3 $C_{18}H_{34}O_3$ | _ | _ | _ | _ | _ | 88-89.6 | _ | _ | _ |
| Arachidic 20:0 $C_{20}H_{40}O_2$ | _ | _ | _ | _ | _ | _ | _ | _ | _ |
| Refs | (Osorio-González *et al.*, 2020) | (Orozco *et al.*, 2017) | (Demirbas, 2003; Ong and Bhatia, 2010) | (Demirbas, 2003; Ong and Bhatia, 2010) | (Ameen *et al.*, 2017) | (Demirbas, 2003; Taufiqurrahmi and Bhatia, 2011) | (Taufiqurrahmi and Bhatia, 2011) | (Khan *et al.*, 2019) | (Khan, *et al.*, 2019) |

## 2.3. Alternative chemical production process

### 2.3.1. Pyrolysis

Vegetable oil pyrolysis can be thermal and catalytic (Anene *et al.*, 2018). The primary products obtained from pyrolysis can be gaseous, liquid, or solid (charcoal) depending on the employed process or the operating conditions (Patel and Shah, 2015). The final product produced from pyrolysis can be altered based on reaction conditions, this is one main advantage of pyrolysis over transesterification (Gregory, 2015). The goal for Pyrolysis is to produce bio-oil of high

value through thermal or catalytic cracking that will eventually displace non-renewable fossil fuels. In this section, thermal and catalytic pyrolysis will be discussed.

#### 2.3.1.1 Thermal cracking

Thermal cracking also referred to as pyrolysis, is a thermal decomposition of triglycerides by heat in the absence of oxygen to produce solids, liquids, and gasses at elevated temperatures with or without catalyst assistance (Da Mota *et al.*, 2014; Wiggers *et al.*, 2017). Pyrolysis of multiple triglycerides was used during world war I and II to produce fuels in different countries (Lima *et al.*, 2004). Thermal cracking is mostly conducted in temperature ranges of 400-600 °C, (Gebremariam and Marchetti, 2017) while with the vegetable oils thermal cracking is conducted at 300-500 °C an atmospheric pressure to produce about 70% hydrocarbons (Satyarthi *et al.*, 2013). Based on the reaction operating parameters (temperature, residence time, and heating rate), pyrolysis can be classified into conventional/slow pyrolysis and short resistance time pyrolysis (fast, flash, rapid, ultra-pyrolysis) (Yaman, 2004). Conventional pyrolysis is characterized by a long resistance time of 5-30 minutes and a low heating rate of 10 °C.$s^{-1}$ and produces charcoal. Fast pyrolysis is characterized by moderate to high heating rates of up to 1000 °C.$s^{-1}$, short resistance time below 0.5 seconds at a higher temperature of 750-1000 °C, and the use of feedstock particles less than 0.2 mm in diameter to produce liquid products (Salvi *et al.*, 2013).

Pyrolysis oil (biomass-produced bio-oil) is a dark brown viscous liquid (Veses *et al.*, 2015; Demirbas *et al.*, 2017). Bio-oils maximum product yield can be obtained at a low-temperature range which is between 400 and 500 °C with heating rates that are high in the range of $10^3$-$10^5$ °C.$s^{-1}$ and lower than 2sec short gas residence time process *(*Lu *et al.*, 2009; Westerhof *et al.*, 2010) . Either way, several studies have shown that certain amounts of oil can be obtained at temperatures of 350 °C and 450 °C and 550 °C and 600 °C of which are outside the range. The oil obtained at these temperatures has the potential to produce higher quality in certain applications than the oil obtained at maximum temperatures (Westerhof *et al.*, 2010). Bio-oil from biomass has thermal efficiencies that are the same as petroleum diesel and have the capability as a Carbon-containing source to substitute petroleum diesel (Yaman, 2004). These oils are highly viscous, corrosive, and relatively unstable with poor heating rates (Al-Sabawi and Chen, 2012; Molefe *et al.*, 2019). The pyrolysis oils have 15-30% water content and high oxygen content which makes them not to be ideal for direct use in diesel and gasoline engines (Fagernas, 1995). The corrosive nature of these products due to high acidity is also not ideal

for an automobile engine. Alternatively, the bio-oils can be upgraded and the upgrading processes can be implemented by catalytic hydroprocessing in order to overcome delays associated with ignition (Sadaka and Boateng, 1914; Al-Sabawi and Chen, 2012). Catalytic hydroprocessing of raw bio-oil can yield 30-50% cleaner oil based on operating conditions (Al-Sabawi and Chen, 2012). Lima *et al.*, (2004) conducted pyrolysis of soybean, palm tree, and castor oil. The bio-oil from soybean was catalytically upgraded at 400 °C with HZMS-5 zeolite catalyst to yield deoxygenated and enhanced hydrocarbon diesel-like fuel. Bio-oil upgrading via Catalytic hydroprocessing (Hydrocracking) is the best option, however above 95% of deoxygenation levels are required in order to produce bio-oils that meet the specifications of the crude oil that are used in refineries (Al-Sabawi and Chen, 2012). A lot of bio-oils do not meet the specifications of the petroleum fuel refineries and they cannot be commercially accepted (Lu et al., 2009). In other words, this means that thermal cracking on its own is not ideal to produce biogasoline and bio-jet fuel.

#### 2.3.1.2 Catalytic cracking

Catalytic cracking of recycled cooking grease, plant oils, and animal fats are some of the feedstocks that can be utilized for the production of biofuels that are acceptable for gasoline engines that contain linear and cyclic paraffin, olefins, aldehydes, ketones, and carboxylic acid (Huber, Connor and Corma, 2007). Catalytic cracking entails pyrolysis (thermal cracking) of vegetable oils in the presence of a solid catalyst that enhances gasoline production and organic liquid yield (OLP). The catalytic cracking has been demonstrated to produce poor quality and quantity of hydrocarbons and a high yield of coke roughly of 8-25 wt% (Taufiqurrahmi and Bhatia, 2011). The generation of coke on the cracking catalyst leads to the deactivation of the catalyst. Generally, gases, organic liquid products, water, and coke are the products produced by catalytic cracking. The OLP comprises hydrocarbons that match the boiling point ranges of 60-120 °C, 120-180 °C, and 180-200 °C respectively for gasoline fraction, kerosene fraction, and diesel fraction (Gary, Handwerk and Kaiser, 2007). Catalytic cracking when compared to hydrocracking is advantageous as no hydrogen is required, operating costs are reduced due to processing under atmospheric conditions, and the temperature used is the same as those used for bio-oil production(thermal cracking) (Huber *et al.*, 2007). When catalytic cracking is compared to transesterification it's still has a low processing cost advantage, flexibility with regard to the source of oil/fat, and compatibility with infrastructure (Dewanto *et al.*, 2017). Catalytic cracking is favorable for gasoline production and reduces the output of hefty fuel oils

and light gases at much lower temperatures in comparison with thermal cracking (Taufiqurrahmi and Bhatia, 2011; Anene *et al.*, 2018).

The pyrolysis parameters and catalysts may also favour the production of lighter hydrocarbons, gasoline, kerosene, etc for example this can be observed in Figure 2 on Yigezu and Muthukumar, (2014) study on six selected metal oxides as potential catalysts for the production of biofuels from vegetable oil while investigating the temperature effect and Twaiq et al., (2003) study on the palm oil while investigating the catalyst ratio. The maximum quantity of light hydrocarbons and Gasoline were found to be the highest at 320 °C with 18.73% and 33.62% when the vegetable oil was catalyzed with $MoO_3$ and $V_2O_5$ respectively. At 350 °C a maximum amount of kerosene was 24.91% when NiO was used as a catalyst. The heavy oil was found to be high throughout all the temperatures. Gasoline content is the most important biofuel fraction, the maximum yield observed was 33.62% with $V_2O_5$ at 320 °C. The gasoline value was slightly low than the value reported at 387 °C by Demirbas, (2003) for sunflower oil cracking with $ZnCl_2$. From the obtained results it was concluded that the synthesized catalyst can be utilized for biofuel production by catalytic cracking of vegetable oil, while the obtained results from the catalysts ratio study, it was found that gasoline increased with the catalyst ratio of 10 and the further catalyst increase resulted in decreased and increased gasoline fraction. Other studies reported on the pyrolysis of vegetable oils using different catalysts at different temperatures are presented in Table 3.

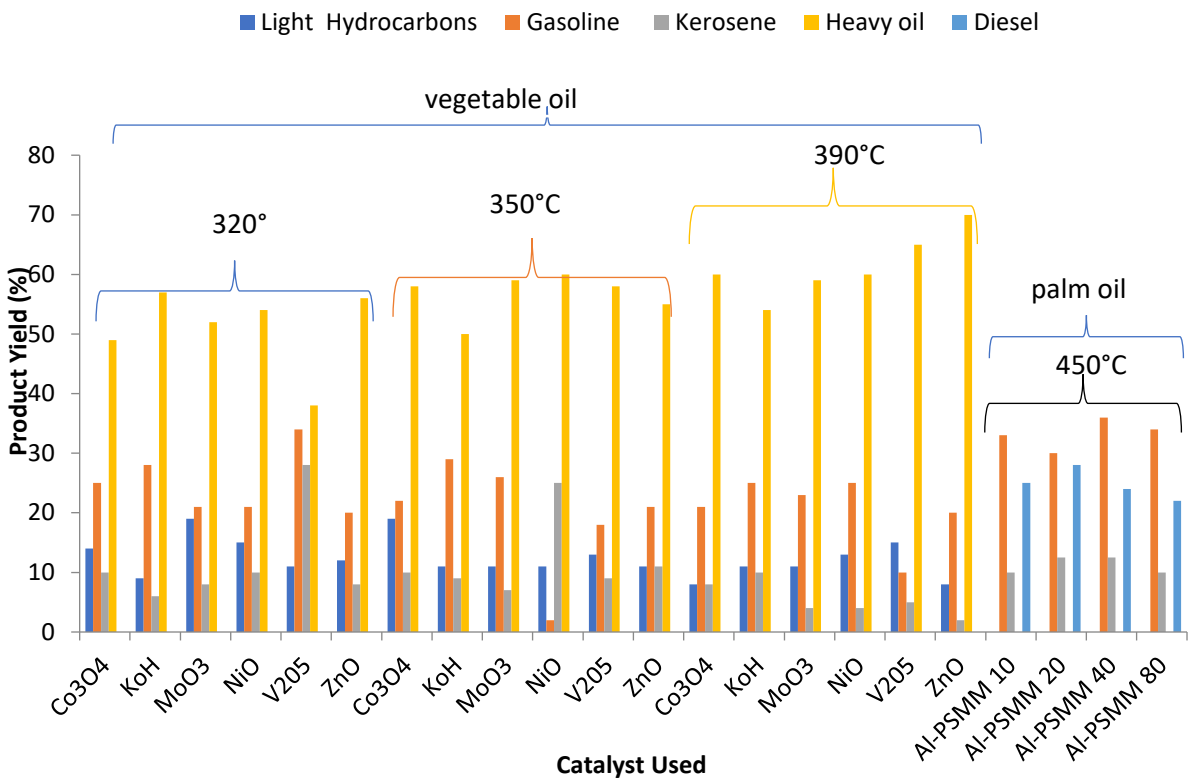


**Figure 2:Used catalysts effect on product yield at 320, 350, 390 and 450 °C (Twaiq *et al.*, 2003; Yigezu and Muthukumar, 2014b)**

Microporous (Zeolites), mesoporous (MCM-41 and SBA-15), microporous (silica-alumina, alumina), composite microporous, and mesoporous catalyst have reportedly been studied for biofuels production from palm oil, soya bean oil, fatty acid mixture, sunflower oil, canola oil, and waste oil (Taufiqurrahmi and Bhatia, 2011). Microporous (Zeolite) catalysts are most favored in vegetable oil cracking due to their selectivity for biofuel products like biogasoline and biodiesel. Mesoporous and macroporous catalysts as there both been used for cracking, have advantages over microporous catalysts regarding hydrothermal and thermal stability. The large pore size of the mesoporous catalyst MCM-41 and SBA-15 makes them selective for the generation of petroleum diesel fractions and this makes them also be more suitable for bulky molecules. The mesoporous catalyst's lower acidity results in elevated coke formation and lower gaseous products (Taufiqurrahmi and Bhatia, 2011).

**Table 3: Studies of a variety of feedstocks, catalyst, and reaction conditions effect on product yield**

| Feedstocks | Catalyst | Temperature[◦C] | Product yield [wt.%] | References |
|---|---|---|---|---|
| Soybean oil | Me-Al-MCM-41. Mesoporous catalyst (Me=La, Ni or Fe) | *T*=450 | Green gasoline=9.1, green diesel =48.8 and tar | (Yu *et al.*, 2013) |
| residual sunflower oil | $Na_2CO_3$ (1, 5, 10 and 20%) | *T*=400 and 420 | Olefins=32.50 Paraffins=32.50 Aromatics=4.16 | (Dandik and Aksoy, 1998) |
| Crude palm oil | 20% $Na_2CO_3$ | *T*=450 | OLP=65.86 non-condensable • gases=30.24 • water=2.5, • Coke=1.4 Green Diesel=91.38 • paraffins=31.27 • Olefins=54.44 • Naphthenics=5.67 | (Da Mota *et al.*, 2014) |
| palm oil | Pt | *T*=300-500 | n-alkenes and I-alkanes =95.55 | (Alencar et al., 1983) |
| Waste cooking oil | ZSM-5 | *T*=450-550 | $_{C5}$-$C_{11}$ –Paraffin= 20.12 Olefins=11.51 Cyclic=1.02 Aromatic=34.60 $C_{12}$-$C_{15}$-Paraffin=22.01 Olefins=3.78 $C_{16}$-$C_{20}$-Paraffin=1.94 Olefins=3.55 Cyclic=0.35 | (Dewanto *et al.*, 2017) |

### 2.3.2 Transesterification

According to Schuchardt *et al.,* (1998) Trans-esterification is the word generally used to outline a group of organic reactions, where an ester reacts with alcohol and is converted into another through the alkoxy moiety interchange. The transesterification process is also referred to as alcoholysis. Transesterification can be carried out in dual processes which include: a) catalytic transesterification and b) Non-catalytic transesterification (Gebremariam and Marchetti, 2017). Transesterification is usually conducted with alcohols such as Butanol, ethanol, methanol, propanol, and amyl alcohol with the participation of base homogenous catalysts like NaOH (sodium hydroxide) or KOH (potassium hydroxide ) in order to chemically break the raw renewable oil molecule into methyl or ethyl ester of the renewable oil and resulting in glycerol being a by-product (Demirbas, 2003). Both methanol as well as ethanol are the most regularly used alcohols, mostly methanol due to their low cost, availability, and advantages physically and chemical (Polar and shortest chain of alcohol) (Patel and Shah.,2015; Sivaprakasam and Saravanan, 2007). The downside related to transesterification is the utilization of large quantities of methanol and the production of glycerol as a by-product (Kim *et al.,* 2016). Transesterification has been largely used to significantly reduce the oil viscosity, (Baskar *et al.,* 2019) thus enhancing fuel atomization and consequently the characteristics of fuel combustion (Bokade and Yadav, 2009; Pinto *et al.,* 2005). The oil's high viscosity can be restrained by other ways which include dilution/blending, microemulsion, and pyrolysis (thermal cracking) (Ameen *et al.*, 2017; Littlejohns *et al.*, 2018).

The transesterification reactions are reversible therefore an alcohol excess is mostly used to shift the equilibrium to the product formation. Often the resulted product of transesterification requires upgrading using other methods. Figure 3 illustrates a general transesterification reaction of Triglyceride (TG) with methanol.

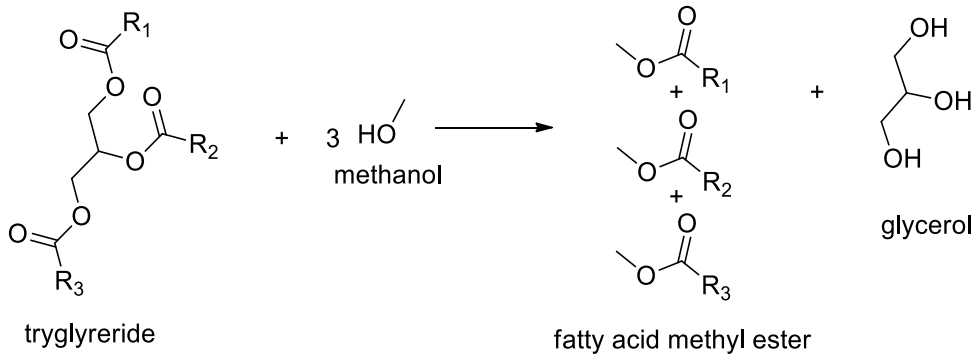


**Figure 3:formation of fatty acids methyl esters and glycerol**

Catalytic hydrodeoxygenation (HDO) is used as a substitute for the triacylglycerides direct conversion to diesel-grade hydrocarbons (green diesel). HDO process requires large hydrogen gas inputs to decrease the catalytically oxygenated lipid functional groups (Kim *et al.*, 2016). In the transesterification process, the homogenous catalyst is sensitive to water and FFA in the feedstock. The FFA reaction with the basic catalyst can form soap. The saponification leads to less biodiesel production and higher cost due to the required purification process (Shi *et al.*, 2012).

#### 2.3.2.1 Homogenous catalysed transesterification

The alkaline catalysts (KOH, NaOH, and $CH_3OK$ (Potassium methanolate) and acid catalysts (Hydrochloric acid (HCl) and Sulfuric acid ($H_2SO_4$) are the catalysts that are particularly commonly used in the transesterification of fat/oil (triglycerides) (Mumtaz *et al.*, 2017). The alkaline catalysed transesterification is the most commercially used transesterification since it is considered to be faster than acid-catalysed transesterification and is less caustic to industrial equipment. Metal alkoxides are the highly active catalyst off all the homogeneous catalysts while the alkaline metal hydroxides such as KOH and NaOH are less active but cheaper (Shereena and Thangaraj, 2009). Acid-catalysed transesterification is a pre-step for the base-catalysed transesterification reaction to esterify FFA greater than 2% (Ejikeme *et al.*, 2010).

#### 2.3.2.2 Heterogeneous catalysed transesterification

Heterogeneous catalysts are said to be solid catalysts or enzymes. Heterogeneous catalysts (especially the solid acid) can be recycled as well as re-used, as compared to the homogenous catalysts (Refaat and Refaat, 2010). The heterogeneous catalysts have the advantage that they simultaneously catalyse the triglycerides transesterification and esterification of FFA's and thus triglycerides low grade with a high content of FFA can also be transformed without any

pre-treatment (Peng, 2012). This catalyst results in easy and better separation of the final product, (Refaat and Refaat, 2010) evading the washing and neutralization process which makes the process more economic (Saez *et al.*,2014). The heterogeneously catalyzed transesterification is more tolerant to water and FFA's in the feedstock.

#### 2.3.2.3 Enzymed catalysed transesterification

The enzyme lipases extracted from different microbial strains have been used as a biocatalyst for the production of biodiesel (Mumtaz *et al.*, 2017). The enzyme catalyst can also be applied on a high FFA feedstock and more oil is converted. The enzyme lipase is costly, requires a longer reaction time, and is inhibited by methanol. Enzyme catalysts have the potential to overcome problems related to the chemical production of diesel (Shimada *et al.*, 1999).

#### 2.3.2.4 Non-catalytic transesterification

As the name suggests, this method is conducted in the absence of any catalyst, but only by using supercritical alcohol (methanol) at pressure and temperature above its critical point (Gebremariam and Marchetti, 2017). The supercritical method is designed in response to challenges associated with the reactant's poor immiscibility and technical problems caused by the catalysts. This method provides simple product separation with faster reaction time but has high operating costs as well as high alcohol requirements (Refaat and Refaat, 2010).

### 2.4. Production mechanism

#### 2.4.1 General hydrocracking process

According to Scherzer and Gruia, (1996) Hydrocracking is a catalytic process in which heavy feedstocks are converted to saturated lighter products. Hydrocracking is occasionally referred to as hydroprocessing or hydrogenation (Šimáček *et al.*, 2010). Hydrocracking is viewed as a severe form of hydrotreating and it involves hydrotreating first in order to make the cracking products lighter and contain a minimal amount of undesired impurities (Al-Sabawi, 2012; Molefe et al.,2019). This process takes place in temperature ranges of 350 to 450 °C with pressure in the range of 40 to 150 bar in conventional petroleum refineries (Peng, 2012). The hydrotreating process is preferred when the desired product is in the diesel range fuel, and it eliminates hetero atoms, and the number of atoms remains intact after C-C saturation (De and Luque, 2014). However, hydrocracking favours the C-C bond breakage, while drastically reducing the molecular weight in order to give rise to gasoline range fuel (De and Luque, 2014). This implies that the biodiesel can be transformed into bio-gasoline along with bio-jet fuel (or

bio-aviation fuel) via hydrocracking as Usomboon *et al.*, (2012) and Liu *et al.*, (2015a) have demonstrated.

There different reactions that occur during hydrocracking which include: HDO (hydrodeoxygenation), HDS (hydrodesulfurization), (HDM ) hydrodemetallization (Rana *et al.*, 2013; Saab *et al.*, 2020). This review's focus is on the best process to produce biofuel, so the focus will be on the HDO process.

Hydrodeoxygenation is a process that removes oxygen from a feedstock and results in high content of hydrocarbon in order to upgrade biodiesel (Mohammad *et al.*, 2013; Zhou *et al.*, 2016). HDO preference is based on its ability to form hydrocarbons in a narrow range of molecular weight. There other different alternatives for upgrading, methods such as catalytic cracking, esterification, emulsion, and steam reforming. Cracking is unattractive due to high yields of light hydrocarbons ($C_1$-$C_4$) and short-chain alkanes ($C_5$-$C_{15}$) with lower energy densities. The HDO reaction rates, as well as the mechanism, are highly determined by the used feedstock and catalyst type (Mohammad *et al.*, 2013). As mentioned, that hydrocracking is a severe form of hydrotreating, it can transform heavy feedstocks into more valuable products. The triglycerides based feedstock contains oxygen content that ranges from 8 to 22%, (Khan *et al.*, 2019) of which can be removed by the deoxygenation reactions in the presence of hydrogen pressure and catalysts, but first, the unsaturated triglycerides bonds are transformed into saturated hydrocarbons through the addition of hydrogen (Hydrogenation), this is then followed by C-O bond scission of the triglycerides molecule to result in free fatty acids (Alwan, 2014). The free fatty acids will be subjugated to 3 major reactions reported to eliminate oxygen: Decarbonylation, Decarboxylation, and hydrodeoxygenation (Peng, 2012; Gosselink *et al.*, 2013; Zhou *et al.*, 2016). Decarboxylation and decarbonylation both produce hydrocarbons with one carbon atom less than the initial fatty acid and also produces a mole of $CO_2$ and CO and water respectively (Vásquez et al., 2017). The decarboxylation major products are $C_{15}$ – $C_{17}$ hydrocarbons (Santillan-Jimenez and Crocker, 2012; Silva *et al.*, 2016). HDO produces alkanes with the same number of C-atoms and 2moles of water. HDO produces $C_{16}$ and $C_{18}$ hydrocarbon products (Veriansyah *et al.*, 2012; Verma *et al.*, 2015). Liquid fuels produced after oxygen removal will have a high energy content as well as high thermal stability being obtained (Vásquez *et al.*, 2017). The produced alkanes will need to be subjected to isomerization and cracking reactions based on their ultimate composition. This will help improve combustion properties and obtain iso-alkanes and lighter hydrocarbons (Vásquez *et al.*, 2017). Figure 4 depicts the general deoxygenation process.

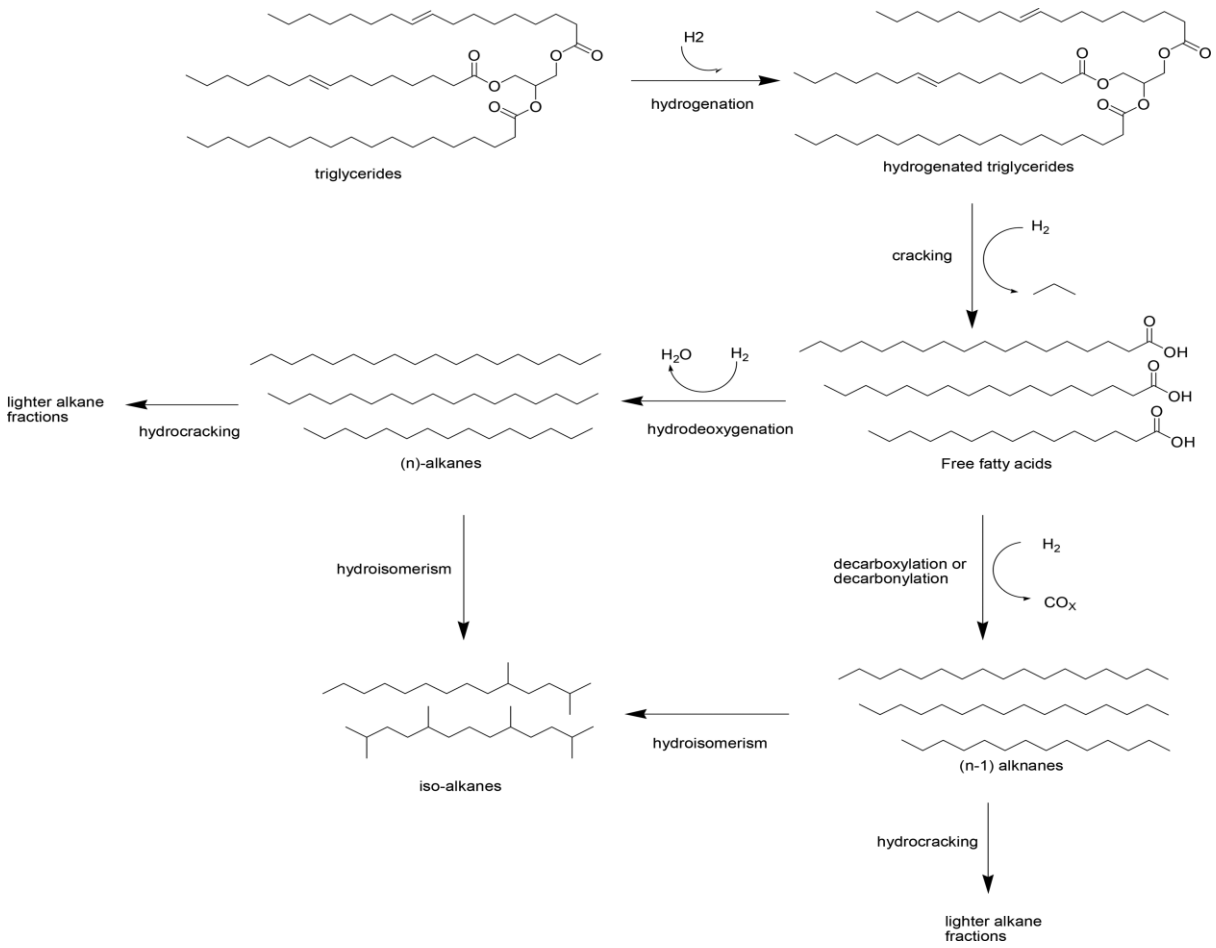


**Figure 4: Triglyceride's deoxygenation process (Molefe *et al.*, 2019)**

Hydrocracking is mostly conducted with bi-metallic/ bifunctional catalysts of which typically have a key role in the deoxygenation of vegetable oils. Bimetallic catalysts have proven to have higher oxygen removal rates when compared to monometallic catalysts (Al-Sabawi and Chen, 2012). This was validated by Kubička and Kaluža, (2010) on their hydrotreating of rapeseed oil (RSO) study. Deoxygenation rates of 3.5 were obtained using $NiMo/Al_2O_3$ this was 19 times greater than those obtained using single metals $Mo/Al_2O_3$ and $Ni/Al_2O_3$ catalysts respectively. At a given reaction temperature, the Mo and Ni catalyst contact time had to be doubled and fourfold respectively for the same rates of deoxygenation to be obtained with $NiMo/Al_2O_3$. In their study, the presence of Ni increased the activity of the bimetallic catalyst $NiMo/Al_2O_3$ because it functioned as Mo catalyst activity promoter in the deoxygenation of triglycerides.

The hydrocracking catalysts mostly comprise oxides Mo or W and either Co or Ni sulfides on alumina comprised support (Al-Sabawi and Chen, 2012). These catalysts have a small diameter of 1.5 mm to 3.0 mm and a length/diameter of 3 to 4 (Robinson, 2015). However other kinds of catalysts can be used or have been suggested.

Hydrcocraking's mains objective is to provide high conversions of vegetable oils and produce high yields of middle distillates (Kerosene, Jet fuel, diesel, and heating oil) and not gasoline in petroleum refineries, though different catalyst can be used to modify it in order to produce biogasoline (Šimáček *et al.*, 2009). For example, the Pt-Zeolite catalyst displayed a strong (effective) catalytic activity for cracking to yield gasoline due to its strong Bronsted acid side (Liu *et al.*, 2015a).

### 2.4.2 Hydrocracking via hydrolysis process

The direct hydrogenation of triglycerides is proven to be expensive due to the hydrogen price at elevated pressure thus the triglycerides normally hydrolysis with high-pressure steam is favored. Generally, the reaction is carried out using a 0.4-1.5 wt% water-to-oil ratio at 100-260°C and 100-7000 kPa (Ngaosuwan *et al.*, 2009; Díaz *et al.*, 2011). The esters hydrolysis takes place by the acyl-oxygen break with an excess of steam/water at elevated temperature or by the utilization of an acid catalyst that is appropriate to hydrolyse the glycerol pillar in the ester group of any triglyceride, di-glycerides, and mono-glycerides (García-Sánchez *et al.*, 2019). The hydrolysis reaction of triglycerides produces 3mol of FFA and 1mol of glycerol (Gly) (Figure 5). This reaction is a homogenous first-order reversible reaction and can be written as:

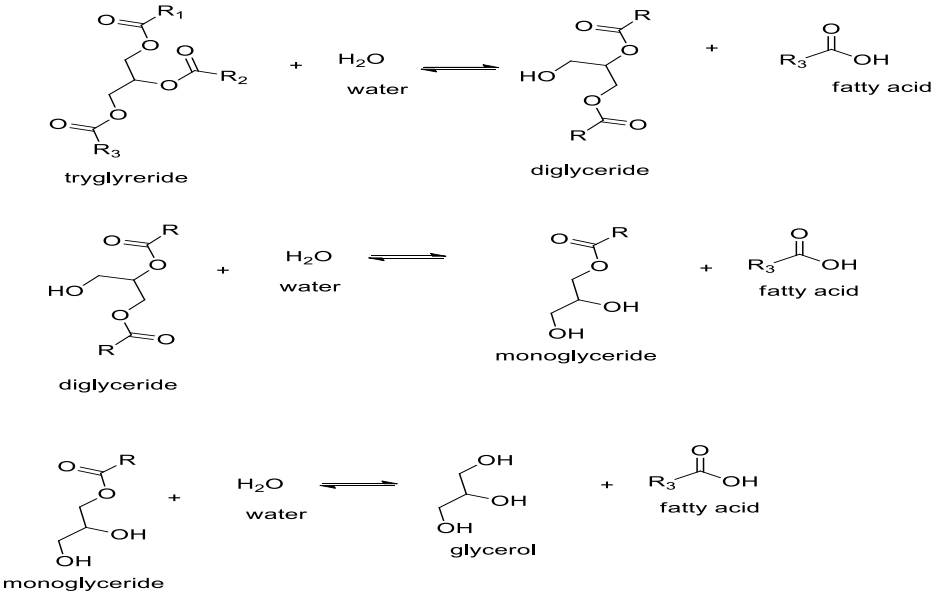


**Figure 5: Triglyceride's hydrolysis reaction**

The produced FFA's as main products have a high degree of purity and can be utilized in multiple industries such as the cosmetics and pharmaceutical industry. The saturated FFA can undergo deoxygenation via decarboxylation in the same hydrothermal medium as hydrolysis to produce n-alkanes chains (Snåre *et al.*, 2006). The produced glycerol on the other hand plays an essential function when dealing with unsaturated fatty acids. The glycerol is catalytically gasified to produce hydrogen via APR (aqueous phase reforming) or hydrothermal catalytic reforming. The hydrogen will accelerate hydrolysis and facilitate hydrogenation of the unsaturated fatty acids into saturated fatty acid (Costa *et al.*, 2020). Therefore, the saturated fatty acid will undergo hydrogenation, hydrodeoxygenation, decarbonylation, and decarboxylation reactions, which will rely on the catalyst used during the hydrothermal reaction (Peng, 2012; Kim *et al.*, 2016; Costa *et al.*, 2020).

## 2.5. Catalyst and reaction parameters

### 2.5.1. Hydrocracking catalyst

Catalyst's typical features are to crack the reactant as well as to accelerate the reaction rate without undergoing any chemical change. Hydrocracking catalysts are bifunctional catalysts that consist of the hydrogenation/dehydrogenation function or acid function and the hydrogen activation function (Ahmed *et al.*, 2002; Saab *et al.*, 2020). The catalyst acid function is provided by the support, such as the amorphous silica-alumina or Zeolites (Meller *et al.*, 2016; Türkmen *et al.*, 2017). The catalyst's acid sites are required for the isomerization and cracking process (Liu *et al.*, 2015b). Hydrogenation/dehydrogenation functions on the metal side can be provided by impregnated metals of which are noble metals such as palladium and platinum or the non-noble metals from group VIA such as molybdenum and tungsten and group VIIIA such as cobalt and nickel, mainly in their sulfided form (Alwan, 2014; Ndimande, 2014). The balance between the metal and acid is a key element in designing the catalyst in order to improve the selectivity, durability, and activity of the catalyst (Roussel *et al.*, 2003; Weitkamp, 2012; Alwan, 2014).

#### 2.5.1.1 Noble metals

Noble metals are most widely used for the triglycerides-based oils oxygen removal and are typically used with zeolites or oxides as supported catalysts (Galadima and Muraza, 2015). The noble metals with suitable support have the potential to display maximum catalytic performance in biofuel and jet fuel production due to different component's synergistic effects

and favoring the catalytic cracking activity. The likes of Pt, Pd, Ir, Rh, and Ag metals were generally used in TG's based oils for oxygen removal (Khan *et al.,* 2018; Yang *et al.,* 2019). Veriansyah *et al.,* (2012) investigated 3 various noble metal catalysts: Pt, Pd, and Ru, with γ - $Al_2O_3$ as support, these catalysts were used for conversion of the soybean oil by HDO. Pt and Pd catalysts were found to be more exceptional than Ru catalyst for the removal of oxygen and hydrocarbon yield. Pd/γ -$Al_2O_3$ had the highest oxygen removal of 90% compared to Pt/ γ - $Al_2O_3$ with 56.4% and Ru/ γ-$Al_2O_3$ with 15.5%. Noble metals are expensive and are used in amounts of 1wt%, so non-noble metals are used as a potential alternative for noble metals because they are less expensive and have high activity.

#### 2.5.1.2. Sulfided/Non-sulfided catalyst

Noble metals and transition metals are mostly used in hydrocracking in their sulfided or reduced form. Sulfided/non-sulfided catalysts have higher activity of which makes them result in being the widely used catalysts for HDO of oil for jet fuel production. Sulfided catalysts are highly active and selective towards the transformation of triglycerides feedstock (Mohammad *et al.,* 2013). Most authors reported that sulphided Ni-Mo/ γ-$Al_2O_3$ and Co-Mo/ γ-$Al_2O_3$ and non-sulfided catalyst can convert vegetable oils triglycerides into jet fuel by HDO process (Khan *et al.,* 2019). However, sulfided catalysts are associated with sulfur content contamination of the final product (Mohammad *et al.,* 2013).

Ni/Mo catalysts have been researched for both hydrotreating and hydrocracking studies. Current developments of using hydrotreating technologies for upgrading fractions of waste oil into transportation fuels that are usable were reported by De and Luque, (2014). The focus was particularly fixed on the selection of the catalyst and the catalyst function in hydrotreating and hydrocracking processes. The following conclusions were made from their findings:

a) A combined sulfided Ni-Mo/$Al_2O_3$ catalyst has a high selectivity for the product in the diesel range($C_{15}$-$C_{18}$) from waste soya oil and gas oil mixture because of minimum cracking,
b) The sulfided NiW/$SiO_2$-$Al_2O_3$ catalyst produces a substantial product in the jet range as a result of cracking.
c) The catalyst NiMo is adequate for the removal of oxygen from triglycerides by hydrodeoxygenation.

d) Ni-W catalyst is highly adequate for both decarboxylation and decarbonylation due to its higher acidity.
e) The NiMo catalyst is examined for co-processing studies that can focus on both hydrotreating and hydrocracking.

Gusmão *et al.*, (1989) also carried out a hydrocracking experiment on vegetable oils (Soybean and babacu) using either a sulfided Ni-Mo/y-$Al_20_3$ or reduced $Ni/SiO_2$ catalysts under a partial hydrogen pressure of 10-200 bars at 350-400 °C. Their research's main objective was to optimize the yield in biodiesel ($C_{12}$-$C_{20}$) acquired from vegetable oils. The $Ni/SiO_2$ was exposed to sulfur poisoning, while the Ni-Mo/Y-$Al_2O_3$ was said to incorporate both the hydrogenation activity with sulfur poisoning resistance.

da Rocha Filho et al.,1993, carried out a hydrocracking experiment in order to investigate the effect of different degrees of saturation and chain length using sulfided Ni-Mo/Y-Al203 catalyst on the resulted products. The produced products were mostly in the diesel range in different quantities based on the used reaction temperature.

Similarly, Sotelo-Boyás *et al.*, (2011), conducted hydrocracking of rapeseed oil, in order to inspect the effect of bi-functional catalyst: sulfided NiMo/γ -Al2O3 catalyst and non-sulfided (Pt/H-Y and Pt/H-ZSM-5). Both the non-sulfided catalysts resulted in more iso-paraffin than n-paraffin with $C_5$ to $C_{22}$ range. The Pt/H-ZSM-5 acid sites had stronger 10 ring zeolites than Pt/H-Y and cracking products which were higher. However, the higher production of $C_{17}$-$C_{18}$ was due to the lower acidity of Pt/H-Y catalyst. Higher diesel yield was observed with Pt/H-Y catalyst, while Pt/H-ZSM-5 was more relevant for green gasoline $C_5$-$C_{12}$ production. This was due to that both zeolites experienced cracking ability that was strong and favored the higher formation of isoparaffin. The sulfided $NiMo/Al_2O_3$ catalyst has been reported to effectively promote triglycerides hydrocracking and carboxylic acid at 350 °C and 8MPa in 3hours (Sotelo-Boyás *et al.*, 2011).

#### 2.5.1.3 Supports

It is very important to choose the catalyst support carefully because it plays the main role in active phase dispersion and it is an important factor in HDO activity determination and selectivity of hydrocarbon (Saab *et al.*, 2020). Various supports such as Zeolites (ZSM-5, H-Beta), Mesoporous material (SAPO-11, Al-MCM 41, SBA-15), and metal oxides ($TiO_2$, $AlO_3$) are all potential supports that were studied (Khan *et al.*, 2019). However, Zeolites are the most generally preferred supports than other supports mainly because of the features they possess,

which include higher catalytic activity, higher resistance to deactivation, good product selectivity, and higher regeneration capability (Li *et al.*, 2015). Supports with average acidity are also favored because of their high productivity and selectivity, while high acidity supports were acknowledged to result in more cracking and decrease the product selectivity (Galadima and Muraza, 2015).

Kim *et al.*, (2017) study demonstrated an increase in selectivity towards bio-jet production using hydrocracking of Palm oil over zeolites (Bulk-ZSM-5, Nano-ZSM-5, and nano beta) as acid supports for Pt catalyst at a temperature of 220-240 °C. The Pt/nano was the best hydrocracking catalyst producing the greatest yield of bio-jet in both the single and the two-step process (hydrotreating and hydrocracking). The two-step process produced high yields of jet fuel range ($C_8$-$C_{16}$) with 71.5 wt%, while the single-step produced high levels of light hydrocarbons (≤C7). In the single-step process, the lighter hydrocarbons remained as the dominating cracking product, while the isomerized $C_8$-$C_{16}$ selectivity continued to be low. The results show that the single-step direct conversion of triglycerides using a bifunctional catalyst is less effective in the production of bio-jet fuel compared to the two-step process concerning product selectivity and catalyst deactivation. So, now the challenge will be to produce bio-jet in one process (Kim *et al.*, 2017).

Tiwari *et al.*, (2011) employed hydrocracking on waste soya oil mixture in order to investigate the mesoporous silica-alumina ($SiO_2$-$AlO_3$) and alumina oxide ($AlO_3$) effect as supports with sulfided Ni-W and Ni-Mo catalysts. At a temperature of 140-250 °C sulfided Ni–W/$SiO_2$–$Al_2O_3$ was discovered to be selective via decarboxylation or decarbonylation for kerosene range hydrocarbons from $C_8$-$C_{18}$ formation which increased with the oil's degree of saturation and, furthermore this alkane's selectivity increased with increasing temperature up to a specific point before dropping again past that point. At a temperature of 250-380 °C sulfided Ni-Mo/$SiO_2$-$AlO_3$ was discovered to be a less acidic catalyst and more selective for diesel range hydrocarbons from $C_{15}$-$C_{18}$, this catalyst is mostly preferred for the HDO pathway for the elimination of oxygen from triglycerides (Tiwari *et al.*, 2011).

Figure 6 represents the effect of different bimetallic hydrocracking catalysts and supports on product distribution that was investigated by different authors. When soybean was catalyzed with NiMo/$Al_2O_3$ and NiMo/25USY (14)60A they both produced mostly diesel, while hydrocracking using NiMo/25HY (5.5)60A slightly increased the gasoline yield. NiMo/25Beta (37)60A resulted in the highest gasoline production of about 70% and RON (research octane

number) value of more than 80%. The NiMo/25-ZSM (90)60A caused hydrocarbon over-cracking to yield great amounts of gaseous products which resulted in decreased iso-/n-ratio. In contrast, the NiMo/25ZSM(1770)60A selectively produced an 80% yield of diesel with iso-/n-ratio of 0.13 between those of NiMo/25USY(14)60A and NiMo/$Al_2O_3$ (Ishihara *et al.*, 2014).

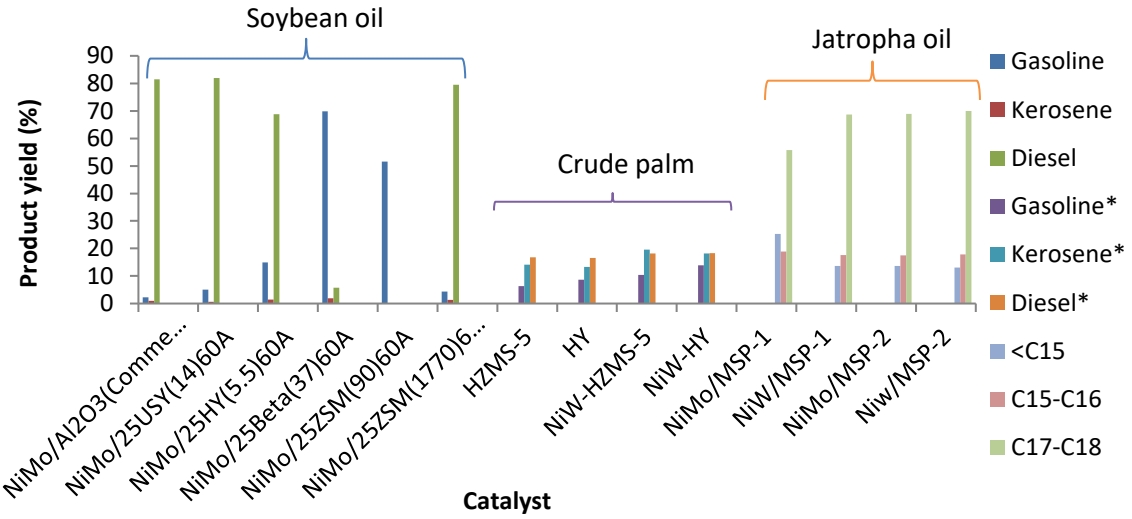


**Figure 6: Catalyst effect on product yield from soya and Jatropha oil (Ishihara *et al.*, 2014; Verma *et al.*, 2015; Subsadsana and Ruangviriyachai, 2016**)

Furthermore, an intensified increase in liquid biofuel production of gasoline, kerosene, and diesel fractions was observed on hydrocracking of crude palm oil, this was to investigate the effect of bimetallic catalyst. The NiW-HY produced a greater yield of gasoline in contrast to NiW-HZMS-5 zeolite catalyst and the NiW-HZMS-5 produced a higher yield of kerosene as compared to the NiW-HY. The results indicate that the catalyst doped with NiW had better hydrocracking performance, compared to the catalyst that was not metallically modified (Subsadsana and Ruangviriyachai, 2016). The NiW was again used for hydrocracking with NiMo in their sulphided form for a conversion comparative study on Jatropha oil at a temperature of 400 °C and 425 °C. The sulphided NiMo and NiW were in combination with the hierarchical mesoporous SAPO-11(MSP-1 and MSP-2). It was observed that higher temperatures alongside the supports acidic character were more selective for the kerosene production, due to hydrocracking activity favored for those conditions. NiMo (MSP-1 and MSP-2) and NiW (MSP-1 and MSP-2) catalysts resulted in a kerosene range of 25-38% and 22-38% respectively. The slightly higher acidic NiW/ MSP-2 produced 30% more kerosene

yield at 450 °C than the lower acidic NiW/MSP-1 (Verma *et al.*, 2015). The acid strength influenced the selectivity of HDO production.

During the hydrocracking process, the final product composition differs as it is mostly influenced by different variables including the selected feedstock, the catalyst used, reaction conditions, among others (Vásquez et al., 2017). The hydrocracking variables and product yields obtained based on different author's studies can be observed in Table 4.

**Table 4:An overview of different oil sources and product yield under different catalysts and operating conditions**

| Material used | Content and operating conditions<br>Temperature (*T*)<br>Reaction time (*Rt*)<br>Hydrogen Pressure (*Hp*)<br>Liquid hourly space velocity (*LHSV)* | Catalyst | Activity | references |
|---|---|---|---|---|
| Coconut oil | Zeolite 0.05wt%<br>Ni & Fe 5wt%<br>*T*=350,375 and 400°C<br>Rt =2hrs | Ni-Fe/ HZSM-5 | n-Paraffin=39.24%<br>Gasoil=18.4%<br>Kerosene=18.1% | (Muttaqii *et al.*, 2019) |
| Waste cooking oil (WCO) | *T*-330-398°C,<br>*Hp*=1200 Psig,<br>*LHSV*=1.0$h^{-1}$,<br>$H_2$*/Oil*=4071 scfb,<br>liquid feed=0.33mi.$min^{-1}$<br>and gas feed =0.4scfh | Commercial hydrocracking catalyst | Diesel=90.1%<br>Gasoline=10.25%<br>Conversion=90% | (Bezergianni *et al.*, 2010) |
| Rapeseed oil | NiO-3.8wt%<br>MoO3-17.3wt%<br>$P_2O_5$-6.7wt%<br>Liquid feed flow=100g $h^{-1}$<br>$H_2$ *flow*=0.1$Nm^3h^{-1}$<br>*WHSV*=1$h^{-1}$<br>Gas/oil=1$h^{-1}$ /920$NM^3$<br>*Hp*=7 and 15Mpa | Ni-Mo/$Al_2O_3$ (commercial) | n-alkane = 6.3wt%<br>n-heptadecane=24.9<br>n-Octadecane=51.1<br>n-alkanes>n-$C_{18}$=3.6<br>conversion<br>>99% @310°C<br>100% @360°C | (Šimáček *et al.*, 2010) |

| | | | | |
|---|---|---|---|---|
| | *T*=310 and 360°C (for results) | | | |
| Waste soya oil plus refinery oil mixture | SiO2-Al2O3=49.38-47.09wt%<br>Al2O3=96.7wt%<br>WO3=26.7wt%<br>NiO=3.3 and 9.8wt%<br>MoO3=14.7wt%<br>*T*= 340-380°C<br>*Hp*=50 bar<br>*LHSV*= 2.4$h^{-1}$<br>*$H_2$/Feed*=1500ml $H_2$gas/ml liquid feed | Sulfided Ni-Mo/ $Al_2O_3$<br>Ni-W/SiO2-$Al_2O_3$ | Diesel=85-95%<br>Kerosene=51% | (Tiwari *et al.*, 2011) |
| Castor oil | CoO- 4wt%<br>MoO3-12wt%<br>Al-84wt%<br>Spiking agent Dimethyl disulphide (DMDS, 2 wt.%)<br>*T*=325°C<br>*Hp*=50 bar (LHSV from 2$h^{-1}$) | CoMO/$AL_2O_3$ | Conversion=87% | (Zaher *et al.*, 2015) |
| Jatropha oil plus its mixtures with gas oil | SiO2=29.38%<br>Al2O3=27.09%,81.97% and 85.0%<br>NiO=26.9%, 3.3%<br>$WO_3$ = 26.7%,<br>MoO3=14.7% and 12.0<br>CoO=3.0%<br>*T*= 340-380°C<br>*Hp*= 50 bar<br>*LHSV*= 1,2$h^{-1}$<br>*$H_2$ to feed ratio*= 1500ml $H_2$ gas per ml liquid feed | Sulfided Ni-W/ $SiO_2$<br>Co-Mo/ $Al_2O_3$<br>NiMo/ $Al_2O_3$ | Diesel =80.8%<br>Diesel=49.2%<br>Diesel=97.9% | (Kumar *et al.*, 2010) |
| Jatropha oil | non-sulfide catalyst, Ni=4.0wt% | PTA-NiMO/ZSM-5 | BTX (Benzene, toulene and xylenes) =59wt% | (Yang *et al.*, 2017) |

| | | | | |
|---|---|---|---|---|
| | Mo=12wt%<br>*T*=380°C, p= 3Mpa,<br>*LHSV*=1.0$h^{-1}$,<br>*$H_2$/Oil ratio* of 1000(v/v) | | | |
| waste virgin coconut oils | Mole ratio silica -alumina of the zeolite (80:1wt%)<br>*T*= 350- 400°C<br>*Rt* (1-3 hrs)<br>*Hp*=20-40 bar | silica -alumina HZSM-5 | Gasoline=4<br>Kerosene=22.4%<br>Diesel=70%<br>Conversion=80% | (Yotsomnuk and Skolpap, 2018) |
| Soybean | *T*=200-280°C, *RT*=2-4hrs, interval of 0.5hr,<br>*Hp*=10MPa | Ni-W | Liquid yield 81.76% and n-alkanes 32.29%, | (Zhou *et al.*, 2016) |
| Jatropha oil | *T*=280-400, *Rt*=10-163h<br>10g catalyst, *Hp*=3.5Mpa,<br>*LHSV*=0.9$h^{-1}$, *$H_2$* to feed *ratio*=1000mL $H_2$ gas/m<br>Liquid feed | NiMoCe/$Al_2O_3$ | Alkanes($C_{15}$-$C_{18}$) =80%,<br>Selectivity= 90%<br>conversion=89% | (Liu *et al.*, 2012) |

### 2.5.2 Temperature

Temperature is the dominating parameter for catalyst effectiveness and has a dominating effect on the product yield. Temperature below 200 °C have been reported to show a significant effect on double bond hydrogenation and resulting in correlating saturated TG's (Khan *et al.*, 2019). As the temperature was increased from 230-280 °C caused the degradation of hydrogenated triglycerides into multiple intermediates and free fatty acids. Further temperature increases to roughly 300 °C increased the hydrocarbon yield and temperature of 350 to 375 °C are said to be the optimal temperatures for the fatty acids C=O bond scission with the least formation of coke during the HDO (Satyarthi *et al.*, 2013; Arun *et al.*, 2015). Figure 7 depicts the study results of the effect of temperature on soybean and waste virgin coconut oil at different temperatures.

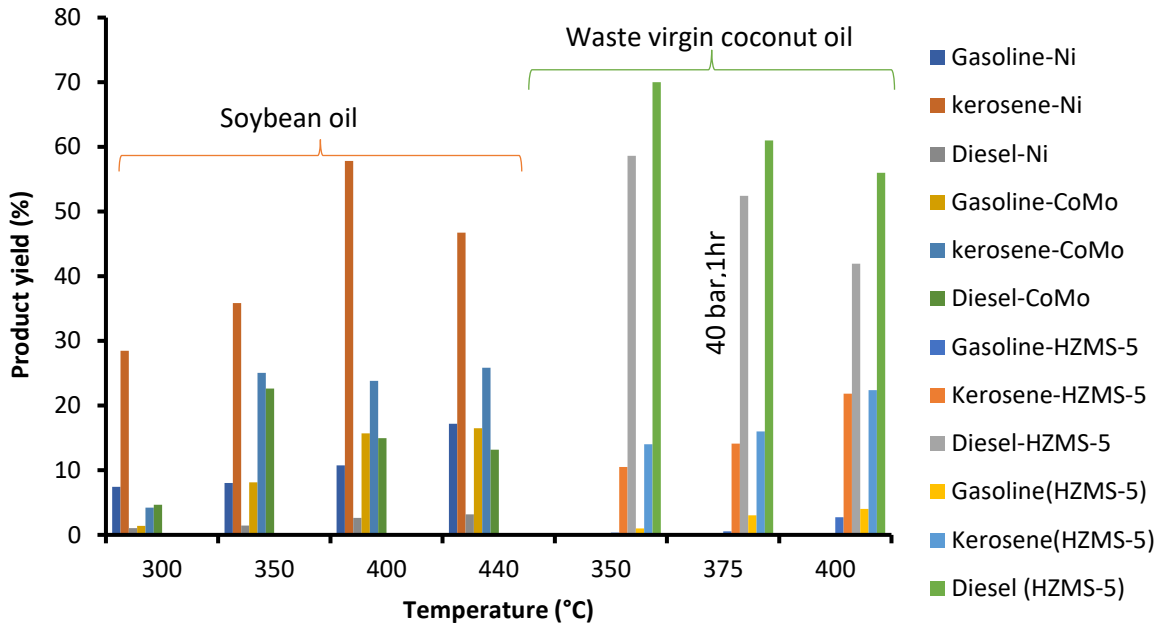


**Figure 7:Temperature effect on production yield of Waste virgin coconut oil and soybean oil (Kim *et al.*, 2013; Yotsomnuk and Skolpap, 2017,2018)**

An increasing temperature from 300 to 400 °C in soybean oil exhibited an increase in diesel yield this was when Ni catalyst was used, at 400 °C both the diesel yield and conversion were on their maximum values because the decarbonylation and decarboxylation reactions were the dominating reaction pathways for the triglyceride's deoxygenation reaction. At 350 °C the CoMosx catalyst produces a higher yield of diesel than what was obtained with the Ni catalyst (Kim *et al.*, 2013).

The kerosene yield from the waste virgin coconut oil was observed to be increasing with increasing temperature, while the diesel yield decreased. At 400 °C kerosene reached the highest product yield and the highest conversion of the coconut oil. At 350 °C diesel was the highest produced product. The biofuels conversion decreased with increasing temperature, this is attributed to that HZMS-1 catalyst contains only an acidic site short of a metallic site (Yotsomnuk and Skolpap, 2017, 2018).

### 2.5.3. Hydrogen pressure

During hydrocracking, pure $H_2$ can be used in combination with other inert gases like Argon (Ar), Nitrogen ($N_2$), Helium (He), etc. An increasing reaction $H_2$ pressure is known to be most favorable in increasing the aromatics conversion into by-products that are saturated, thus increasing the jet fuel and diesel quality with a higher/elevated viscosity index which is exceptional.

from the parameters investigation conducted by, Anand *et al.,* (2016). It was discovered that hydrocracking of vegetable oil at a temperature of 420 °C and hydrogen pressure greater than 60 bar, the C-O bond scission was improved, which resulted in an elevated yield of naphtha and kerosene-like jet fuel hydrocarbons while hydrogen pressure lower than 60 bar displayed more C-C bond cleavage and dehydrogenation instead. When the pressure was further increased to 90 bars the was a slow increase in the formation of naphtha and kerosene (2-10%). Furthermore, the hydrogen pressure increase also favored cracking and lower range hydrocarbons formation, (Anand *et al.*, 2016). From the investigation, it can be said that higher hydrogen pressure is more acceptable to reduce heavy product formation in order to improve the selectivity of the lower range hydrocarbons in hydrocracking (Khan, *et al.*, 2019).

Šimáček *et al.*, (2009, 2010), hydrocracked rapeseed oil using Ni-Mo/$Al_2O_3$, under a hydrogen pressure of 7 and 15 Mpa and temperature of 260-340 °C. It was found out that a higher reaction temperature above 310 °C and pressure of 7 Mpa resulted in a drastic increase in n-alkanes n-C17 and n-C18. The high temperature increased the formation of i-alkanes formed from the n-alkanes and improved low-temperature properties of the biodiesel (product) due to the increase of i-alkanes (Šimáček *et al.*, 2009, 2010), while an increase in pressure in the waste virgin slightly affected the biofuel yield increase (Yotsomnuk and Skolpap, 2018). This pressure effect on product yield can be observed in Figure 8.

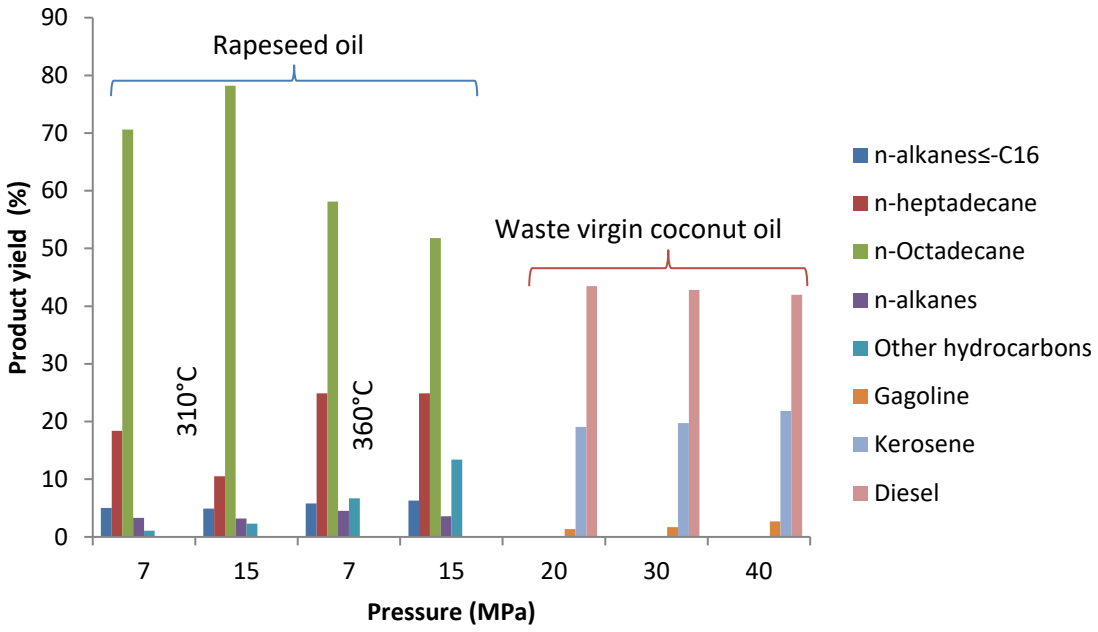


**Figure 8: Effect of pressure on the product yield of rapeseed (Šimáček *et al.*, 2010; Yotsomnuk and Skolpap, 2018)**

### 2.6. Hydrocracking mechanism

Four different mechanisms have been proposed for hydrocracking reactions this includes the bi-functional mechanism, hydrogenolysis, thermal cracking, and Haag-Dessau mechanism (Weitkamp, 2012). Out of all the mechanisms the bi-functional hydrocracking mechanism is the focus as sketched in Figure 9.

Paraffinic feed molecule dehydrogenation takes place on the metal site resulting in alkane's formation. Then the alkanes desorb and migrate to a Bronsted acid site by diffusion through the fluid phase, where it is protonated into a carbenium ion. Subsequently, the carbenium ion undergoes skeletal isomerization (such as alkyl shift or protonated cyclopropane) and cracking (Ndimande, 2014). The carbenium ions β scission results in an olefin and shorter carbenium ions, the olefin can either be cracked to a greater extent on the acid site of the catalyst (secondary cracking), (Burnens, 2011; Thybaut and Marin, 2016) or it can be subjected to a hydrogenation reaction over a metal particle. The produced shorter carbenium ions can be deprotonated to form an olefin, which migrates from the acid site by fluid-phase diffusion (Saab *et al.*, 2020).

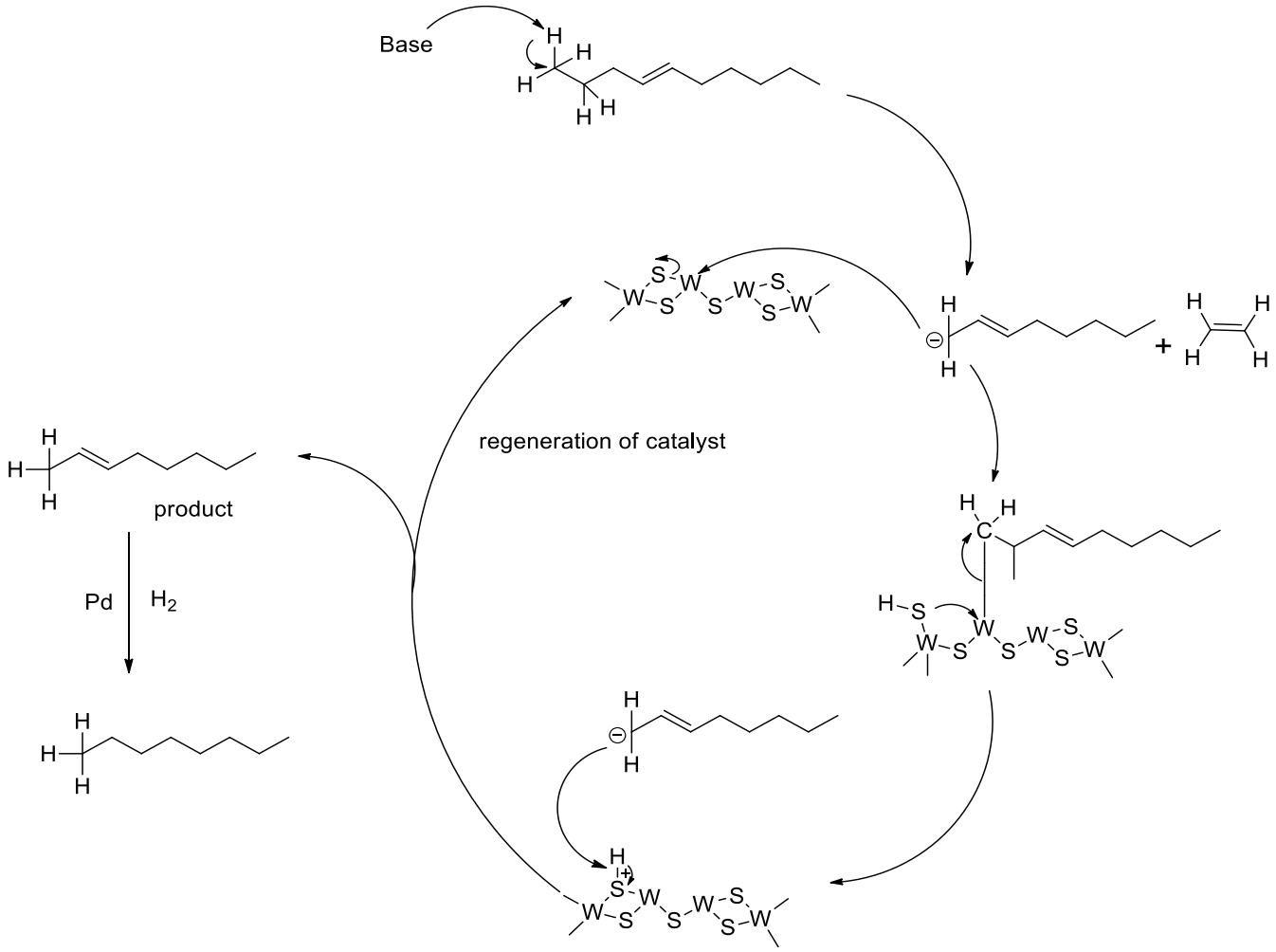


**Figure 9: Proposed hydrocracking mechanism of n-decane**

## 2.7 Conclusion

Transesterification is the most used method for the transformation of feedstocks to biofuels, while on the other hand hydrocracking as a two in one process incorporating hydrotreating and cracking has proven to have a potential in producing biofuels with better fuel properties. Hydrocracking can take place via hydrolysis since direct hydrogenation is said to be expensive. Different studies displayed the influence of several parameters such as catalyst, temperature, and pressure on hydrocarbon selectivity (Anand et al., 2016; Khan et al.,2019). The most used catalyst in hydrocracking are Ni-Mo and Co-Mo catalysts and produces biofuels with a higher yield at high pressure and temperature. Hydrocracking catalysts have a longer lifetime of which makes them superior to the pyrolysis catalysts because it deactivates to a lesser extent. The higher resistance to coke formation in the hydrogen present makes the catalysts to be highly durable. An advantage of using $H_2$ is that the catalyst will deactivate to a lesser extent in

comparison to other inert gases. The bifunctional mechanism for the Hydrocracking mechanism can result in more than one cracking and isomerization product.

## 2.8 References


Adhikari, S., Nam, H., and Chakraborty, J. P., (2018), Conversion of solid wastes to fuels and chemicals through pyrolysis, *Elsevier B.V.*, 239-263.

Al Alwan, B. A., (2014), Biofuels Production Via Catalytic Hydrocracking Of Ddgs Corn Oil And Hydrothermal Decarboxylation Of Oleic Acid Over Transition Metal Carbides Supported On Al-Sba-15, 1-188.

Ahmed, S., Alam, K., and Al-Suaibi, H., (2002), Characterization of hydrocracking catalyst: Metal-Acidity balance, 133–135.

Alencar, J. W., Alves, P. B., and Craveiro, A. A., (1983), Pyrolysis of Tropical Vegetable Oils, *J. Agric. Food Chem.*, 31(6),1268–1270.

Al Muttaqii, M., Kurniawansyah, F., Prajitno, D. H., and Roesyadi, A., (2019), Hydrocracking of Coconut Oil over Ni-Fe/HZSM-5 Catalyst to Produce Hydrocarbon Biofuel, *Indones. J. Chem*, 19(2), 319 – 327.

Al-Sabawi, M., and Chen, J., (2012), Hydroprocessing of biomass-derived oils and their blends with petroleum feedstocks: A review, *Energy and Fuels*, 26(9), 5373–5399.

Anand, M., Farooqui, S.A., Kumar, R., Joshi, R., Kumar, R., Sibi, M.G., Singh, H., Sinha, A.K., ( 2016), Optimizing renewable oil hydrocracking conditions for aviation bio-kerosene production, *Fuel Process. Technol.*, 151, 50–58.

Anene, A. F., Fredriksen, S. B., Sætre, K. A., and Tokheim, L., (2018), Experimental Study of Thermal and Catalytic Pyrolysis of Plastic Waste Components, *Sustainability.*, 10, (3979), 1–12.

Ameen, M., Tazli, M., Yusup, S., Ramli, A., and Yasir, M., (2017), Catalytic hydrodeoxygenation of triglycerides : An approach to clean diesel fuel production, *Renew. Sustain. Energy Rev.*, 80,1072–1088.

Atabani, A. E., Silitonga, A.S., Ong, H. C., Mahlia, T. M. I., Masjuki, H .H., Badruddin, I. A., Fayaz, H., (2013), Non-edible vegetable oils :A critical evaluation of oil extraction, fatty acid compositions, biodiesel production, characteristics, engine performance and emissions production, *Renew. Sustain. Energy Rev.*, 18, 211–245.

Arun, N., Sharma, R. V., and Dalai, A. K., (2015), Green diesel synthesis by hydrodeoxygenation of bio-based feedstocks: Strategies for catalyst design and development, *Renew. Sustain. Energy Rev.*, 48, 240–255.

Baskar, G., Kalavathy, G., Aiswarya, R., and Selvakumari, I. A., (2019), Advances in bio-oil extraction from nonedible oil seeds and algal biomass, *Elsevier Ltd.*, 187-210.

Bezergianni, S., Dimitriadis, A., Kalogianni, A., and Pilavachi, P. A., (2010), Hydrotreating of waste cooking oil for biodiesel production. Part I: Effect of temperature on product yields and heteroatom removal, *Bioresour. Technol.*, 101(17), 6651–6656.

Bezergianni, S., Kalogianni, A., and Vasalos, I. A., (2009), Hydrocracking of vacuum gas oil-vegetable oil mixtures for biofuels production, *Bioresour. Technol.*, 100(12), 3036–3042. Biswas, S., and Sharma, D. K., (2014), Effect of different catalysts on the cracking of Jatropha oil, *J. Anal. Appl. Pyrolysis*, 110, 346–352.

Bokade, V. V., and Yadav, G. D., (2009), Transesterification of Edible and Nonedible Vegetable Oils with Alcohols over Heteropolyacids Supported on Acid-Treated Clay, 9408–9415.

Burnens, G., Bouchy, C., Guillon, E., and Martens, J. A., (2011), Molecule on bifunctional silica – alumina and ultrastable Y zeolite catalysts, 282, 145–154.

Capodaglio, A. G., and Callegari, A., (2018), Feedstock and process influence on biodiesel produced from waste sewage sludge, *J. Environ. Manage.*, 216, 176–182.

Costa, C. Z., Sousa-aguiar, E. F., Antonieta, M., and Gimenes, P., (2020), Hydrothermal Treatment of Vegetable Oils and Fats Aiming at Yielding Hydrocarbons : A Review, Catalysts, 10(843), 1-34.

Da Mota, S. D. P., Mancio, A. A., Lhamas, D. E. L., de Abreu, D. H., da Silva, M. S., dos Santos, W.G., de Castro, D. A. R., de Oliveira, R.M., Araújo, M. E., Borges, L. E. P., Machado, N. T., (2014), Production of green diesel by thermal catalytic cracking of crude palm oil (Elaeis guineensis Jacq) in a pilot plant, *J. Anal. Appl. Pyrolysis*, 110(1), 1–11.

Dandik, L., and Aksoy, H. A., (1998), Pyrolysis of used sunflower oil in the presence of sodium carbonate by using fractionating pyrolysis reactor, *Fuel Process. Technol.*, 57( 2), 81–92, 1998.

Da Rocha Filho, G. N., Brodzki, D., and Djéga-Mariadassou, G., (1993), Formation of alkanes, alkylcycloalkanes and alkylbenzenes during the catalytic hydrocracking of vegetable oils, *Fuel*, 72(4), 543–549.

Dasari, S., and Goud, V., (2013), Comparative Extraction of Castor seed Oil Using Polar and Non polar Solvents, *Int. J. Curr. Eng. Technol.*, 1, 121–123.

De, S., and Luque, R., (2014), Upgrading of waste oils into transportation fuels using hydrotreating technologies, *Biofuel Res. J.*, 1(4), 107–109.

Demirbas, A., (2003), Biodiesel fuels from vegetable oils via catalytic and non-catalytic supercritical alcohol transesterifications and other methods : a survey, 44, 2093–2109.

Demirbas, A., Al-Ghamdi, K., Sen, N., Aslan, A., and Alalayah, W. M., (2017), Gasoline- and diesel-like products from heavy oils via catalytic pyrolysis, *Pet. Sci. Technol.*, 35(15). 1607–1613.

Dewanto, M. A. R., Januartrika, A. A., Dewajani, H., and Budiman, A., (2017), Catalytic and thermal cracking processes of waste cooking oil for bio-gasoline synthesis, *AIP Conf. Proc.*, 1-8.

Díaz, G. C., Perez, R. S., De, N., and Om, C., (2011), Hydrolysis - Hydrogenation of soybean oil and tallow, 3(7), 530–534

Ejikeme, P. M., Anyaogu, I. D., Ejikeme, C. L., Nwafor, N. P., Egbuonu, C. A. C., Ukogu, K., Ibemesi, J. A., (2010), Catalysis in Biodiesel Production by Transesterification Processes-An Insight, 7(4), 1120–1132.

El Khatib, A. S., Hanafi, A. S., Arief, M., and Al-Amrousi, F. E., (2017), Production of Petroleum-like Fractions from Waste Cooking Oil, 60, (1),147–160.

Elwan, E., Arief, Y. Z., Muhamad, N. A., Bashir, N., and Adzis, Z., (2014), Solid waste as a renewable feedstock: A review, *ARPN J. Eng. Appl. Sci.*, 9(8) ,1297–1310.

Fagernas, L.,(1995), Chemical and Physical Characterization of Biomass-Based Pyrolysis Oils, 1-120.

Fodor, Z., and Klemeš, J. J., (2011), Municipal solid waste as alternative fuel - Minimising emissions and effluents, *Chem. Eng. Trans.*, 25, 31–38.

Galadima, A., and Muraza, O., (2015), Catalytic upgrading of vegetable oils into jet fuels range hydrocarbons using heterogeneous catalysts: A review, *J. Ind. Eng. Chem.*, 29, 12–23.

García-Sánchez, M., Sales-Cruz, M., Lopez-Arenas, T., Viveros-García, T., and. Pérez-Cisneros, E. S., (2019), An Intensified Reactive Separation Process for Bio-Jet Diesel Production, *Processes*,7(655), 1-17.

Gary, J. H., Handwerk, G. E., and Kaiser, M. J., (2007), Petroleum Refining: Technology and Economics, Fifth Edition

Gebremariam, S. N., and Marchetti, J. M., (2017), Biodiesel production technologies : review, *AIMS Energy*, 5 (30), 425-457.

Gosselink, R. W., Hollak, S. A. W., Chang, S.-W., van Haveren, J., de Jong, K. P., Bitter, J. H., van Es, D. S., (2013), Reaction pathways for the deoxygenation of vegetable oils and related model compounds," *ChemSusChem*, 6( 9) 1576–1594.

Gregory, J. A., (2015), Thermal Conversion of Triglycerides of Vegetable Oil for Production of Renewable Lamp Fuel,Master thesis, 1-139

Gusmão, J., Brodzki, D., Djéga-Mariadassou, G., and Frety, R., (1989), Utilization of vegetable oils as an alternative source for diesel-type fuel: hydrocracking on reduced Ni/SiO2 and sulphided Ni-Mo/γ-Al2O3, *Catal. Today*, 5(4), 533–544

Huber, G. W., Connor, P. O., and Corma, A., (2007), Processing biomass in conventional oil refineries : Production of high quality diesel by hydrotreating vegetable oils in heavy vacuum oil mixtures, 329, 120–129.

Ishihara, A., Fukui, N., Nasu, H., and Hashimoto, T., (2014),Hydrocracking of soybean oil using zeolite-alumina composite supported NiMo catalysts, *Fuel*, 134, 611–617.

Keera, S. T., El Sabagh S. M., and Taman A. R., (2018), Castor oil biodiesel production and optimization, *Egypt. J. Pet.*, 27(4), pp. 979–984.

Khan S., Lupa A. N. K., Qureshi K. M., Abnisa F., Daud W. M. A. W., Patah M. F. A., (2019), Journal of Analytical and Applied Pyrolysis A review on deoxygenation of triglycerides for jet fuel range hydrocarbons, *J. Anal. Appl. Pyrolysis*, 140, 1–24.

Kim S. K., Brand S., Lee H. S., Kim Y, and Kim J., (2013), Production of renewable diesel by hydrotreatment of soybean oil: Effect of reaction parameters,*Chem. Eng. J.*, 228, 114–123.

Kim M. Y., Kim J. K., Lee M. E., Lee S., and Choi M., (2017) ,Maximizing Biojet Fuel Production from Triglyceride: Importance of the Hydrocracking Catalyst and Separate Deoxygenation/Hydrocracking Steps, *ACS Catal.*, 7(9), 6256–6267.

Kim, D., Vardon, D. R., Murali, D., Sharma, B. K., and Strathmann, T. J., (2016), Valorization of Waste Lipids through Hydrothermal Catalytic Conversion to Liquid Hydrocarbon Fuels with in Situ Hydrogen Production, *ACS Sustainable Chem. Eng*., 1775−1784.

Klemetsrud, B., Ukaew S, Thompson V. S., Thompson, D. N., Klinger, J., Li L., Eatherton, D., Puengprasert P., and Shonnard, D., (2016), Characterization of Products from Fast

Micropyrolysis of Municipal Solid Waste Biomass, *ACS Sustainable Chem. Eng*, 4, 5415−5423.

Kubička, D. and Kaluža, L., (2010), Applied Catalysis A : General Deoxygenation of vegetable oils over sulfided Ni , Mo and NiMo catalysts,372, 199–208.

Kumar, R., Rana, B. S., Tiwari, R., Verma, D., Kumar, R., Joshi R. K., Garg, M. O., Sinha, A. K., (2010), Hydroprocessing of jatropha oil and its mixtures with gas oil, *Green Chem.*, 12(12),2232–2239.

Lee, S. Y., Sankaran, R., Chew, K. W., Tan, C. H., Krishnamoorthy, R., Chu, D-T.,Show, P-L., (2019), Waste to bioenergy: a review on the recent conversion technologies, *BMC Energy*, 1(1), 1–22.

Li, D., Xin, H., Du, X., Hao, X,. Liu, Q., and Hu C., (2015), Recent advances for the production of hydrocarbon biofuel via deoxygenation progress, *Sci. Bull.*, 60(24), 2096–2106.

Li, J., Xia, H., Wu, Q., Hu, Z., Hao, Z., and Zhu, Z., (2016), Hydrocracking of the crude oil from thermal pyrolysis of municipal wastes over bi-functional Mo-Ni catalyst, *Catal. Today*, 271, 172–178.

Lima ,D. G., Soares, V. C. D., Ribeiro, E. B., Carvalho, D. A., Cardoso, É. C.V., Rassi, F. C., Mundim, K.C., Rubim, J.C., Suarez P. A. Z., (2004), Diesel-like fuel obtained by pyrolysis of vegetable oils, *J. Anal. Appl. Pyrolysis*, 71(2), 987–996.

Littlejohns, L., Rehmann, L., Murdy, R., Oo, A., and Neill, S., (2018), Current state and future prospects for liquid biofuels in Canada, 17, 759–779.

Liu, J., Fan, K., Tian, W., Liu, C., and Rong, L., (2012), Hydroprocessing of Jatropha oil over NiMoCe/Al 2O 3 catalyst, *Int. J. Hydrogen Energy*,. 37(23), 17731–17737.

Liu, S., Zhu, Q., Guan, Q., He, L., and Li, W., (2015), Bio-aviation fuel production from hydroprocessing castor oil promoted by the nickel-based bifunctional catalysts, *Bioresour. Technol.*, 183, 93–100.

Lu, Q., Li, W. Z., and Zhu, X. F., (2009), Overview of fuel properties of biomass fast pyrolysis oils, *Energy Convers. Manag.*, 50(5),1376–1383, 2009.

Meller, E., Aizenshtat, Z., and Sasson, Y., (2016), Catalytic Hydrocracking -Hydrogenation of Castor Oil Fatty Acid Methyl Catalytic Hydrocracking -Hydrogenation of Castor Oil Fatty

Acid Methyl Esters over Nickel Substituted Polyoxometalate Catalyst, *Chemistry Select*, 1, 6396–6405

Meller, E., Green, U., Aizenshtat, Z., and Sasson, Y., (2014), Catalytic deoxygenation of castor oil over Pd/C for the production of cost effective biofuel, *Fuel*, 133, 89–95.

Matsakas, L., Gao, Q., Jansson, S., Rova, U., and Christakopoulos, P., (201), Green conversion of municipal solid wastes into fuels and chemicals Green conversion of municipal solid wastes into fuels and chemicals, *Electron. J. Biotechnol.*, 26, 69–83.

Mohammad, M., Kandaramath, T., Yaakob, Z., and Chandra, Y., (2013), Overview on the production of paraffin based-biofuels via catalytic hydrodeoxygenation, *Renew. Sustain. Energy Rev.*, ( 22), 121–132.

Mohammad, M., Hari, T. k., Yaakob, Z., Sharma Y. C., and Sopian, K., (2013), Overview on the production of paraffin based-biofuels via catalytic hydrodeoxygenation, *Renew. Sustain. Energy Rev.*, 22, 121–132.

Molefe, M., Nkazi, D., and Mukaya, H. E., (2019), Method Selection for Biojet and Biogasoline Fuel Production from Castor Oil : A Review, *Energy & Fuels*.,5918−5932.

Moodley, K., (2015), Catalytic hydrocracking of waste vegetable oil over transition metal-based catalysts : selective production of jet fuel range alkanes, 1-178.

Morais, S., Mata, T. M., Martins, A. A., Pinto, G. A., and Costa, C. A. V., (2010), Simulation and life cycle assessment of process design alternatives for biodiesel production from waste vegetable oils, *J. Clean. Prod.*, 18( 13), 1251–1259.

Mumtaz, M. W., Adnan, A., Mukhtar, H., Rashid, U., and Danish, M., (2017), Biodiesel Production Through Chemical and Biochemical Transesteri fi cation : Trends , Technicalities , and Future Perspectives,*Elsevier Inc.*, 465-485.

Ndimande, C., (2014), Ideal Hydrocracking Catalysts for the Conversion of FT Wax to Diesel, *Cent. Catal. Res. Dep. Chem. Eng. Cape T.*, 1–128.

Nekhavhambe, E., Mukaya, H. E., and Nkazi, D. B., (2019), Development of castor oil–based polymers: A review, *J. Adv. Manuf. Process.*, 1(4), 1–13.

Neuling, U., and Kaltschmitt, M., (2017), Review of biofuel production – feedstock processes and markets, 29(2), 137–167.

Ngaosuwan, K., Lotero, E., Suwannakarn, K., Goodwin, J. G., and Praserthdam, P., (2009),

Hydrolysis of triglycerides using solid acid catalysts, *Ind. Eng. Chem. Res.*, 48, (10),4757–4767.

Okullo, A., Temu, A., Ogwok, P., and Ntalikwa, J., (2017), Physico-Chemical Properties of Biodiesel from Jatropha and Castor Oils, *Int. J. Renew. Energy Res.*, 2 (1) *47-52*.

Ong, Y. K., and Bhatia, S., (2010), The current status and perspectives of biofuel production via catalytic cracking of edible and non-edible oils, *Energy*, 35( 1), 111–119.

Orozco, L. M., Echeverri, D. A., Sánchez, L., and Rios, L. A., (2017), Second-generation green diesel from castor oil : Development of a new and efficient continuous-production process, *Chem. Eng. J.*, 322, 149–156.

Osorio-González, C. S., Gómez-Falcon, N., Sandoval-Salas, F., Saini, R., Brar, S. K., and Ramírez, A. A., (2020), Production of biodiesel from castor oil: A review, *Energies*,. 13(10), 1–22.

Patel, V. R., Dumancas, G. G., Viswanath, L. C. K., Maples, R., and Subong, B. J. J., (2016), Castor Oil : Properties ,Uses , and Optimization of Processing Parameters in Commercial Production, *Libertas academia*, 1–12.

Patel, N. K., and Shah, S. N., (2015), Biodiesel from Plant Oils. *Elsevier Inc.*, 277-307.

Peng, B., (2012), Transformation of triglycerides and fatty acids into biofuels with sulfur-free catalysts, 1-148,.

Pinto, A. C., Guarieiro, L. L. N., Rezende, M. J. C., Ribeiro, N. M., and Ednildo, A., (2005), Biodiesel : An Overview, 16( 6), 1313–1330.

Prajitno, D. H., Roesyadi, A., Al-muttaqii, M., and Marlinda, L,, (2017), Hydrocracking of Non-edible Vegetable Oils with Co-Ni /HZSM-5 Catalyst to Gasoil Containing Aromatics, 12(3) 318–328.

Rana, B. S., Kumar, R., Tiwari, R., Kumar, R., Joshi, R. K., Garg, M. O., and Sinha, A. K., (2013), Transportation fuels from co-processing of waste vegetable oil and gas oil mixtures, *Biomass and Bioenergy*, 56, 43–52.

Refaat, A. A., and Refaat, A. A., (2010), Different techniques for the production of biodiesel from waste vegetable oil, 7(1),183–213.

Robinson, P.,( 2015), Hydrotreating and Hydrocracking *: Fundamentals Chapter 7* .

Rodríguez-Fernández, J., Hernández, J. J., Calle-Asensio, A., Ramos, Á., and Barba, J., (2019), Selection of blends of diesel fuel and advanced biofuels based on their physical and thermochemical properties, *Energies*,12(11), 1-13.

Roussel, M., Lemberton, J., Guisnet, M., and Cseri, T., (2003), Mechanisms of n -decane hydrocracking on a sulfided NiW on silica-alumina catalyst, 218,427–437.

Saab, R., Polychronopoulou, K., Zheng, L., Kumar, S., and Schiffer, A., (2020), Synthesis and performance evaluation of hydrocracking catalysts : A review,*J. Ind. Eng. Chem.*, 89, 83–103.

Sadaka, S., and Boateng, A. A., (1914), Pyrolysis and Bio-Oil, *Agric. Nat. Resour.*, 1,1–6.

Saez, B., Santana, A., Ramírez, E., Maçaira, J., Ledesma, C., Llorca, J., and Larrayoz, M. A., (2014), Vegetable Oil Transesterification in Supercritical Conditions Using Co-solvent Carbon Dioxide over Solid Catalysts : A Screening Study, *Energy Fuels*, 28, 6006−6011.

Salvi, B. L., Subramanian, K. A., and Panwar N. L, (2013), Alternative fuels for transportation vehicles: A technical review, *Renew. Sustain. Energy Rev.*, 25, 404–419.

Santillan-jimenez, E., and Crocker, M., (2012), Catalytic deoxygenation of fatty acids and their derivatives to hydrocarbon fuels via decarboxylation / decarbonylation, 87, 1041–1050.

Satyarthi, J. K., Chiranjeevi, T., Gokak, D. T., and Viswanathan, P. S., (2013), An overview of catalytic conversion of vegetable oils/fats into middle distillates, *Catal. Sci. Technol.*, 3(1)70–80.

Scherzer, J., and Gruia, A. J., (1996), Hydrocracking Science and Technology . New York: Marcel Dekker.

Schuchardt, U., Sercheli, R., and Matheus, R., (1998), Transesterification of Vegetable Oils : a Review, *J. Braz. Chem. Soc.*, 9(1),199–210.

Shereena, K. M., and Thangaraj, T., (2012), Biodiesel : an Alternative fuel Produced From Vegetable Oils by Transesterification, 5(3), 67–74.

Shi, F., Wang, P., Duan, Y., Morreale, B., Shi, F., and Wang, P., (2012), Recent developments in the production of liquid fuels via catalytic conversion of microalgae : experiments and simulations, 9727–9747.

Shimada, Y., Watanabe, Y., Samukawa, T., and Sugihara, A., (1999), Conversion of Vegetable Oil to Biodiesel Using Immobilized Candida antarctica Lipase, *JAOCS*, 76(7), 789-793.

Silva, L.N., Fortes, I. C. P., De Sousa, F. P., and Pasa, V. M. D., (2016), Biokerosene and green

diesel from macauba oils via catalytic deoxygenation over Pd/C, *Fuel*, 164, 329–338.

Šimáček, P., Kubička, D., Šebor, G., and Pospíšil, M., (2010), Fuel properties of hydroprocessed rapeseed oil, *Fuel*, 89(3) 611–615.

Šimáček, P., Kubička, D., Šebor, G., and Pospíšil, M., (2009), Hydroprocessed rapeseed oil as a source of hydrocarbon-based biodiesel, *Fuel*, 88(3) 456–460.

Sivaprakasam, S., and Saravanan, C. G., (2007), Optimization of the Transesterification Process for Biodiesel Production and Use of Biodiesel in a Compression Ignition Engine, 4, 2998–3003.

Skaggs, R.L., Coleman, A. M., Seiple, T. E., and Milbrandt, A. R., (2018), Waste-to-Energy biofuel production potential for selected feedstocks in the conterminous United States, *Renew. Sustain. Energy Rev.*, 82, 2640–2651.

Snåre, M., Kubičková, I., Mäki-Arvela, P., Eränen, K., and Murzin, D. Y., (2006), Heterogeneous Catalytic Deoxygenation of Stearic Acid for Production of Biodiesel, *Ind. Eng. Chem. Res*., l 45, 5708–5715.

Sotelo-Boyás, R., Liu, Y., and Minowa, T., (2011), Renewable diesel production from the hydrotreating of rapeseed oil with Pt/zeolite and NiMo/Al2O3 catalysts, *Ind. Eng. Chem. Res.*, 50(5), 2791–2799.

Subsadsana, M., and Ruangviriyachai, C., (2016), Effect of niw modified HZSM-5 and HY zeolites on hydrocracking conversion of crude palm oil to liquid hydrocarbons, *Orient. J. Chem.*, 32(2), 839–844.

Taufiqurrahmi, N., and Bhatia, S., (2011), Catalytic cracking of edible and non-edible oils for the production of biofuels, *Energy Environ. Sci.*, 4,( 4), 1087–1112.

Thybaut, J. W., and Marin, G. B., (2016), Multiscale Aspects in Hydrocracking : From Reaction Mechanism Over Catalysts to Kinetics and Industrial Application, 1st ed., *Elsevier* Inc., 59.

Tiwari, R., Rana, B.S., Kumar, R., Verma, D., Kumar, R., Joshi, R. K., Garg, M. O., Sinha, A. K., (2011), Hydrotreating and hydrocracking catalysts for processing of waste soya-oil and refinery-oil mixtures, *Catal. Commun.*, 12(6), 559–562.

Türkmen, M. B., Yüzüak, B., Atmaca, D. O., Bayat, A., and Balci, V., (2017), Effects of Material Characteristics on the Performance of Hydrocracking Catalysts, *JOTCSB*,1(1), 13–

24.

Twaiq, F. A., Rahman, A., and Bhatia, S., (2003), Liquid hydrocarbon fuels from palm oil by catalytic cracking over aluminosilicate mesoporous catalysts with various Si/ Al ratios, 64, 95–107.

Usomboon, N., Santikunaporn, M., and Butnar, S., (2012), Bio-Gasoline Production from Bio-Diesel via Catalytic Cracking Reaction on Platinum Zeolite Catalyst, 6, 17–22.

Veriansyah, B., Han, J. Y., Kim, S. K., Hong, S-A., Kim, Y. J., Lim, J. S., Shu, Y-W., Oh S-G, Kim, J., (2012), Production of renewable diesel by hydroprocessing of soybean oil : Effect of catalysts, *Fuel*, 94,578–585.

Verma, D., Rana, B. S., Kumar, R., Sibi, M. G., and Sinha, A. K., (2015), Diesel and aviation kerosene with desired aromatics from hydroprocessing of jatropha oil over hydrogenation catalysts supported on hierarchical mesoporous SAPO-11, *Appl. Catal. A Gen.*,490(1) ,108–116.

Veses, R. C., Shah, Z., Kuamoto, P. M., Caramão, E. B., Machado, M. E., and Silva, R., (2015), Fundamentals of Renewable Energy and Applications Bio-Oil Production by Thermal Cracking in the Presence of Hydrogen, *J Fundam Renew. Energy*, 6(1), 1–7.

Vásquez, M. C., Silva, E. E., and Castillo, E. F., (2017), Biomass and Bioenergy Hydrotreatment of vegetable oils : A review of the technologies and its developments for jet biofuel production, 105, 197-206.

Weitkamp, J., (2012), Catalytic Hydrocracking — Mechanisms and Versatility of the Process 292–306.

Westerhof, R. J. M., Brilman, D. W. F., Van Swaaij, W. P. M., and Kersten, S. R. A., (2010), Effect of temperature in fluidized bed fast pyrolysis of biomass: Oil quality assessment in test units, *Ind. Eng. Chem. Res.*, 49, (3) 1160–1168.

Wiggers, V. R., Beims, R. F., Ender, L., Simionatto, E. L., Meier, H. F., (2017), Renewable Hydrocarbons from Triglyceride's Thermal Cracking, *Frontiers in Bioenergy and Biofuels*, 407-424

Yaman, S., (2004), Pyrolysis of biomass to produce fuels and chemical feedstocks, *Energy Convers. Manag.*, 45( 5), 651–671.

Yang, J., Xin, Z., He, Q(S)., Corscadden, K., and Niu, H., (2019), An overview on performance

characteristics of bio-jet fuels, *Fuel*, 237, 916–936.

Yang, X., Liu, J., Fan, K., and Rong, L., (2017), Hydrocracking of Jatropha Oil over non-sulfided PTA-NiMo/ZSM-5 Catalyst, *Sci. Rep.*, 7,1–14.

Yigezu, Z. D., and Muthukumar, K., (2014), Catalytic cracking of vegetable oil with metal oxides for biofuel production, *Energy Convers. Manag.*, 84, 326–333.

Yotsomnuk, P., and Skolpap, W., (2017), Biofuel Production from Waste Virgin Coconut Oil by Hydrocracking Over HZSM-5 Zeolite, *Int. J. Adv. Sci. Eng. Technol.*, 5(1), 54–57.

Yotsomnuk, P., and Skolpap, W., (2018), Effect of process parameters on yield of biofuel production from waste virgin coconut oil, *Int. J. Adv. Sci. Eng. Technol.*, 22(6), 21–35.

Yu, F., Gao, L., Wang, W., Zhang, G., and Ji, J., (2013), Bio-fuel production from the catalytic pyrolysis of soybean oil over Me-Al-MCM-41 (Me = La, Ni or Fe) mesoporous materials, *J. Anal. Appl. Pyrolysis*, 104, 325–329.

Zaher, F. A., El Sayed, H. A., Heakal, B. H., and Hamed, S. F., (2015), Potential of Castor Oil as a Feedstock for the Production of Bio-fuel via Catalytic Hydro- Cracking, 443–449.

Zhang, Y., Dubé, M. A., McLean, D. D., and Kates, M., (2003), Biodiesel production from waste cooking oil: 1. Process design and technological assessment, *Bioresour. Technol.*, 89, (1), 1–16.

Zhang, Z., Wang, Q., Chen, H., and Zhang, X., (2017), Hydroconversion of waste cooking oil into green biofuel over hierarchical USY-Supported NiMo catalyst: A comparative study of desilication and dealumination, *Catalysts*, 7(10).

Zhao, X.,Wei, L., Cheng, S., and Julson, J., (2017), Review of heterogeneous catalysts for catalytically upgrading vegetable oils into hydrocarbon biofuels, *Catalysts*, 7(3), 1-25.

Zheljazkov, V. D.,Vick, B. A., Ebelhar, M. W., Buehring, N., Baldwin, B. S., Astatkie, T., Miller, J. F., (2008), Yield, oil content, and composition of sunflower grown at multiple locations in Mississippi, *Agron. J.*, 100(3),635–642.

Zhou, Z., Zhang, W., Sun, D., Zhu, L., and Jiang, J., (2016), Renewable biofuel production from hydrocracking of soybean biodiesel with a commercial petroleum Ni-W catalyst, *Int. J. Green Energy*, 13(12), 1185–1192.

# Chapter 3: Development of nano-catalysts supported on carbon onions.

## 3.1 Introduction

Multiple methods have been utilised for the synthesis of CNO's and flame pyrolysis was found to be the most promising method for its advantages such as cost effectiveness and higher yields of CNO's (Mykhailiv *et al.,* 2017). The flame pyrolysis synthesis method as well as the two different catalyst synthesis methods which are the co- impregnation (Li, Xu, and Guthrie., 2000) and the sequential impregnation (Nugrahaningtyas *et al.,* 2016) methods are detailed in this section. The precursor salts used are $NiCl_2 \cdot 6H_2O$ and $ZnNO_3 \cdot 6H_2O$ with ≥98 purity.

## 3.2: Catalyst Synthesis

### 3.2.1 Synthesis of the CNO'S (Carbon nano onions) using the pyrolysis method.

The carbon onions (CNO's) were prepared from olive oil. A glass pot was filled with olive oil wherein a pure wick was inserted into the oil through a created hole on the pot lid. The wick that was immersed in oil was ignited to create a flame under ambient air conditions. The glass pot was then placed underneath a collecting brass plate to generate soot and about 30 mm distance was maintained between the nozzle and the brass plate (Mongwe *et.al.,* 2018; Shaku *et.al.,* 2020). The created soot was collected from the brass plate. The synthesized samples of carbon nano onions were then dispersed in water with continuous sonication.

### 3.2.2: Co-impregnation method

The $NiCl_2.6H_2O$(s) and $N_2O6Zn.6H_2O$(s) were dissolved together with distilled water and, they were continuously stirred to form a mixture. Hydrazine was added to the Ni-Zn mixture and subsequently, 5mg/ml NaBr4 (Sodium borohydride) solution was also added dropwise to the mixture to start the reduction reaction process of the salts. The hydrazine hydrate solution was prepared by 2 moles of hydrazine in a 250 mL conical flask with distilled water. The reduced Ni-Zn mixture was then introduced into the prepared dispersed CNO's solution with continuous sonication to form Ni-Zn/CNO's. The formed Ni-Zn/CNO's was then centrifuged and dried overnight at 120 °C for 12 hours.

### 3.2.3: Sequential impregnation

The $NiCl_2.6H_2O(s)$ and $N_2O6Zn.6H_2O(s)$ were firstly reduced separately to NiO and ZnO using the same reduction method used in co-impregnation (section 3.2.2). Thus, the reduced Zn(O) was loaded first to the CNO's solution with continuous sonication to form Zn/CNO. The formed Zn/CNO was then centrifuged and dried in an oven at 120 °C for 12 hours. Thereafter, the reduced Ni solution was introduced to the formed Zn/CNO's composite with continuous sonication to form Ni-Zn/CNO catalyst. The Ni-Zn catalyst was dried at 120 °C for 12 hours. Both the synthesized catalysts were calcined at 500 °C in a muffle furnace for 2 hours (Marlinda *et.al.*, 2017).

## 3.3: Catalyst characterization techniques

This section details the characterization techniques that were used in this research project. Various instruments that are mostly used or combinedly used in different research projects to obtain complimentary details on the properties of the catalysts, with the presence of different characteristics in the synthesized Ni-Zn/CNO catalysts were herein studied using the TGA, BET, SEM, TEM, XRD, and FTIR characterization techniques.

### 3.3.1: Thermogravimetric Analysis (TGA)

The catalyst's thermal stability was determined using TGA. The instrument was first tared with an empty aluminium oxide crucible and then a 10.0 mg of sample was placed in a mini crucible. The thermal stability of the sample was obtained using the SDT Q600 V20.9 instrument under nitrogen gas flow while heating the sample from 30 – 1110 °C at a heating rate of 20 $^{\circ}Cmin^{-1}$. The samples were analysed for 74 minutes per sample.

### 3.3.2: Brunauer-Emmet Teller (BET) Analysis

The catalyst's textural properties were acquired using the micromeritics Trista 3000 equipment. The BET method was used to calculate the surface area, while the BHJ formalism was used to acquire the pore size distribution. Nitrogen gas was used to degasses 200 mg of all the catalyst samples at 150-200 °C for 3hours.

### 3.3.3: Scanning Electron Microscopy (SEM) Analysis

Scanning Electron Microscope was used to analyse the extrinsic morphology of the catalysts. The ethanol dispersed samples were dripped on the aluminium stamps and allowed to dry. Furthermore, the samples were coated with gold-palladium, then analysed using the FEI Quanta 200 ESEM.

### 3.3.4 Energy Dispersive X-ray Spectroscopy (EDS) Analysis

EDS was used in co-existance with SEM to analyse the catalysts elemental composition of all the samples. EDS utilizes energy source such as the electron beam which excites the samples and subsequently dissipates some of the absorbed energy by emitting core-shell electrons and thus release X-rays. The analyses can be presented as peak patterns, spectrums etc,

### 3.3.5: Transmission Electron Microscopy (TEM) Analysis

Transition Electron Microscope (TEM) was used to study the intrinsic structural morphology of the prepared Ni-Zn/CNO catalyst. This was carried out using the FEI Tecnai T12instrument. The powdered samples were sonicated in ethanol to form a suspension. The suspension drop was dripped on carbon film-coated copper grids and allowed to dry at room temperature. The grid was analysed while mounted onto the sample holder and placed in the instrument chamber

### 3.3.6: X-Ray Diffraction (XRD) Analysis

X-Ray Diffraction (XRD) was used for the identification of the catalyst crystallinity and the present metal phases. All the samples measurement were conducted using a Bruker D2 phaser Powder XRD, with Co-Kα irradiation, which operates at 30KV and 30mA, with a scanning speed of 1.52 per minute in the $10 \leq 2\Theta \leq 90^{\circ}C$ range.

### 3.3.7: Fourier Transform Infrared (FTIR) spectroscopy Analysis

The FTIR instrument was used to determine different functional groups present in the Ni-Zn/CNO catalysts. Samples were each placed on the Bruker Tensor 27 FTIR analyser instrument and the transmittance scans were performed producing the IR spectra of the samples. The spectra that serve as unique molecular fingerprints were generated and were easily differentiated from the other molecule's absorption patterns.

### 3.4: Results and discussion

#### 3.4.1 Effect of metals loading

The influence of impregnation of Ni-Zn with different metal ratios on the catalyst properties of co-impregnated and sequentially impregnated catalysts was investigated using the described characterization methods mentioned in Section 3.3, and the results are discussed herein. EDX was used to confirm the loading ratios.

##### 3.4.1.1 Thermal stability analysis of the synthesized catalysts

TGA is one technique that allows the monitoring of the mass of the material as a function of temperature under a running controlled temperature program (Amjad, 2019). In this research project, the TGA was used to analyse the thermal stability of the synthesized co-impregnated and sequentially impregnated Ni-Zn/CNO catalysts in Figures 10 and 11. From both Figures, the catalysts demonstrate the thermal decomposition behaviours of the catalysts/composites in different stages. At the first stage all the catalysts from Figure 10 and 11 displays an initial weight loss at temperatures from 100 to 220 °C, this corresponded to water molecules reduction (dehydration) and -OH ions from the surface of the particles.

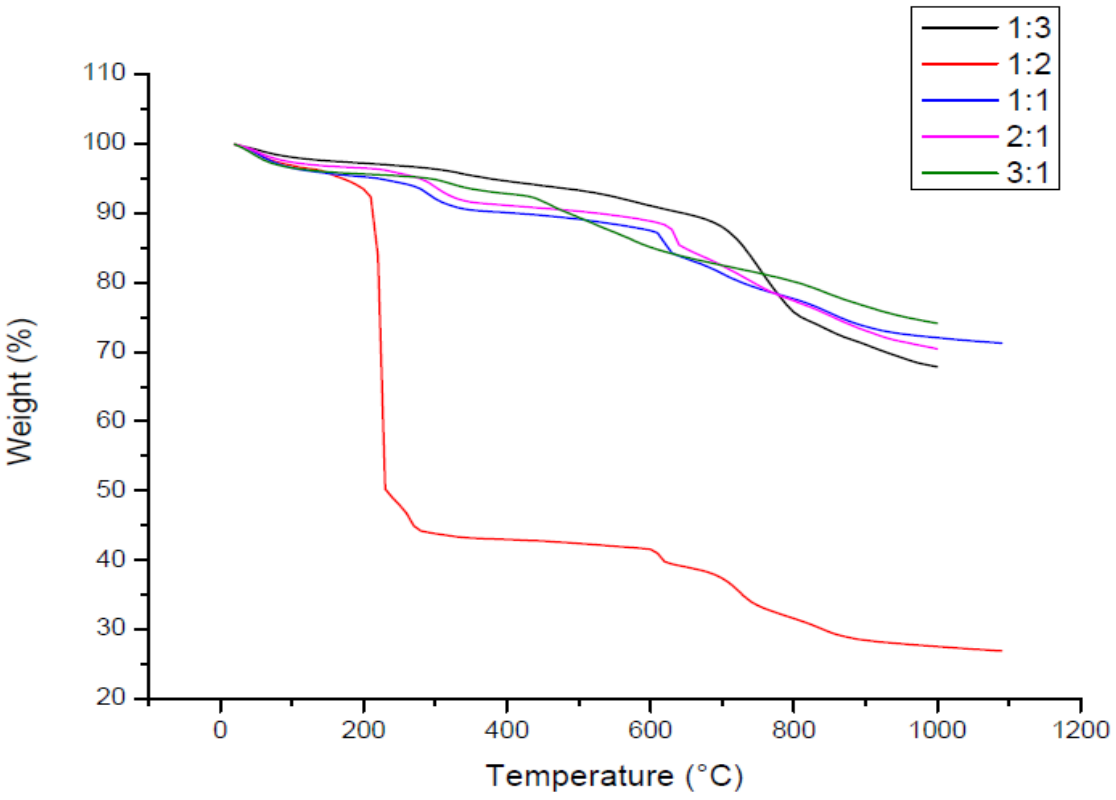


**Figure 10: Thermal degradation of the co-impregnated catalysts as a function of temperature**

In Figure 10 the 1:2 catalyst was observed to have the sharpest weight loss, losing 49% of its weight from 230 to 280 ˚C, this is associated with the first weight loss of the support of which might have been due to the support losing its organic functional groups (like C=O, O-H) or organic material (Mongwe *et al.*, 2018). All the other catalysts were degrading at a steady rate throughout and these catalysts experienced the last support weight loss in temperature ranges from 600 to 800 ˚C, this corresponded to the loss of the remaining carbon (Mongwe *et al.*, 2018).

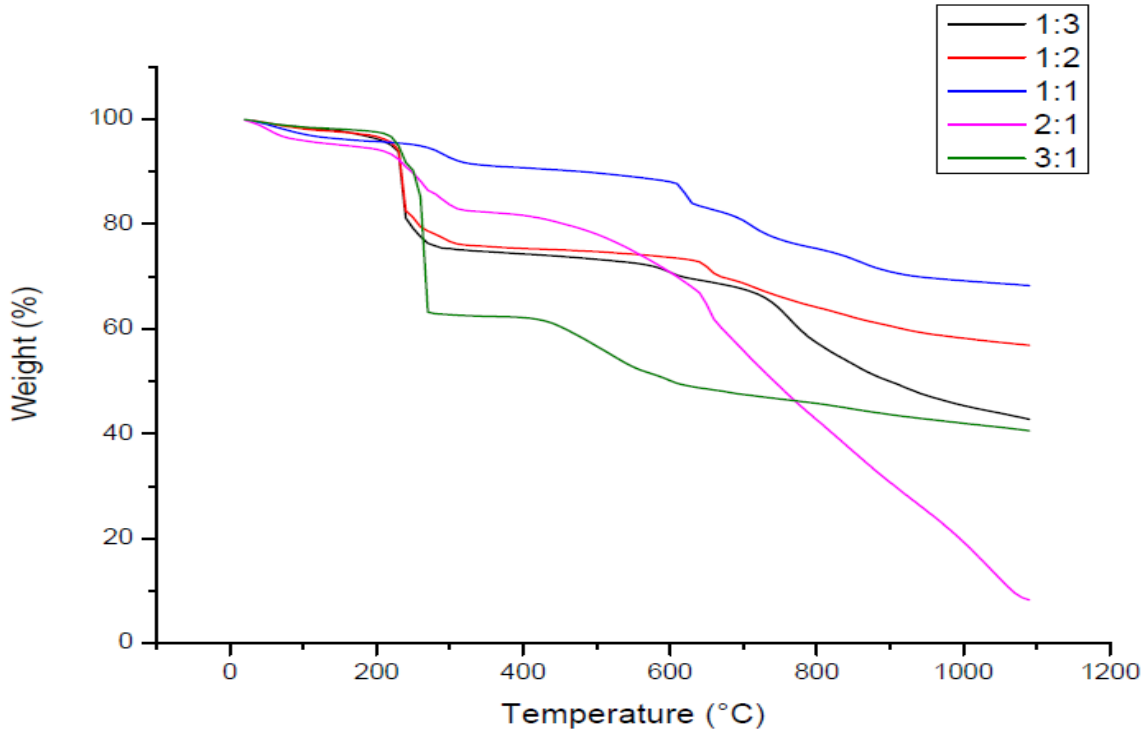


**Figure 11: Thermal degradation of the sequential impregnation catalysts as a function of temperature**

When TGA was used to analyse the sequentially prepared catalysts in Figure 11, it was observed that at temperatures from 240 to 260 °C the catalysts displayed weight losses, of which the catalysts 3:1, 1:2, and 1:3 ratios had the largest weight drops losing 37, 23 and 22% of their weights respectively. This corresponded to the conversion/transition of the metals $NiCl_2(OH)^{-1}$ and $Zn(OH)_2$ to NiO and ZnO, respectively. The catalysts ratios of 1:1, 1:2, and 1:3 at temperatures from 220 °C to roughly 600˚C were observed to be in a plateau stage, while the 3:1 had the shortest plateau stage from 230 to 410 °C. At temperatures of 610 °C the catalysts lost their weights again this was due to thermal decomposition of their supports

(CNO's) of which corresponds to literature that carbon fullerenes burn at temperatures between 500 °C and 600 °C, while more graphitic structure burn between 600 and 800 °C (Charisiou *et al.*, 2019), these weight losses were also observed in the co-impregnation catalysts. Catalyst 2:1 had an accelerated degradation above 600 °C meaning that it had the weakest thermal stability and the 1:1 was observed to be the most stable catalyst.

#### 3.4.1.2 Physical adsorption/desorption of $N_2$ analysis for the catalysts (BET)

According to Brunauer−Emmett−Teller (BET), the $N_2$ adsorption-desorption details in table 5 indicates the textural properties of the synthesized Ni-Zn/CNO catalyst calcined at 500 °C. The evenly spreading of the metals on the catalyst supports surface was expected to increase the surface areas (Nugrahaningtyas, Nuryono and Widjonarko 2010; Dewajani, Purwono and Budiman, 2017), but in counter from table 5 increasing the metal loading ratios resulted in a decrease in some of the surface areas, this was also observed by (Mohiuddin, Mdleleni and Key, 2018) on Fe and Cr impregnated ZSM-5 in the 0.5-5 range. This has resulted due to the metal build-up on the mouth of the channel's pore or the metals were unevenly dispersed on the surface, resulting in the $N_2$ gas being less absorbed so that the catalyst surface was decreased with increasing metal loadings (Dewajani, Purwono and Budiman, 2017).

Catalysts from 1:2 to 2:1 (Co-impregnation) their surface areas are increasing with increasing metal loading ratios and the 1:1 and the 2:1 catalyst are observed to have the highest surface area compared to the other catalysts, while the 1:2 and 3:1 have the smallest surface areas. The increasing metals loading, and larger surface areas are generally linked to higher catalyst efficiency. With the sequential impregnation catalysts, the 1:3 was found to have the highest surface area. The catalysts with high surface areas are associated with a lamella or plate-like structures compared to the other ones (Wang *et al.*, 2015). So, the 2:1 (co-impregnation) and the 1:3 (sequential impregnation) are the optimum ratios to be used.

The formed catalyst pore sizes influence the porosity, the available surface area for $N_2$ adsorption and also affect the extent to which the molecules can be spread onto a solid. The pore sizes, as well as the pore volumes from Table 5, are observed to be increasing and decreasing with the increasing metal loadings this was due to the pile-up of agglomerates.

**Table 5: BET textural properties of co-impregnated and sequential impregnated Ni-Zn/CNO's catalyst with different ratios calcined at 500°C and determined by the adsorption and desorption of $N_2$.**

| Catalyst | Surface Area($m^2/g$) | Pore Volume($cm^3/g$) (BJH) | Pore size(nm) |
|---|---|---|---|
| Co- impregnation | | | |
| 1:3 | 82.6050 | 0.262947 | 12.43611 |
| 1:2 | 36.5492 | 0.210985 | 23.56958 |
| 1:1 | 136.8398 | 0.438476 | 12.79979 |
| 2:1 | 147.8331 | 0.668609 | 18.53823 |
| 3:1 | 67.0786 | 0.5378 | 29.08801 |
| Sequential impregnation | | | |
| 1:3 | 13.8932 | 0.074049 | 25.4642 |
| 1:2 | 10.7817 | 0.061370 | 21.026 |
| 1:1 | 10.7184 | 0.061739 | 28.8572 |
| 2:1 | 9.1963 | 0.053719 | 28.1053 |
| 3:1 | 10.8290 | 0.078787 | 29.57074 |

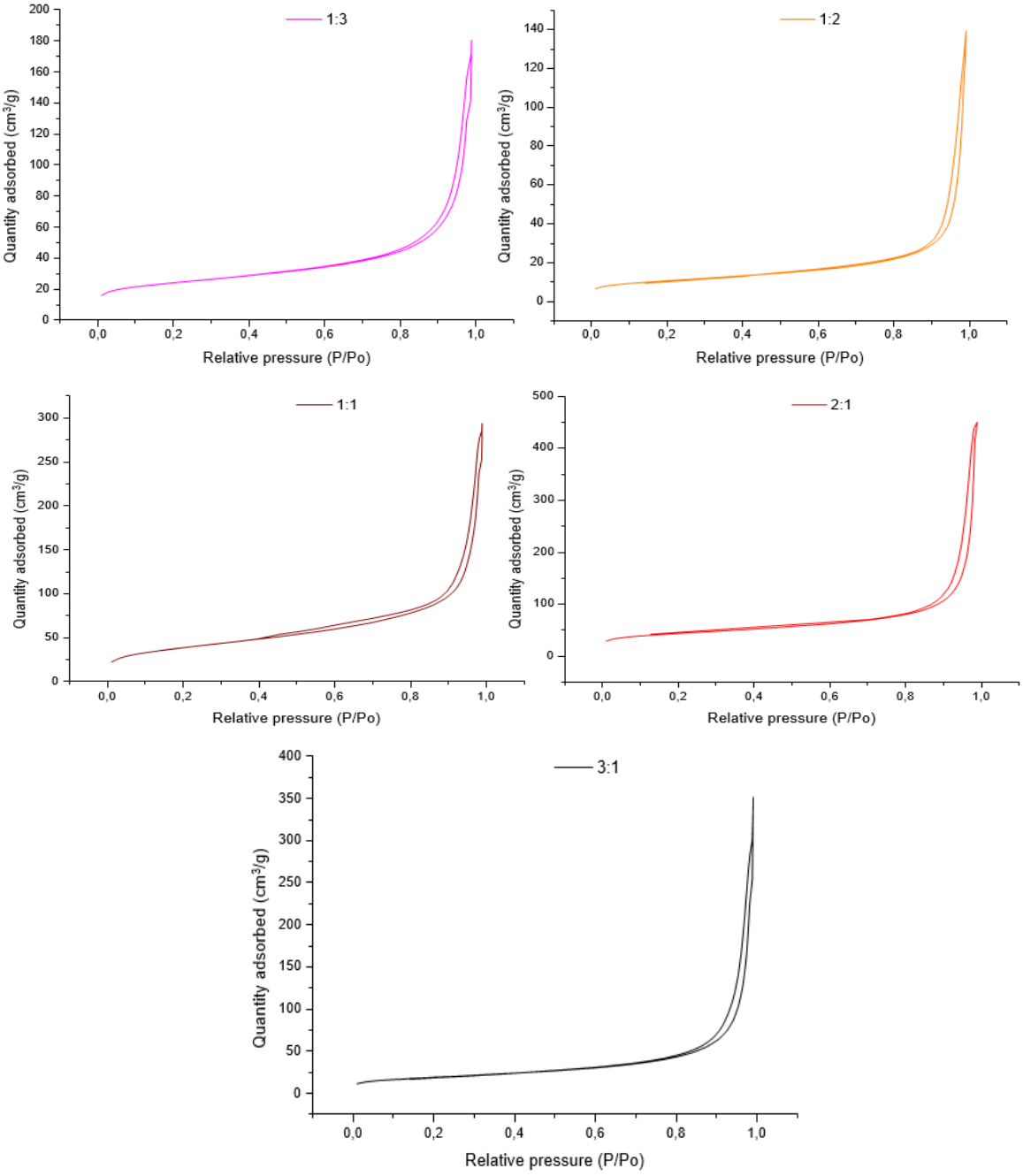


**Figure 12:Isotherms of N2 adsorption or desorption for the Ni-Zn/CNO's co-impregnated catalysts**

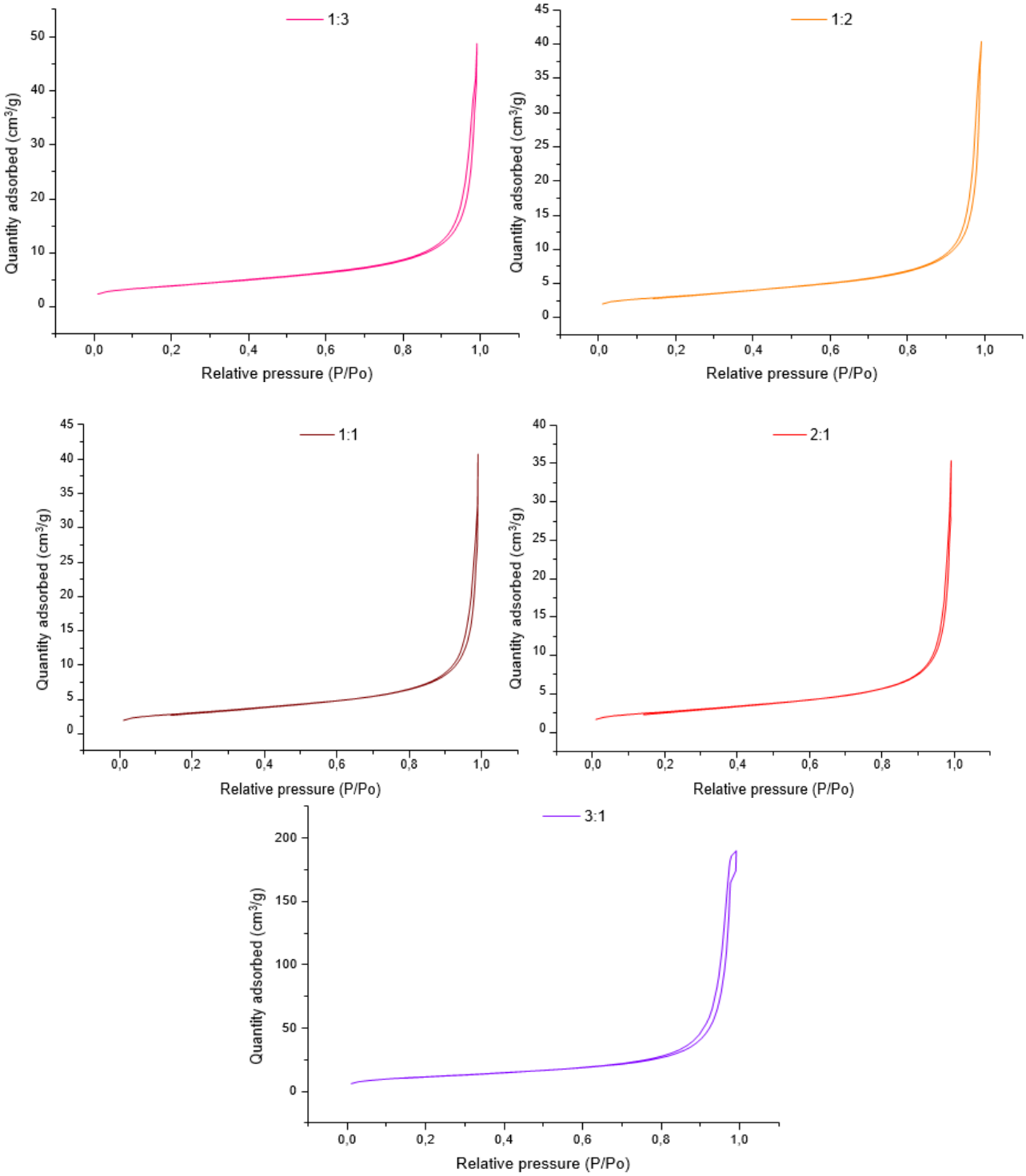


**Figure 13: Isotherms of $N_2$ adsorption or desorption for the Ni-Zn/CNO's sequential impregnated catalysts**

The $N_2$ gas adsorption/desorption isotherm plots represented in Figures 12 and 13 shows that all the curves have the same shape that represents the Langmuir type IV correlated with monolayer to multilayer adsorption followed by pore condensation (Kumar and Jena, 2016). With the graphs having the formation of multilayers, it can be said that the adsorption/desorption was physisorption. All these catalysts possess an H3 hysteric loop

formed at a higher relative pressure (p/po) from above 0.8-1.0 but having the 1:1 catalyst (p/po) starting from 0.4-1.0 in Figure 12. All the H3 shapes are narrow, and they have different pointing ending shapes. This suggests that they possess non-rigid aggregates of plate-like particles (Slit-shaped pores) (Barton *et al.*, 2017). All the isotherms have pores in the mesoporous regions this is according to the IUPAC classification (Thommes *et al.*, 2015).

#### 3.4.1.3 Structural morphology analysis of metal-supported catalysts (SEM and TEM)

In this study, SEM and TEM were used to study both the ex/intrinsic morphologies of the catalysts. The SEM micrographs revealed conglomerated quasi-spherical nanoparticles (i.e. CNOs) with various particle sizes shown in Figures 14 and 15. The observed CNOs nanoparticles morphology was similar to that reported in the literature by Mongwe *et al.*, (2018). SEM micrographs for all samples also showed the presence of nono-quasi-spherical nanoparticles as shown in Figures 14 and 15. This can be an indication of Ni-Zn nanoparticles that are supported onto the CNOs bedding.

Furthermore, it is evident that a bi-metallic catalyst supported on a carbonaceous material was formed in both the methods used. The micrographs also reveal that when the co-impregnation preparation method was used, the Ni-Zn nanoparticles formed different nanoparticulate structures and shapes that are attached to the surfaces of CNOs used as the catalyst support. Hence, CNOs promoted the separation of Ni-Zn nanoparticles to allow for the availability of increased catalyst active sites.

From Figure 15 when the sequential method was used, the prepared catalyst mostly exhibits cuboidal-shaped Ni-Zn nanoparticles. Notably, the particle sizes of these bi-metallic nanoparticles are larger than those of the carbon support. However, CNOs nanoparticles offer the support needed by the Ni-Zn nanoparticles since they are clustered (Wu *et al.*, 2011) as shown in Figure 15. The clustering of the CNOs allows for embedding larger Ni-Zn nanoparticles since CNO's nanoparticles are connected to form larger clusters. Thus, the presence of CNO's material retards the agglomeration of cuboidal Ni-Zn nanoparticles.

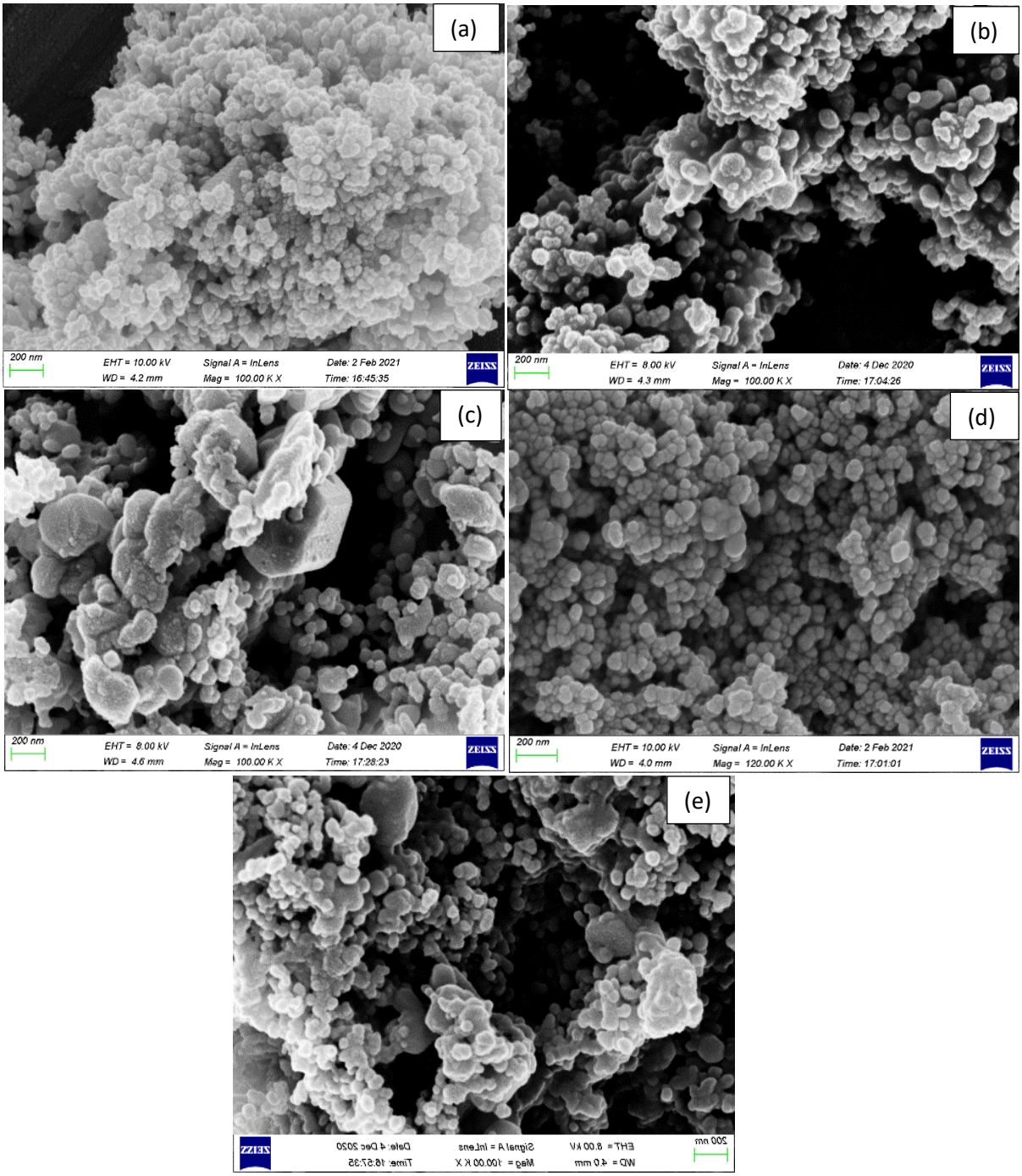


**Figure 14: SEM micrographs of Ni-Zn/CNOs catalyst using different Ni:Zn ratios in co-impregnation preparation method; (a) 1:3, (b) 1:2, (c) 1:1, (d) 2:1 and (e) 3:1 respectively**

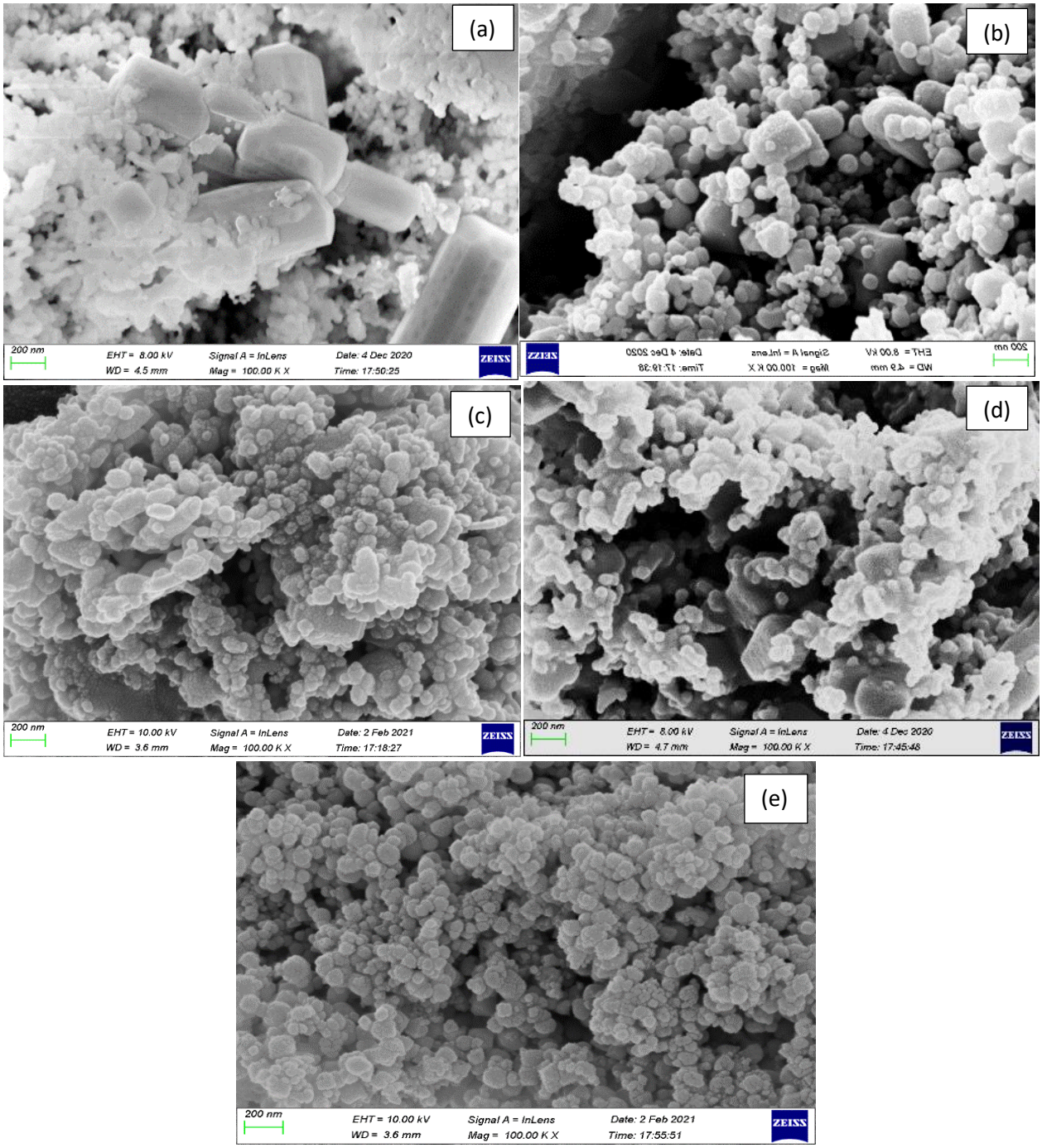


**Figure 15: SEM micrographs of Ni-Zn/CNOs catalyst using different Ni:Zn ratios in a sequential preparation method; (a) 1:3, (b) 1:2, (c) 1:1, (d) 2:1 and (e) 3:1 respectively**

The obtained TEM micrographs also revealed that the prepared bi-metallic catalysts exhibited dense or solid quasi-spherical carbon nanoparticle shapes (i.e. CNO's) with different particle sizes that are less than nm (Velasquez *et al.*, 2016) as shown in Figure 16 and 17.

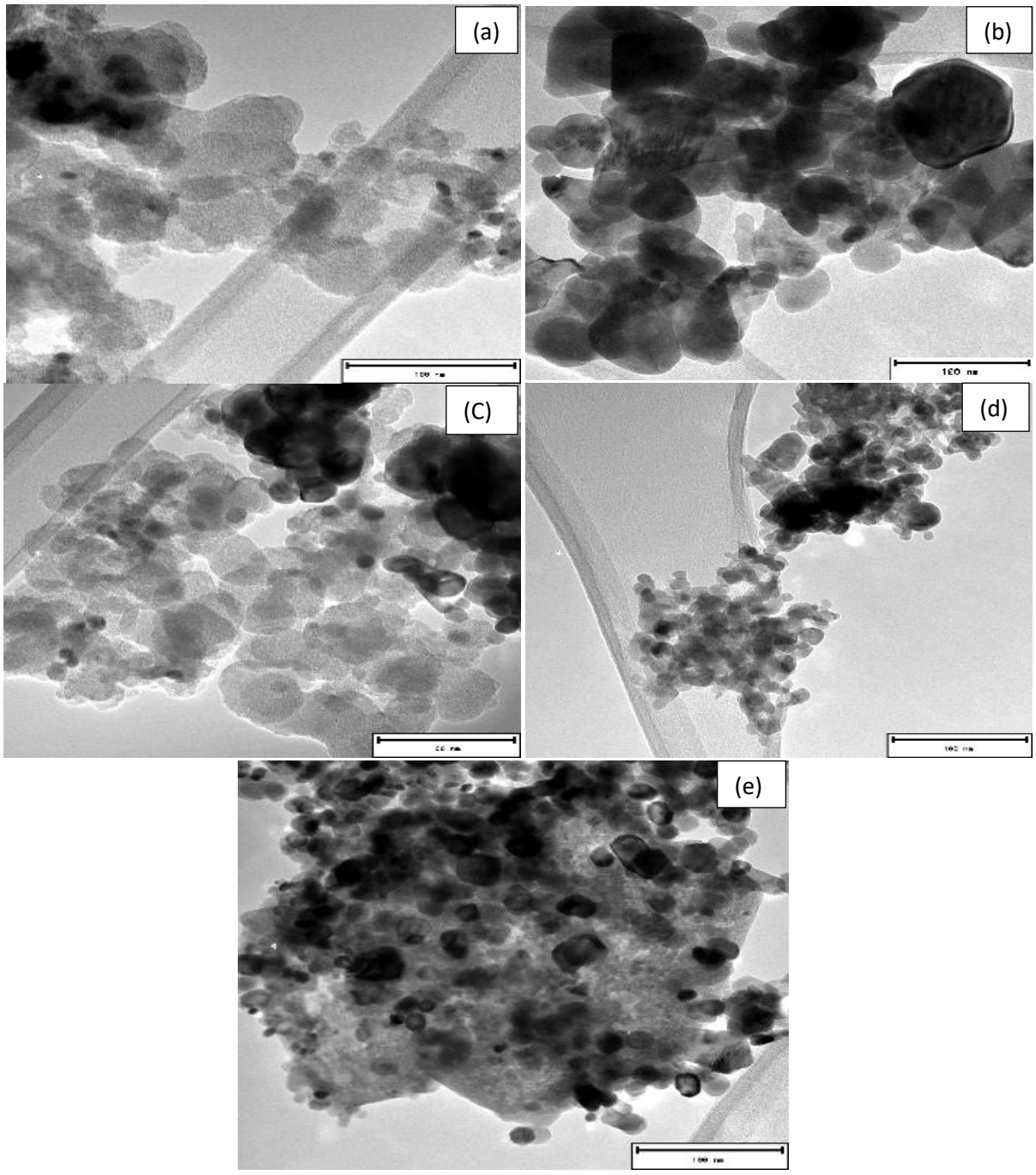


**Figure 16: TEM micrographs of Ni-Zn/CNOs catalyst using different Ni:Zn ratios in a co-impregnation preparation method; (a) 1:3, (b) 1:2, (c) 1:1, (d) 2:1 and (e) 3:1 respectively**

These results support the observations made from the SEM results since they have also shown that the carbon nanoparticles formed conglomerates which can be a result of van der Waals forces leading to linkages of quasi-spherical nanoparticles. It can be seen that the Ni-Zn nanoparticles are present in all samples prepared. However, with the use of different

preparation ratios in the co-precipitation catalyst preparation process. It was observed that larger Ni-Zn nanoparticles were formed when using 1:2 which allowed for possible agglomeration of the bi-metallic nanoparticles (darker regions in Figure 16(b)). Thus, the agglomeration of Ni-Zn nanoparticles can also be seen in other cases as shown in Figure 16. In the same preparation method, when 3:1 was prepared, the Ni-Zn nanoparticles formed were evenly distributed over the carbon support (i.e. CNOs) as can be observed in Figure 16(e). This is an indication that the increased amount of Zn allows for the formation of smaller Ni-Zn nanoparticles that are supported on CNOs (Takahashi *et al.*, 2003). The entire results shown in Figure 16 further reveal that the Ni-Zn nanoparticles form agglomerates which depend on the used ratio of Ni and Zn during the catalyst preparation as well as the nanoparticle sizes formed. In addition, it can be seen from the TEM micrographs that the co-precipitation catalyst preparation process allowed for the formation of cuboidal nanoparticles that are supported onto CNOs (Figure 16).

The TEM microscopy results presented for the sequential impregnation in Figure 17 also revealed that the carbon nanoparticles used as the bi-metals support formed conglomerates.
Thus, the Ni-Zn nanoparticles were mostly supported on a sheet of CNOs when a sequential catalyst preparation method was employed.
However, in some cases, it is shown that the Ni-Zn nanoparticles formed flakes-like nano sheets that are embedded on CNOs this can be observed in Figure 17(a), (c), and (e). The supported Ni-Zn nanoparticles shown by the darker regions in Figure 17(d) exhibit cuboidal shapes with particle sizes that are similar to those of CNOs. Thus, the catalyst prepared using 2:1 can be suggested as the better catalyst due to the Ni-Zn particle sizes formed as well as their CNOs surface distribution.

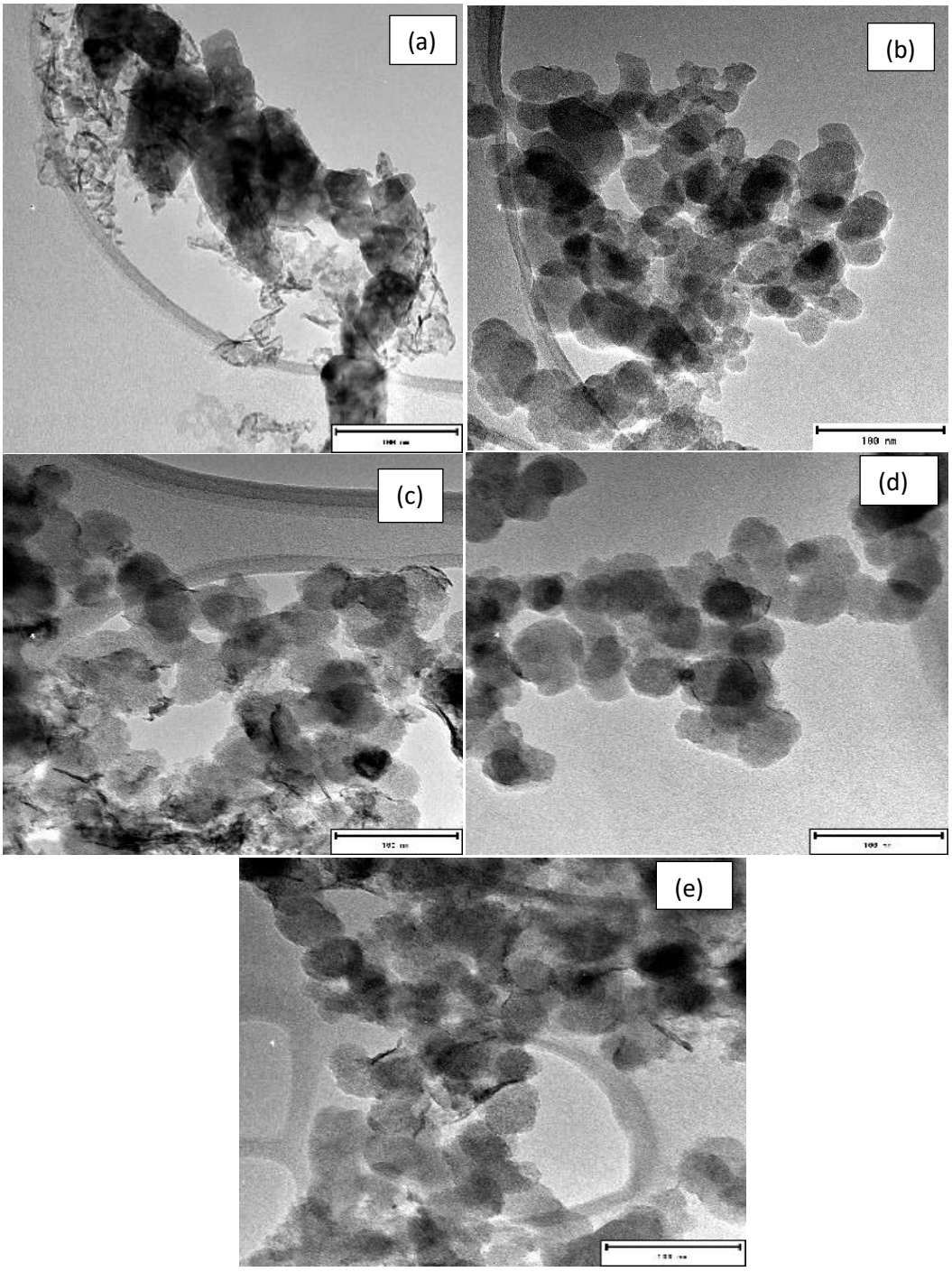


**Figure 17: TEM micrographs of Ni-Zn/CNOs catalyst different Ni:Zn ratio in a sequential preparation method (a) 1:3 (b) 1:2 (c) 1:1 (d) 2:1 and (e) 3:1 respectively**

### 3.4.4 Crystallographic structures identification in the catalysts

The nano Ni-Zn/CNO catalysts crystallinity were investigated by the XRD with all the patterns recorded in 2Θ range from 10 to 90◦C (Figure 18 and 19). From the diffractograms in Figure 18 the metals ratios resulted in differences in the peaks intensity being observed, this might be due to the difference in the components of the crystal scattering intensity or their arrangement in the lattice (Biswas and Sharma, 2014). The was also a slight upshift of peaks with increasing Zn metal content in the CNO support this can be observed from equimolar 1:1 to 1:2 (Zn increase). From 1:1 peaks located at 2Θ= 32.7˚,54.0˚ and 62.8˚ representing ZnO are observed to have shifted to 35.0˚, 57˚ , and 63˚ respectively in the 1:2 ratio, this is because the peaks are moving towards a higher d-spacing value this kind of trend was also observed by (Zaher *et al.*, 2015) in Ni-Zn ferrites.

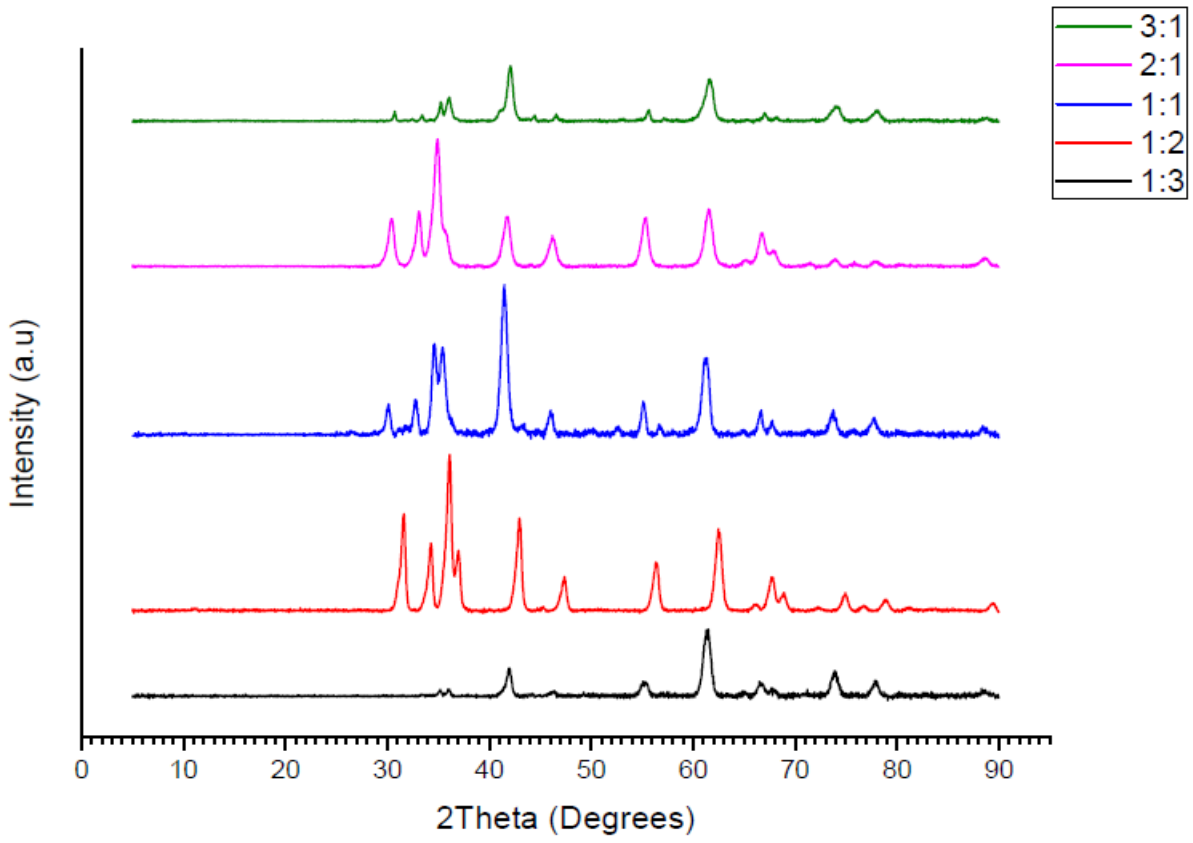


**Figure 18: XRD patterns of the sequentially impregnated Ni-Zn/CNO'S catalyst**

The Ni-Zn/CNO catalysts structures were Further investigated in the sequential impregnation method in Figure 19. The 5 patterns of the nano Ni-Zn/CNO's samples presented are observed to have produced similar diffractograms/patterns. Asymmetric peaks are observed that

attributes to the NiO, ZnO, and Ni-Zn in the range from 31 to 79°. The NiO peaks appear at 2Θ= 37.2,43.3, 62.8,75.4, and 79.4°, and the peaks identified at 2Θ = 31.7°, 34.4°, 36.2°, and 62.8◦ are an indication of the ZnO (Pan and Chen, 2019). The presence of the observed peaks proves that the Ni and Zn have been embedded on the supports surface and with both the NiO and ZnO found at 2Θ=47◦.

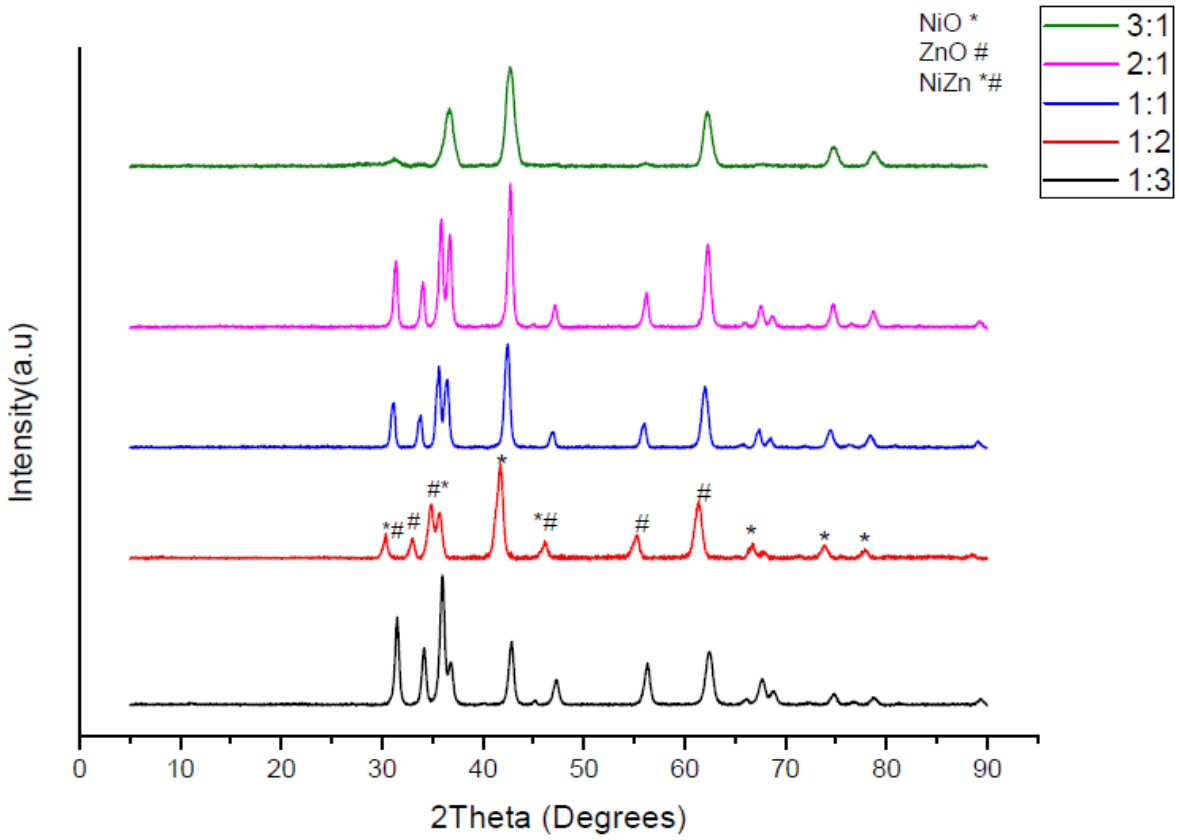


**Figure 19: XRD patterns of the sequentially impregnated Ni-Zn/CNO'S catalyst**

Furthermore, the XRD patterns in Figure 19 also revealed that the composites contain a mixture of different structures the cubic and hexagonal planes and according to (Biswas and Sharma, 2014) the change in phases of the components results in x-ray shielding of which causes the disappearance of some peaks. So, it can be said that the slight disappearance of other ZnO and NiO peaks in the samples at 2Θ was due to the composition changing phases from one form to another.

### 3.4.1.5 Identification of various functional groups in catalysts (FTIR)

The FTIR analysis was done to determine the existing vibration bands (Figures 20 and 21) from co-impregnated and sequential impregnation Ni-Zn/CNO catalysts with the spectra recorded in the 4500-450cm$^{-1}$ ranges. From the obtained results in Figure 20, the broad absorption bands were observed in the range of 3550-3200cm$^{-1}$ for all the samples. These bands are associated with the hydroxyl group (O-H) stretching vibrations, suggesting the existence of water found on the surface of the molecule (Habib *et al.*, 2020). The O-H bands appears sharp and broad, the sharpness or broadness of this bands are based on the extend of the molecule hydrogen bonding. The broader peaks are associated with a very great intermolecular hydrogen bonding, while the sharper peaks are associated with a lesser extend of hydrogen bonding. The bands in the absorbance range of 1622-1573cm$^{-1}$ can be assigned to the vibrations of C=C bonds.

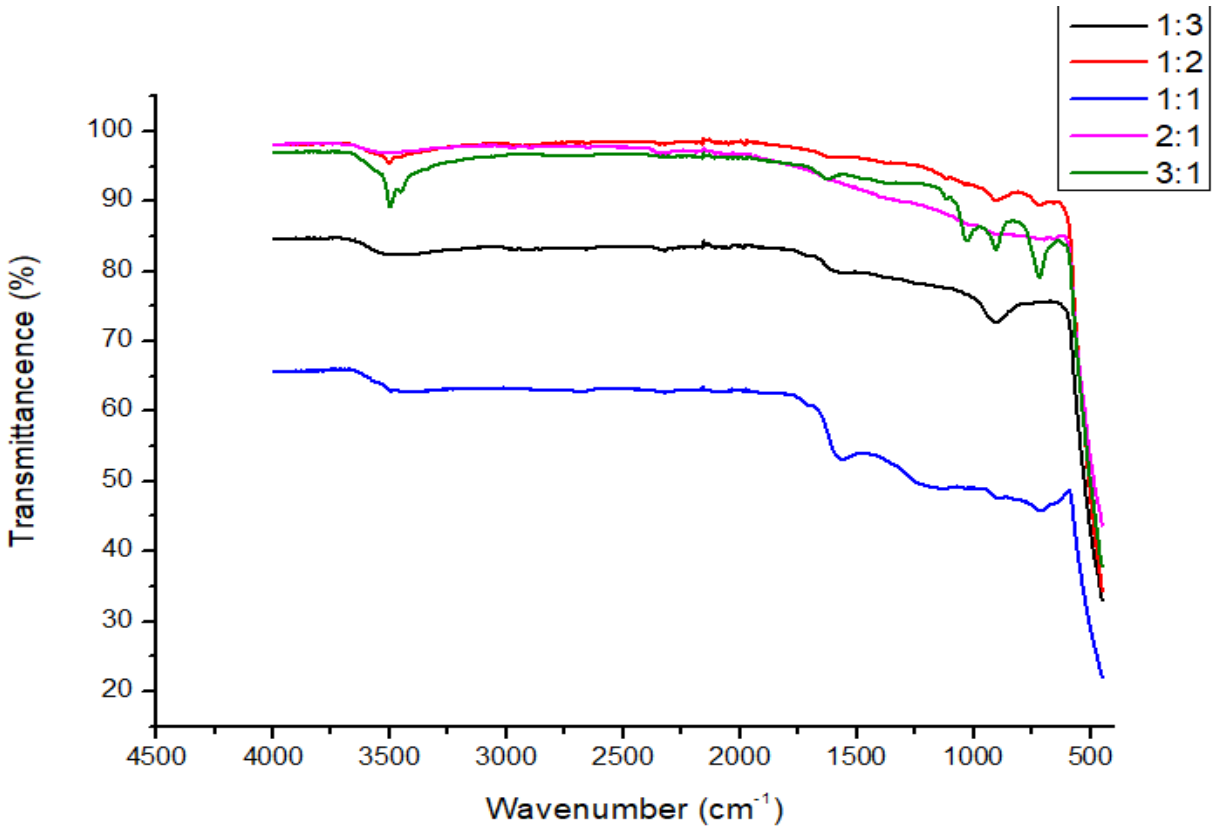


**Figure 20: FTIR spectra's of the co-impregnated Ni-Zn/CNO's catalyst**

More functional groups were further detected in Figure 21, the IR C=O peak at 1752cm$^{-1}$ for 1:1 is observed to be shifting to 1723 cm$^{-1}$ in 1:2, which is a lower frequency when Zn is increased, with further increase of Zn metal in 1:3, the C=O peak shifts to 1739cm$^{-1}$ which is

a higher frequency. These shifts could be due to particle size effect or morphology variation and this trend was also observed by Balakrishnan, and Schwank, (1992) on their FTIR study of bimetallic Pt-Sn/Al2O3 catalyst. In this Figure they are two effects taking place simultaneously, one effect is the second metal (Zn) effect shifting the C=O peak to lower frequencies, while the opposing effect of the particle size shifts the peak to a higher wavenumber. With the effect of particle size domination, it is observed that the is a shift in peak towards the higher wavenumber from 1709 $cm^{-1}$ in 2:1 to 17112 $cm^{-1}$ in 3:1(Peaks shifts are highlighted by the vertical lines)

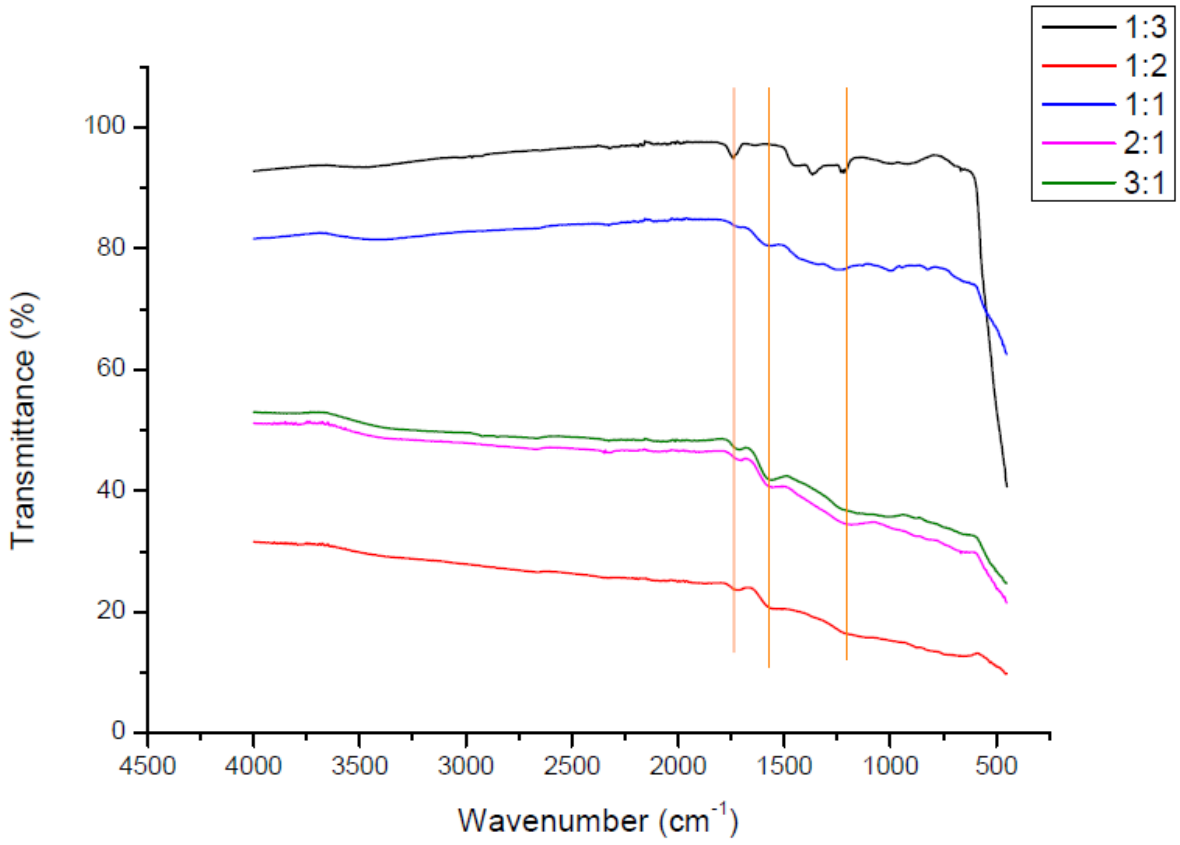


**Figure 21: FTIR spectra of the sequentially impregnated Ni-Zn/CNO's catalyst**

### 3.4.2 Effect of impregnation synthesis methods

Two of the synthesised catalysts from both the synthesis methods were selected based on their high surface areas, the ones with high surface areas were compared based on their synthesis methods. The two selected catalysts were 2:1(co-impregnation) and 1:3(sequential impregnation).

**Comparison of the 2:1 and 1:3 catalysts prepared via the co-impregnation and sequential impregnation methods respectively.**

The TGA graphs of the prepared Ni-Zn/CNO's catalysts are presented in Figure 22, from both Figures the graphs are observed to be losing their water content until 200 °C**,** this is plausible since the water was used as the dispersing medium and has a boiling point of 100 °C. The 2:1 catalyst between temperatures of 230 and 310 °C had the slightest weight loss, it can be said that the weight loss was due to the catalyst losing its functional groups such as like C=O. While the 1:3 ratio had the sharpest weight loss between 240 and 260 °C this weight loss corresponded to the metals transition from $NiCl_2(OH)$ and $Zn(OH)_2$ to NiO and ZnO, respectively. The weight loss of the catalyst above 400 °C can be attributed to the catalysts losing their carbon support (Molina-Ontoria *et al.*, 2013). The 2:1 ratio when observed from Figure 22 proves to be a better catalyst when compared to the 1:3 catalyst because it remained stable even at high temperatures.

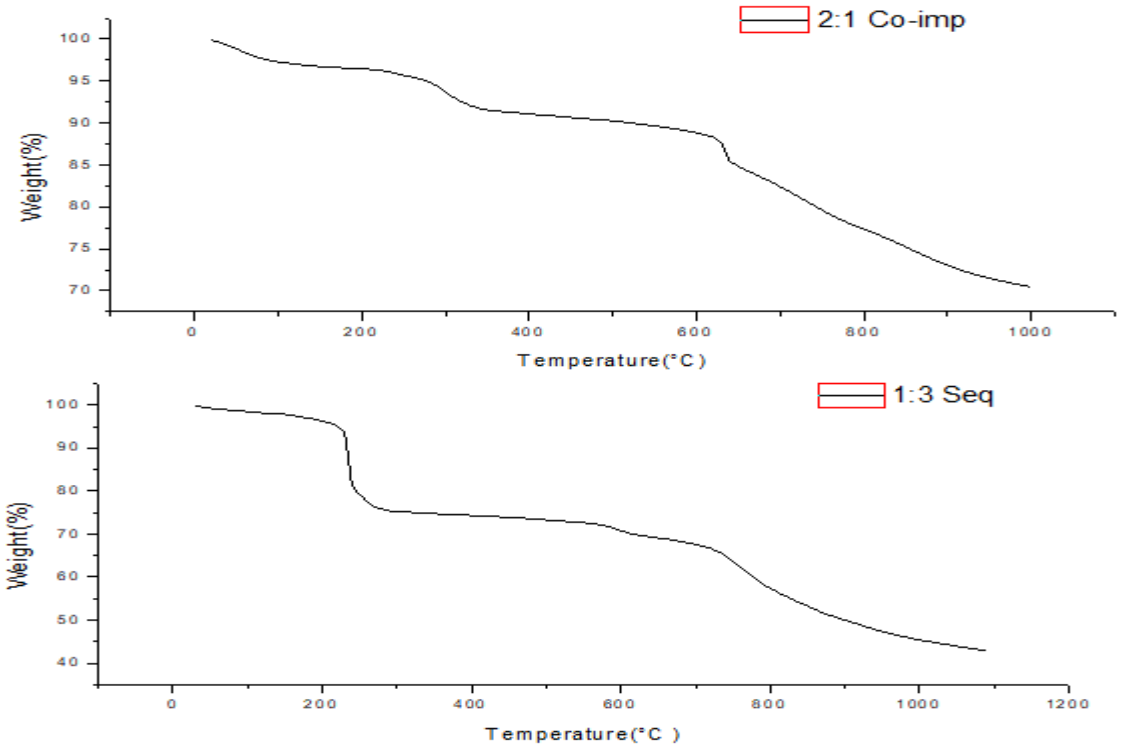


**Figure 22:Thermal degradation of the co-impregnation and sequentially impregnated catalysts with ratios of 2:1 and 1:3 respectively as a function of temperature**

From Table 6 of the catalyst, textural properties study, the catalyst 2:1 had the largest surface area and pore volume, while the 1:3 only exhibits a larger pore size when compared to the 2:1.

**Table 6: BET textural properties of the co-impregnated and sequentially impregnated catalysts with ratios of 2:1 and 1:3 calcined at 500 °C**

| Catalyst | Surface Area($m^2/g$) | Pore Volume($cm^3/g$) (BJH) | Pore size(nm) |
|---|---|---|---|
| 2:1 | 147.8331 | 0.668609 | 18.53823 |
| 1:3 | 13.8932 | 0.074049 | 25.4642 |

From Figure 23 of the $N_2$ adsorption-desorption isotherms of the catalysts, the 2:1 and 1:3 catalysts display type IV isotherms with H3 hysteric loops, which correspond to mesoporous materials (Thommes *et al.*, 2015).

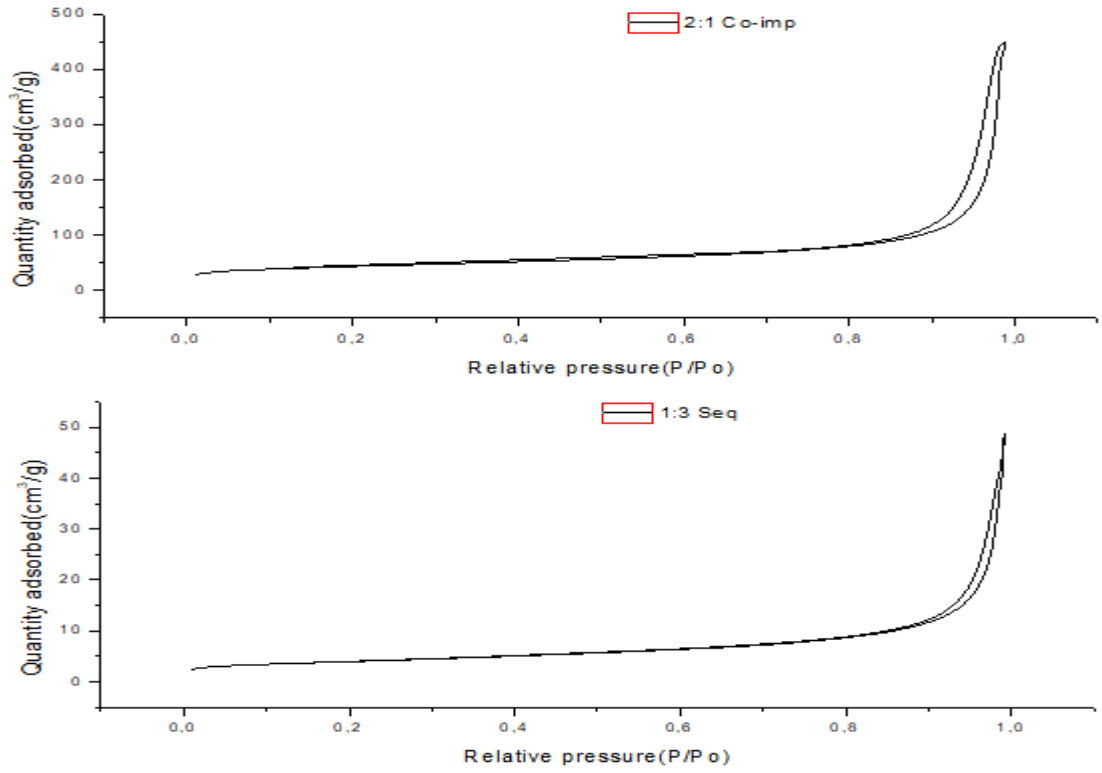


**Figure 23: Isotherms of N2 adsorption or desorption for co-impregnated and sequential impregnated catalysts with ratios of 2:1 and 1:3 respectively**

In this study, the morphologies of the catalysts were probed by the SEM technique with the obtained micrography presented in Figure 24. The 2:1 micrography's revealed coarse aggregated nanoparticles, while the 1:3 displayed flake cubic-like shaped nanoparticles. The change in the size of the cubic nanoparticles on the 1:3 catalyst displays good stability.

Subsequently the area of the observed morphologies in SEM were selected for quantitative elemental analysis. The TEM micrographs in Figure 25 further confirm the presents of the agglomerates observed in SEM, with the agglomerates in the 1:3 formed in a cuboidal form. Cheng *et al.*, (2017) also identified the presence of agglomerates from their TEM images when the Ni-Zn/$Al_2O_3$ catalyst with Ni: Zn percentages of 15%-5%, 10%-10% and 5%-15% respectively.

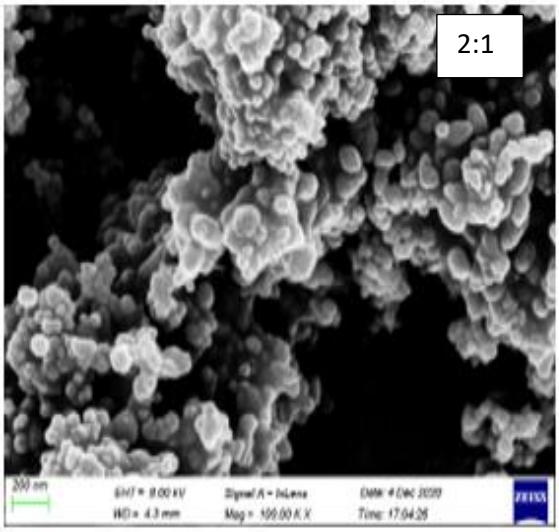


| Element | Weight(%) |
|---|---|
| C | 66.33 |
| O | 17.33 |
| Cl | 6.10 |
| Ni | 7.12 |
| Zn | 3.12 |

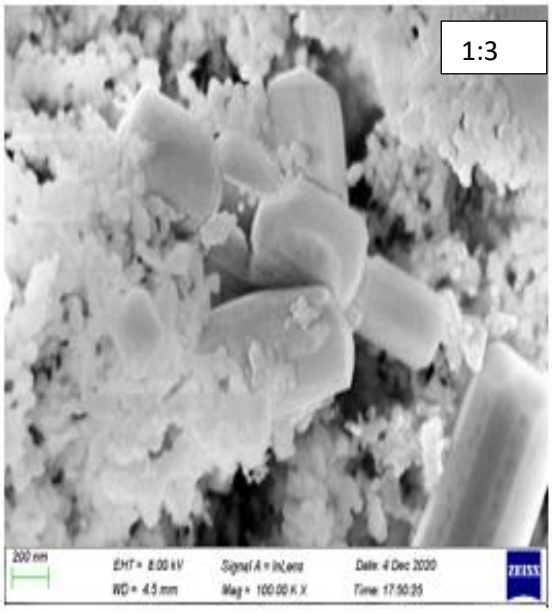


| Element | Weight(%) |
|---|---|
| C | 12.89 |
| O | 17.42 |
| Cl | 16.56 |
| Ni | 24.90 |
| Zn | 28.23 |

**Figure 24: SEM images of the co-impregnated and sequentially impregnated catalysts with ratios of 2:1 and 1:3 respectively**

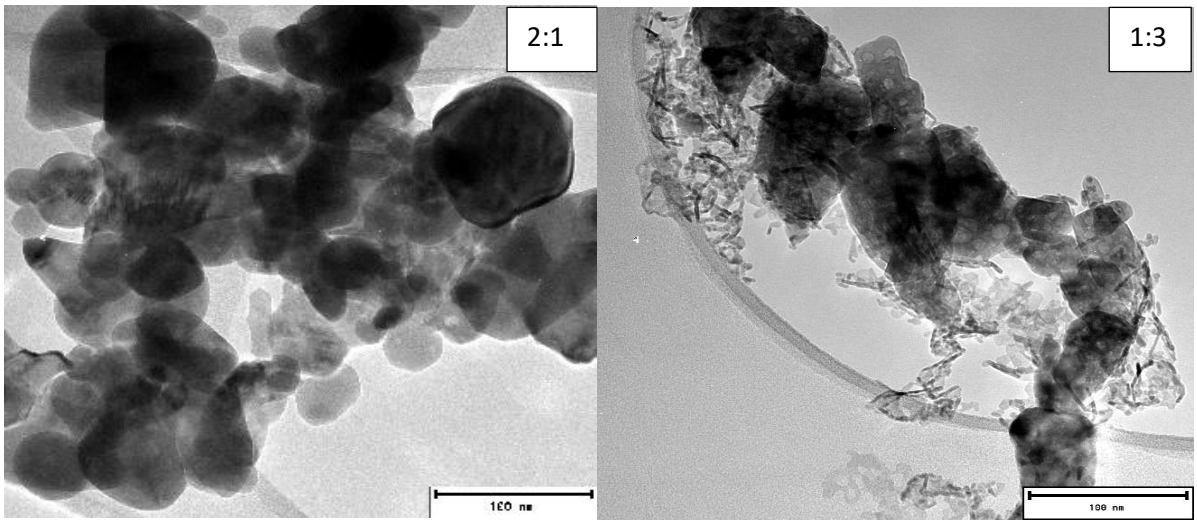


**Figure 25: TEM images of the co-impregnated and sequentially impregnated catalysts with ratios of 2:1 and 1:3 respectively**

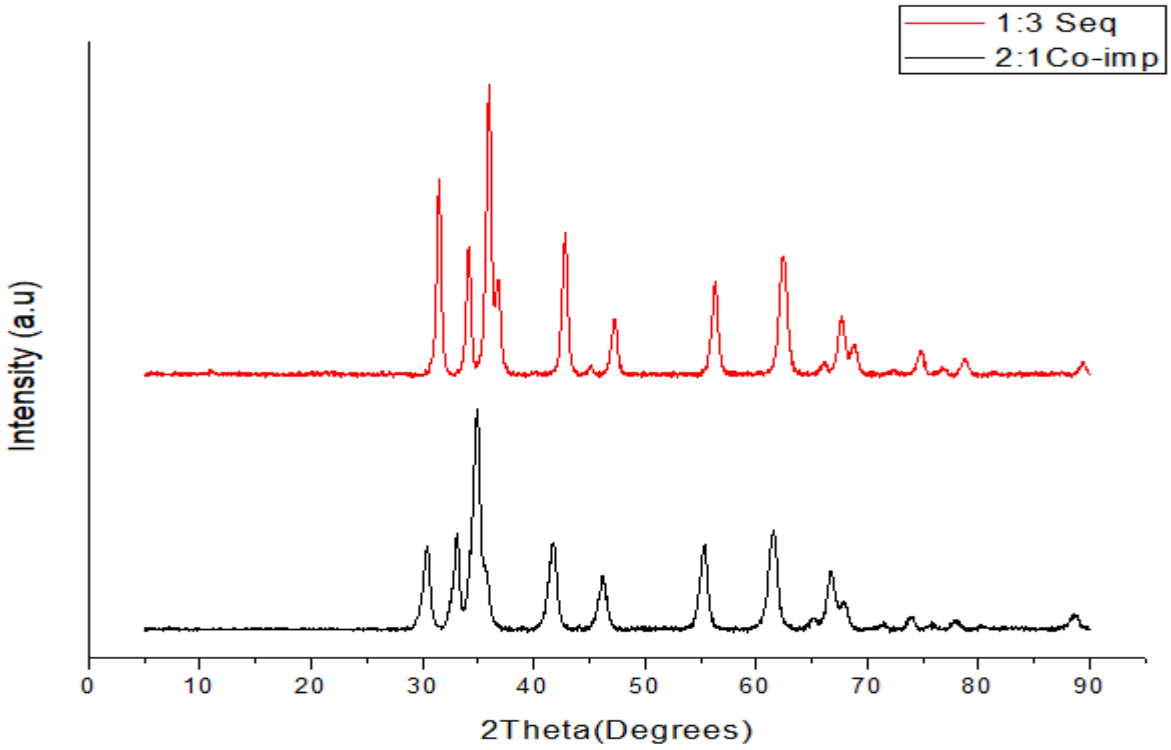


**Figure 26:The XRD patterns of the co-impregnated and sequentially impregnated catalysts with ratios of 2:1 and 1:3 ratio respectively**

Figure 26 represents the XRD patterns of Ni-Zn/CNO's, broader peaks are observed for the 2:1 catalyst, and according to Kim et al., (2018), the presence of broader peaks is due to smaller crystallites which are associated with the Scherrer equation. The crystal particle size trend is consistent with the particle size observed in SEM. The 1:3 catalyst shows a well-formed mesoporous material with both the cubic and the hexagonal planes, this planes are observed due to metals transitions observed in TGA. The peaks of the 1:3 ratio at $2\Theta^{\circ}$ appear sharper and narrow than the 2:1 catalyst, this may be due to the mentioned ascribed cubic and hexagonal phases.

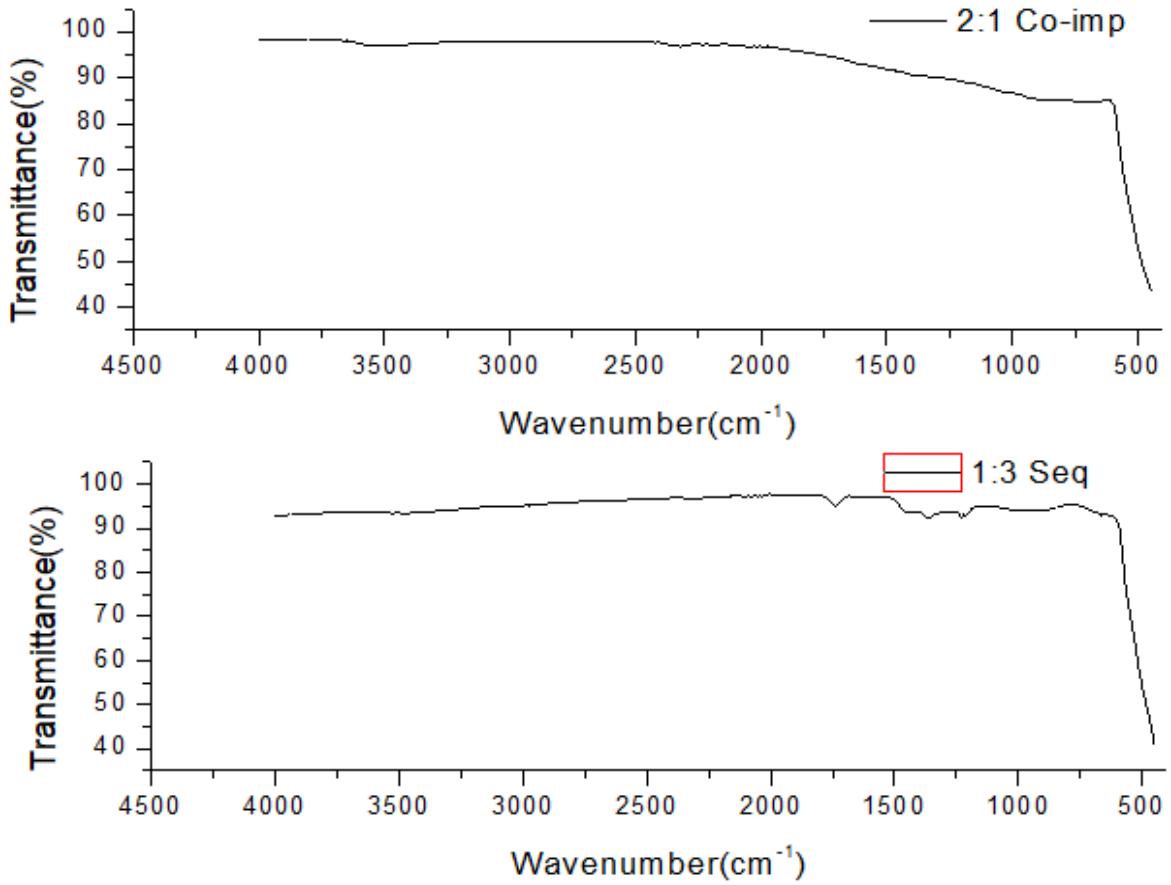


**Figure 27: The FTIR spectra of the co-impregnated and sequentially impregnated catalysts with ratios of 2:1 and 1:3 respectively**

The catalyst prepared by the co-impregnation method had a few bands that are slightly visible than the ones observed in the sequential impregnation method (Figure 27). The vibration bands detected by the FTIR that are observed in the range of 3650-3250$cm^{-1}$ in the co-impregnation

and sequential impregnation were attributed to water molecules. The band at 1622.2cm$^{-1}$ in the 2:1 catalyst ratio is related to the stretching of the C=C group. The bands observed in the range of 1740-1720cm$^{-1}$ and 1420-1330cm$^{-1}$ in the 1:3 are associated with the stretching of strong C=O and medium O-H groups respectively.

### 3.5 Conclusion and recommendations

The above results clearly show that the employed catalysts preparation procedures and metals ratios strongly affect the characteristics of the catalysts (Morphology, chemical composition etc). The co-impregnation catalysts showed more stability with their different metal loading ratios, as they slowly lost their weight and also posed larger surface areas with the 2:1 having the largest surface area compared to the sequentially impregnated catalysts. The larger surface areas of the co-impregnated catalysts mean that they have more active sides available. All the catalysts from both the co-impregnation and the sequential impregnation their shapes of the adsorption isotherms represented the Langmuir type IV. The presented micrographs from SEM and TEM, revealed that CNOs are capable of providing support for Ni-Zn nanoparticles depending on the bi-metallic catalyst preparation ratio used. The surface distribution of Ni-Zn nanoparticles is controlled by their size and this can provide variable catalyst activity (Wong *et al.*, 2018). Moreover, as seen in the TEM micrographs, the Ni-Zn nanoparticle shapes can also contribute to the efficiency of the catalyst as they provide different surface-active sites in respect of the carbonaceous support that can offer additional physicochemical properties (e.g. negatively charged species transport carrier). The Ni-Zn were found to be successfully embedded on the support and had different phases and the existing chemical bonds in the catalysts were observed differently as sharp and broad peaks. The use of capping agents is recommended to reduce the formation of agglomerates. Variation of calcination temperatures is recommended in order to observe more changes in the catalyst's properties.

### 3.6 Reference's

Amjad, S., (2019), Renewable Energy Storage in the Natural Gas Network : Enhancing $CO_2$ Conversion into Synthetic Natural Gas over Zeolite Catalysts by Tuning Ni Particle Size,Dissertation,Tecnico lisboa, 1-72.

Balakrishnan, K., and Schwank, J., (1992) ,FTIR Study of Bimetallic Pt-Sn / $AI_20_3$ Catalysts, *Journal of catalysis*, 138, 491-499.

Barton, R. R.. Carrier, M., Segura, C., Fierro, J. L. G., Escalona, E., and Peretti, S.W., (2017), Ni/HZSM-5 catalyst preparation by deposition-precipitation. Part 1. Effect of nickel loading and preparation conditions on catalyst properties, *Applied Catalysis A: General*, 540, 7–20.

Biswas, S., and Sharma, D. K., (2014), Journal of Analytical and Applied Pyrolysis Effect of different catalysts on the cracking of Jatropha oil, *Journal of Analytical and Applied Pyrolysis*, 110, 346–352.

Cheng, S., Wei, L., Julson, J., Muthukumarappan, K., Kharel, P. R., and Boakye, E., (2017), *Fuel Processing Technology*, 162, 78–86

Charisiou, N. D., Douvartzides, S. L, Siakavelas, G. I., Tzounis, L., Sebastian, V., Stolojan, V., Hinder, S. J., Baker, M. A., Polychronopoulou, K and Goula M.A, (2019), The Relationship between Reaction Temperature and Carbon Deposition on Nickel Catalysts Based on $Al_2O_3$, $ZrO_2$ or $SiO_2$ Supports during the Biogas Dry Reforming Reaction, *Catalysts*, 9(676),1–22.

Dewajani, H., Purwono, S., and Budiman, A., (2017), Effect of modification ZSM-5 catalyst in upgrading quality of organic liquid product derived from catalytic cracking of Indonesian nyamplung oil (Calophyllum inophyllum), *Advances of Science and Technology for Society*, 1–7.

Habib, N., Guellati, O., Harat, A., Nait-Merzoug, A., Haskouri, J. E., Momodu, D., Manyala, N., Begin, D., and Guerioune, M., (2020), Ni – Zn hydroxide - based bi - phase multiscale porous nanohybrids : physico - chemical properties, *Applied Nanoscience*, 10 (8), 2467–2477.

Kumar, A., and Jena, H. M., (2016), Results in Physics Preparation and characterization of high surface area activated carbon from Fox nut ( Euryale ferox ) shell by chemical activation with H3PO 4, *Results in Physics*, 6,651–658.

Mohiuddin, E., Mdleleni, M. M., and Key, D., (2018), Catalytic cracking of naphtha: The effect of Fe and Cr impregnated ZSM-5 on olefin selectivity, *Applied Petrochemical Research*, 8(2),

119–129.

Mongwe, T. H., Matsosoa, B.J, Mutuma, B. K., Covillea, N. J., and Maubane M. S., (2018), Synthesis of chain-like carbon nano-onions by a flame assisted pyrolysis technique using different collecting plates, *Diamond and Related Materials*, 90,135–143.

Nugrahaningtyas, K. D., Nuryono, N., and Widjonarko, D. M, (2010), The application of varied impregnation methods on the characters of non-sulfided NiMo/USY catalyst,1-4

Molina-Ontoria, A., Chaur M. N., Plonska-Brzezinska M. E., Echegoyen, L., (2013), Preparation and characterization of soluble carbon nano-onions by covalent functionalization, employing a Na–K alloy, *Chem. Commun*, 49, 2406—2408

Mykhailiv, O., Zubyk, H., and Plonska-Brzeniska, M. E., (2017), Carbon nano onions: Unique carbon nanostructures with fascinating properties and their potential applications, *Inorganica Chimica Acta*, 468,49-66.

Pan, Z., Wang, R., and Chen, J., (2019), Catalytic deoxygenation of methyl laurate as a model compound to hydrocarbons on hybrid catalysts composed of Ni–Zn alloy and HY zeolite, *J Chem Technol Biotechnol*, 94: 1777–1787.

Takahashi, H., Sunagawa, Y., Myagmarjav, S., Yamamoto, K., Sato, N., and Muramatsu, A., (2003), Reductive Deposition of Ni-Zn Nanoparticles Selectively on TiO2 Fine Particles in the Liquid Phase, *Materials Transactions*, 44, (11), 2414 to 2416.

Thommes, M., Kaneko, K., Neimark, A. V, Olivier, J. P., Rodriguez-Reinoso, F., Rouquerol, J., and Sing, K. S. W., (2015), Physisorption of gases , with special reference to the evaluation of surface area and pore size distribution ( IUPAC Technical Report ), *Pure Appl. Chem.*1-23.

Velasquez, M., Batiot-Dupeyrat, C., Gallego, J., Fernández, J. J., and Santamaria, A., (2016), Synthesis of carbon nano-chains from glycerol-ethanol decomposition over Ni-Fe alloy catalyst, *Diamond & Related Materials*, 70, 105–113

Wang, X., Hu, J., Liu, W., Wang, G., An, J., and Lian, J., (2015), Ni-Zn binary system hydroxide, oxide and sulfide materials: system and high supercapacitor performance, *J. Mater. Chem. A*,3,23333–23344.

Wong, F. H., Tiong, T. J., Leong, L. K., Lin, K-S., and Yap, Y. H., (2018), Effects of ZnO on Characteristics and Selectivity of Coprecipitated Ni/ ZnO/Al2O3 Catalysts for Partial Hydrogenation of Sunflower Oil, *Ind. Eng. Chem. Res*, 57, 3163−3174

Wu, G., Nelson, M., Ma, S., Meng, H., Cui, G., and Shen, P. K., (2011), Synthesis of nitrogen-doped onion-like carbon and its use in carbon-based CoFe binary non-precious-metal catalysts for oxygen-reduction, Ca r b o n, 49 ,3972 –3 982

Zaher, F. A., El Sayed, H. A., Heakal, B. H., and Hamed, S. F., (2015), Potential of Castor Oil as a Feedstock for the Production of Bio-fuel via Catalytic Hydro- Cracking, *Curr. Sci. Int.*, 4(3),443–449.

# Chapter 4: Biofuel production using the synthesized catalysts.

## 4.1 Introduction

The high-quality production of biofuels is strongly dependent on the used catalysts and the reaction parameters. This section contains hydrocracking trial runs results of hydrocracked castor oil in which the performance of the two prepared Ni-Zn/CNO's catalysts with ratios of 2:1(Co-impregnation) and 3:1(Sequential impregnation) were investigated. The main focus was to observe the effect that hydrocracking parameters (Temperature, Time and, catalyst loading) have on the obtained biofuel yield as well as to observe their selectivity. The experimental results were examined in terms of selectivity yield. Furthermore, the catalyst with a higher production yield will be used for the optimization of the bio-jet.

## 4.2 Method

Castor oil as a primary feedstock material was used in hydrocracking with a fixed volume of 100ml. The oil was poured into a 3neck round bottom flask(reactor). Catalysts with ratios of 2:1 and 1:3 prepared by co-impregnation and sequential impregnation methods respectively were utilized at a time throughout the experiments. Catalysts with varied masses of 100,115,130,145 and 160 mg were added one at a time into the oil and the liquid-solid mixture was agitated using an ultra-sonicator for 25 minutes in order for a uniform mixture to be achieved. The reactor was then placed on the heating mantle with the stirrer bar placed in it and the condenser and the inlet nozzles were then connected to the reactor. The experimental setup can be observed as shown in Figure 28. The oil was purged with nitrogen gas for 20 minutes before the reaction in order to remove the remaining air. After purging the reactions were carried out at temperatures of 210, 230, 250, 270, and 290 °C with hydrogen gas, and the reaction times were varied between 0.5-2.5 hours, with a 0.5 hour interval. After the reactions, the reactor was cooled down and the liquid fractional yields of the products were collected and filtered so that can be analysed.

Fractionation

A gas chromatography-mass spectrometer (GCMS) was used to analyse the major liquid biofuel components. The GCMS produced results in the form of total ion chromatography. The product composition was grouped on the basis of their carbon number intervals. They were grouped into four categories with different ranges which are the bio-gasoline ($C_5$-$C_{11}$),bio-

jet($C_{12}$-$C_{15}$), Biodiesel($C_{16}$-$C_{18}$), and long hydrocarbons($C_{19}$+) (Dewajani, Purwono and Budiman, 2017). The peak area percentages were used to calculate the respective fractional yields of each fractional group. The GC-MS results for raw castor oil and the cracked oil are attached in Appendix A. All the yields are reported as percentages.

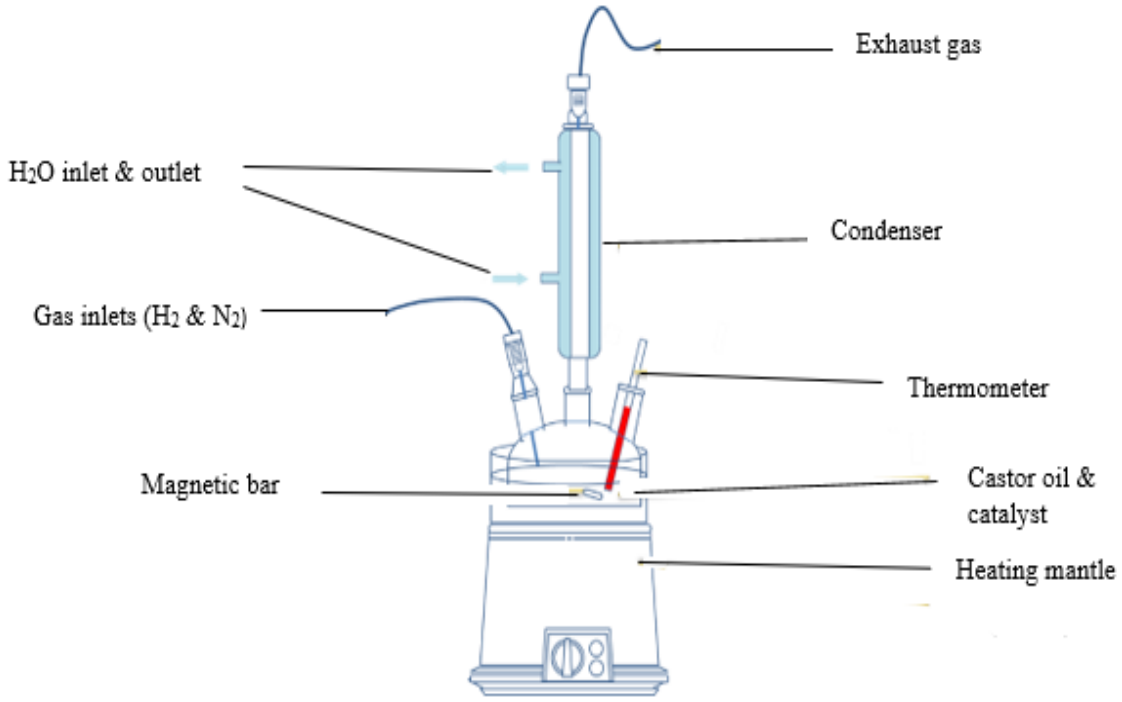


**Figure 28: Hydrocracking set-up for biofuels production**

### 4.3. Process variables for the co-impregnation and sequential impregnation

#### 4.3.1 co-impregnation catalyst

**Effect of temperature**

An increase in temperature increases the activity of the catalyst which result in a faster decay of the catalyst life (Bezergianni and Kalogianni, 2009). The effect of temperature on hydrocracking of castor oil was investigated in temperature ranges of 210 °C to 290 °C with a fixed time.

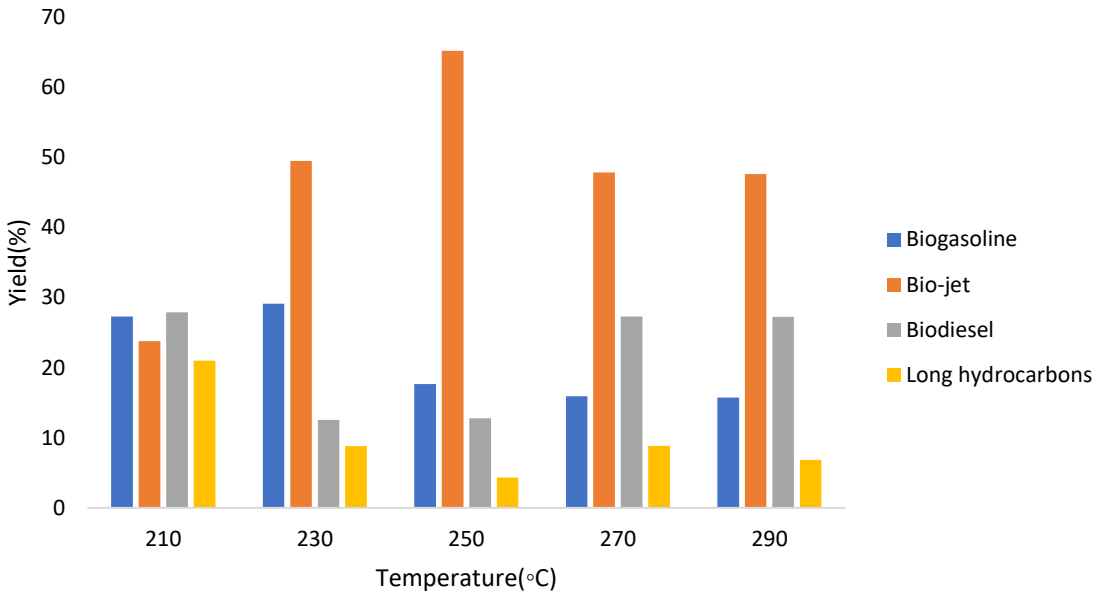


**Figure 29: Temperature effect on the selectivity of bio-jet yield**

From Figure 29 is observed that at a lower temperature of 210 °C the bio-jet yield is at its lowest with a 23.77% yield, as the temperature is increased the bio-jet yield also increased until 250 °C, then with a further temperature increase to 290 °C the bio-jet yield decreased to 44.56%. At 250 °C the bio-jet is at its maximum selectivity with a 65.23% yield and a 100% conversion. Typically temperature increase results in faster cracking on acid sites, yet, very high temperatures limit the hydrocracking of aromatic compounds (Saab *et al.*, 2020). As observed in Figure 29, it can be said that the temperature significantly influenced the desired yields of hydrocarbon biofuels to a certain point.

**Effect of time**

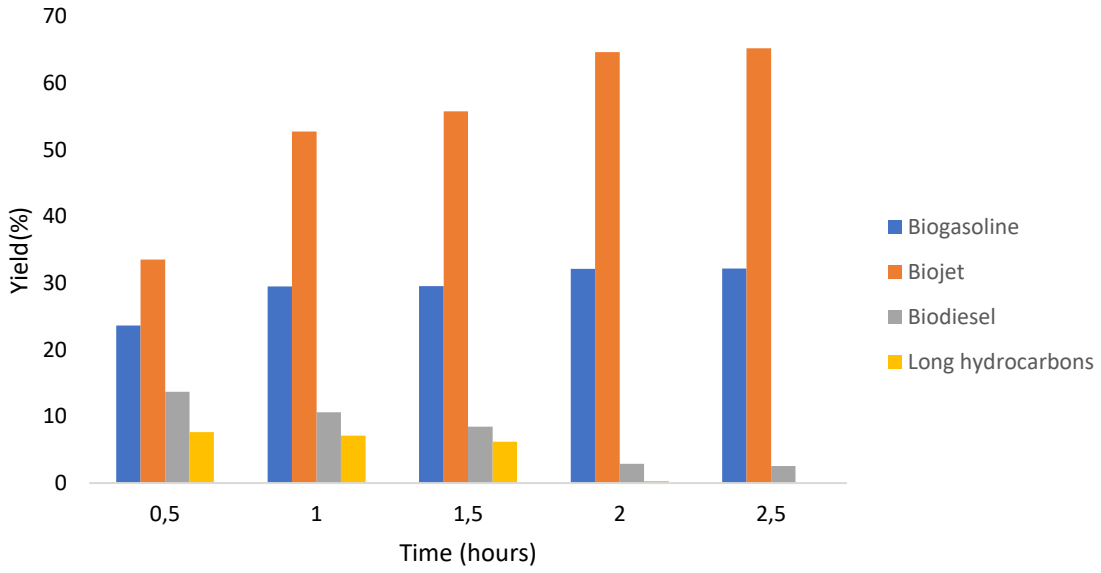


**Figure 30: Time effect on the bio-jet selectivity yield**

Five reaction runs were carried out with 0.1g of catalyst at the temperature of 250 °C in order to determine the effect time has on the bio-jet product yield. An increase in contact time from 0.5 hours to 2.5 hours is observed to increase the bio-jet and bio-gasoline production yield throughout, both the bio-gasoline and bio-jet increased from 23.66 and 33.56% to 32.19 and 65.23% respectively. Time was more selective towards the bio-jet with its highest yield of 65.23% at 2.5 hours, while the biodiesel and the long hydrocarbons are observed to be decreasing with increasing time.

**Effect of catalyst loading**

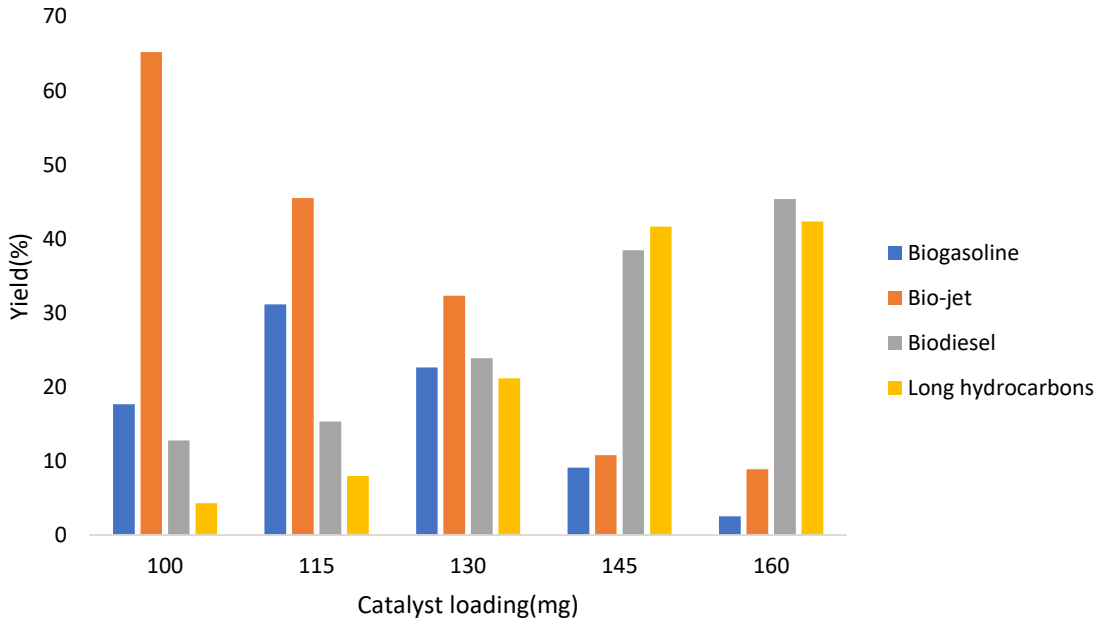


**Figure 31: Catalyst ratio effect on the bio-jet yield**

The effect that catalyst loading has on bio-jet production was studied on castor oil hydrocracking. Five experiments with varied catalyst loadings were carried at a constant hydrogen pressure of 100 kPa and at a reaction temperature of 250 °C. From Figure 31 it can be observed that the bio-jet selectivity is at its maximum at 100 mg and its selectivity decreases as the catalyst loadings are increasing. The catalyst loading increase is observed to increase the biodiesel as well as the long hydrocarbons production. Since the hydrogen pressure was retained constant with all the experiments, it might be said that the hydrogen might have not been sufficient enough for the catalyst weight, then resulting in less cracking of the heavy hydrocarbons. Veriansyah *et al.*, (2012) also encountered a decrease in selectivity when conducting hydroprocessing of soybean oil into renewable diesel. The catalyst oil ratio which increased from 0.044 to 0.088 using the Ni-Mo/γ-alumina catalyst, resulted in reduced selectivity from 92.9 to 91.9% towards diesel as the desired product.

### 4.3.2 Sequential impregnation

#### Effect of temperature

Temperature is the dominating parameter for the catalyst effectiveness (Bezergianni, Kalogianni and Vasalos, 2009; Yotsomnuk and Skolpap, 2017) in cracking the C=O bound and has an effect on the product yield. Effect of Temperature on castor oil was studied by conducted hydrocracking experimental trial runs at temperatures of 210 to 290 °C for 2.5 hours. The obtained product yields at different temperatures are represented in Figure 32.

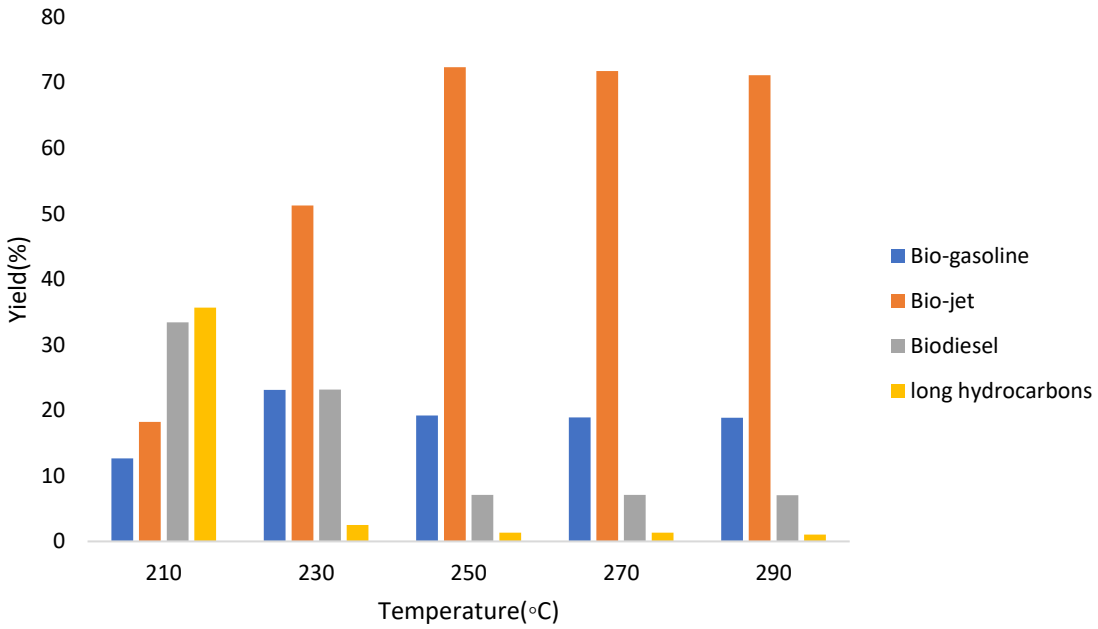


**Figure 32: Effect of temperature on the bio-jet selectivity yield**

As the temperature was increased the was an increase in bio-gasoline and bio-jet, and a further temperature increase resulted in a decrease in both. At the temperature of 230 °C bio-gasoline was at its maximum, while at 250 °C the bio-jet was found to be at its maximum yield selectivity with the main components formed being the tridecane's, pentadecanes, and heptadecanes. At 210 °C, the temperature was not effective enough to break down the long hydrocarbons (Carboxylic acids) and the bio-diesel similar results were also observed by Al-Muttaqii *et al.*, (2019) at 350 °C which was the lowest temperature.

The temperature increase from 230 to 290 °C assisted in improving the hydrocracking activity and helped cleave the long hydrocarbons molecules of the castor oil and also with some diesel molecules being further cracked to produced short hydrocarbons (Bezergianni *et al.*, 2010; Al-Muttaqii *et al.*, 2019). Therefore, since the bio-jet is the desired/targeted product then it can be said that the high yield of bio-jet was due to the cleaved long hydrocarbons transforming to short hydrocarbons. Higher temperatures should be considered for higher bio-jet yields as the experiment was more favorable at higher temperatures and resulted in 100% conversions being obtained than lower temperatures. The optimal temperature for bio-jet fuel production is 250 °C.

**Effect of time**

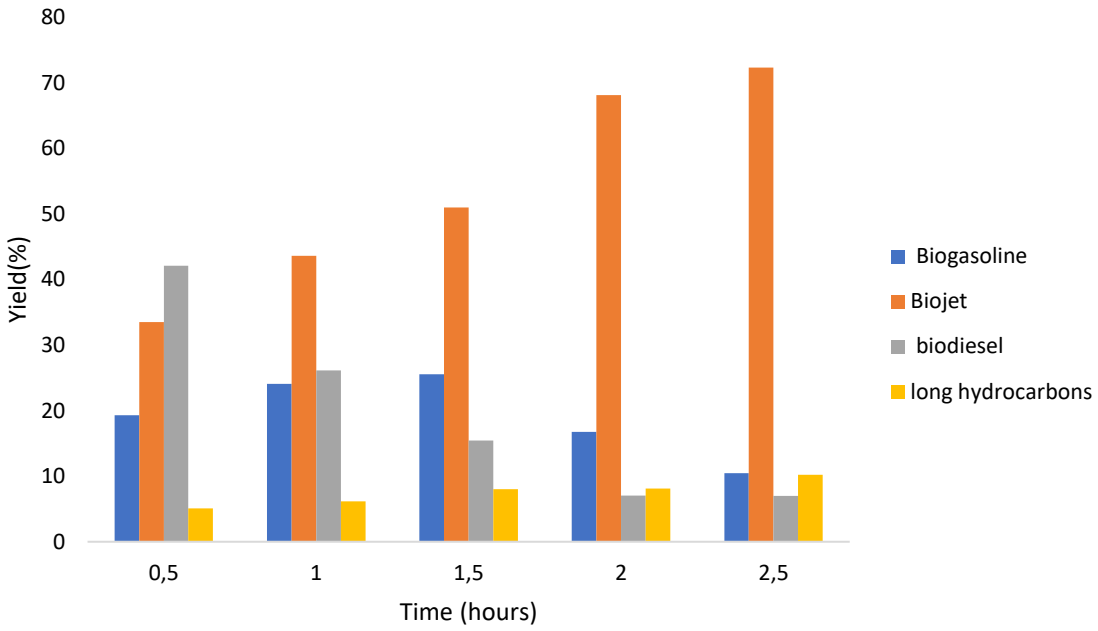


**Figure 33: Effect of reaction time on the bio-jet production yield**

From Figure 33 it can be observed that the increase in contact time from 0.5 hours to 2.5 hours increased bio-jet fraction and the long hydrocarbons, while both bio-gasoline and biodiesel have decreased. The 2.5 hours contact time was more selective to bio-jet as it increased from 33.49% at 0.5 hours to 72.33%. The long hydrocarbons fractions are observed to be increasing from 0.5 until 2.5 hours, this increase is due to the polymerization process. The polymerization process intensifies when the experimental reactants are exposed to a longer reaction time. This process was also observed by (Mampuru, Nkazi and Mukaya, 2020) on hydrocracking of

cooking oil using Ni-Mo/alumina catalyst starting from 0.5 hours. This is evident from Figure 33 with long hydrocarbons increasing from 5.07 to 10.22%

**Effect of catalyst loading**

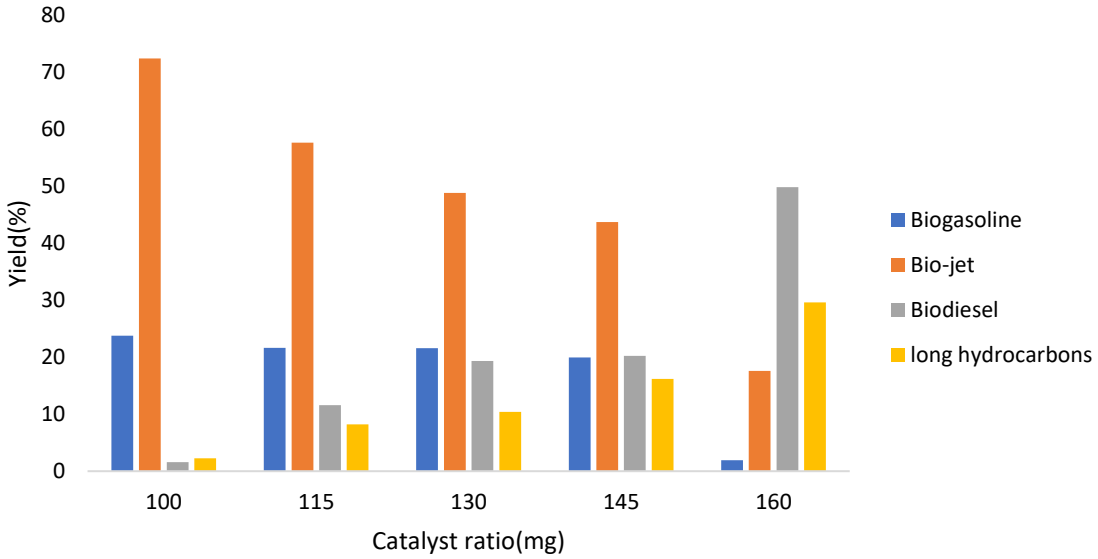


**Figure 34: Effect of catalyst ratio effect on the bio-jet yield**

Five reaction runs were conducted using the 1:3 catalyst for 2.5 hours each to study the effect that catalyst ratio has on the bio-jet yield as the desired product. From Figure 34 the reactions were conducted with catalyst varied from 100-160 mg in 100ml of oil each. It was discovered that bio-jet fraction is at its maximum with 72.33% at a lower catalyst ratio of 100 mg, while with a further catalyst ratio increase to 130 mg and 160 mg the was a decrease in the bio-jet production selectivity from 48.75 and 17.6%. On the other hand, the biodiesel and the long hydrocarbons were highly elevated as the catalysts loading ratios were increased with an increase from 1.58 and 2.26% at 100 mg to 49.8 and 29.56% at 160 mg respectively. It can be said that the catalyst loading increase is no longer selective to bio-jet but the selectivity has shifted to biodiesel and long hydrocarbons with higher catalyst loadings. Liu *et al.*, (2011) reported that the level of catalyst cracking also depends on the catalyst amount.

### 4.4 Catalyst activities and Brunauer−Emmett−Teller (BET) results

The assessment of catalyst activities is sometimes predicted based on the catalyst characterization such as BET (Dewajan et al., 2016). According to Zhao *et al., (*2019) and Liu *et al.,* (2016) catalysts at nanosize scale and with high surface area are expected to give higher catalytic activity.

Two preparation methods were used for the synthesis of the catalysts, the co-impregnation and sequential impregnation.

**Table 7: Table of catalysts ratios with the biggest and smallest surface areas from both the catalysts preparation methods.**

| | Co-impregnation | | Sequential impregnation | |
|---|---|---|---|---|
| ratios | 2:1 | 1:2 | 1:3 | 2:1 |
| Surface Areas ($m^2/g$) | 147.8331 | 36.5492 | 13.89 | 9.1963 |

Based on Table 7 the ratio of 2:1 co-impregnation was supposed to be the catalyst with high activity. However, the hydrocracking results showed the non- expected based on the BET. The 1:3 sequential impregnation catalyst showed high selectivity for bio-jet fuel. Based on this investigation, the following should be considered for the prediction and catalyst activity assessment.

a) Catalyst preparation method.

-The low production yield of the 2:1 ratio might have resulted due to the Ni presence in co-impregnation of which might have restrained the Zn nanoparticle's growth.

-The catalytic activity of the Zn-promoted Ni/CNO in sequential impregnation can be associated with the pre-impregnated Zn role in promoting the Ni activity by enforcing the particle's growth and withdrawing an electron from Ni.(Kim, Kim and Kim, 2018; Adira Wan Khalit *et al.*, 2020)

b) The metal used: the presence of Zn in the sequential impregnation shows high selectivity for bio-jet.

c) Process temperature.

For example, from both temperatures study in Figures 29 and 32, It is observed that when the temperature was increased from 210 to 250 ˚C the sequential impregnated catalyst had the best results throughout than the co-impregnated catalyst. Though the larger surface area forms active sites which are associated with high catalytic activity, the lower production yield of the co-impregnated catalyst can be explained by their relatively smaller pore sizes of 18.53823 nm compared to the sequential impregnated pore size of 25.4642 nm. This showed the hydrocracking activity limitation impact.

### 4.5 Conclusion and recommendations

The results obtained from the hydrocracking study indicate that temperature, time, and catalyst loadings all play an important role in the triglycerides transformation into light bio-fuels. The presence of a larger amount of long hydrocarbons at temperatures of 210 °C is an indication that the temperature is not strong enough to break the strong bonds or convert the long hydrocarbons into short hydrocarbons. Therefore, higher temperatures between 250 °C and 290 °C are recommended when using the 1:3 catalyst, and a higher temperature between 230 °C and 290 °C can be used when the 1:2 catalyst is used to produce higher yields of short hydrocarbons (Bio-jet). But in order for the maximum selectivity to be obtained temperature of 250 °C is highly recommended. An increase in time was observed to increase the bio-jet selectivity, so a high reaction time is recommended. For all the catalysts it was observed that an increase in the metal loading led to a decrease in the catalyst activity. This with first brief observation intuitive, one might expect the catalyst loading increase to result in increasing hydrocracking catalyst activity, since the first step in the hydrocracking reaction, takes place on the metal sites. More availability of metal sites for reaction, therefore, is expected to result in elevated catalyst activity. The observed decrease in the activity thus can be suggested to be due to diffusion limitations resulting from the formed metal clusters or agglomerates in the CNO's pores that were mentioned to have formed in chapter 3. So, it is recommended that the catalyst loading ratios be used in amounts close to 100 mg since above 100 mg selectivity is observed to be sifting. It can also be suggested that the high loadings of the catalysts be done if the desired product is biodiesel since it was highly produced at high catalyst loadings. Generally, it can be concluded that both the catalysts are found to have produced their highest yields based on their active sides and activity since they both had the highest surface areas when compared to the other catalysts that were prepared with the same method. Since it is believed that the nanosize scale catalysts with higher surface area results in higher catalytic activity. When the catalytic activity of the catalysts was analysed, it was discovered that the sequential impregnated catalyst had the highest production yield. In summary the Catalyst preparation method, metal used, and process temperature should be considered for the prediction of the catalyst activity since they had an influence in this investigation. Based on the obtained results from the hydrocracking runs the 1:3 catalyst was further used for the optimization of bio-jet.

## 4.6 References

Adira Wan Khalit, W. N., Marliza, T. S., Asikin-Mijan, N., Gamal, M. S., Saiman, M. I., Ibrahim, M. L., and Taufiq-Yap, Y. H., (2020), Development of bimetallic nickel-based catalysts supported on activated carbon for green fuel production, *RCS Advances*,10, 37218–37232.

Al-Muttaqii, M., Kurniawansyah F, Prajitno D.H, and Roesyadi A, (2019),Hydrocracking of Coconut Oil over Ni-Fe / HZSM-5 Catalyst to Produce Hydrocarbon Biofuel, *Indones. J. Chem*., 19 (2), 319 - 327.

Bezergianni, S., Dimitriadis, A., Kalogianni, A., Pilavachi, P., (2010), Hydrotreating of waste cooking oil for biodiesel production. Part I: Effect of temperature on product yields and heteroatom removal, *Bioresource Technology*, 101(17), 6651–6656.

Bezergianni, S., and Kalogianni, A., (2009), Bioresource Technology Hydrocracking of used cooking oil for biofuels production, *Bioresource Technology*, 100(17), 3927–3932.

Bezergianni, S., Kalogianni, A., and Vasalos, I. A., (2009), Hydrocracking of vacuum gas oil-vegetable oil mixtures for biofuels production, *Bioresource Technology*, 100(12), 3036–3042.

Dewajani, H., Purwono, S. and Budiman, A. (2017), Effect of modification ZSM-5 catalyst in upgrading quality of organic liquid product derived from catalytic cracking of Indonesian nyamplung oil (Calophyllum inophyllum), *AIP Conference Proceedings*, (2016),. 1–7.

Kim, Y., Kim, J., and Kim, D. H., (2018), Investigation on the enhanced catalytic activity of a Ni-promoted Pd / C catalyst for formic acid dehydrogenation : e ff ects of preparation methods and Ni/Pd ratios, *The Royal Society of Chemistry*, 8, 2441–2448.

Liu, J., He, J.,Wang, L.,Li, R., Chen, P., Rao X., Deng L., Rong L., Lei J., (2016), NiO-PTA supported on ZIF-8 as a highly effective catalyst for hydrocracking of Jatropha oil, *Scientific reports*, 1-11

Liu, Y., Sotelo-Boyas, R., Murata, K., Minowa, T., and Sakanishi, K., (2011), Hydrotreatment of Vegetable Oils to Produce Bio-Hydrogenated Diesel and Liquefied Petroleum Gas Fuel over Catalysts Containing Sulfided Ni-Mo and Solid Acids, *Energy Fuels*, 25,4675–4685.

Mampuru, M. B., Nkazi, D. B., and Mukaya, H. E., (2020), Hydrocracking of waste cooking oil into biogasoline in the presence of a bi-functional Ni-Mo/alumina catalyst, *Energy Sources, Part A: Recovery, Utilization, and Environmental Effects*, 42(20), pp. 2564–2575.

Saab, R., Polychronopoulou, K., Zheng, L., Kumar, S., and Schiffer, A., (2020), Journal of Industrial and Engineering Chemistry Synthesis and performance evaluation of hydrocracking catalysts : A review, *Journal of Industrial and Engineering Chemistry*, 89, 83–103.

Veriansyah, B., Han, J. Y., Kim, S. K., Hong, S-A, Kim, Y. J., Lim, J. S., Shu, Y-W., Oh, S-G., and Kim, j., (2012), Production of renewable diesel by hydroprocessing of soybean oil : Effect of catalysts, *Fuel*, 94, pp. 578–585.

Yotsomnuk, P., and Skolpap, W., (2017), Biofuel Production from Waste Virgin Coconut Oil by Hydrocracking Over HZSM-5 Zeolite, *International Journal of Advances in Science Engineering and Technology*, 5(1), 54–57.

Zhao, B. B., Ke, X. K., Bao, J. H., Wang, C-L., Dong, L., Chen, Y-W., and Chen H-L., (2009), Synthesis of Flower-Like NiO and Effects of Morphology on Its Catalytic Properties, *J. Phys. Chem. C*, *113*, 14440–14447

# CHAPTER 5: Optimization of Bio-jet production process variables

## 5.1 Introduction

In this section, the experimental design was done using the design expert software version 11(stat-Ease) in order to investigate the effect that process parameters time, temperature, and catalyst loading have on hydrocracking of castor oil towards the bio-jet fuel production. The 1:3 catalyst was utilised since it was subsequently screened to be the best catalyst. Both the RSM (Response Surface Methodology) and the central composite design (CCD) were used for the development of the conducted experimental runs. RSM is used for modelling and forecasts the response of interest affected by different parameters with the response optimizing being the aim (Liu et al, 2018).

## 5.2 Experimental design

The experimental design was used in order to investigate the effect of parameters in hydrocracking of castor oil towards the production of bio-jet. The RSM has shown to be the strongest tool in terms of optimizing the experimental conditions in order to obtain both minimal and maximum response values, (Abnisa *et al.*, 2010). The bio-jet percentage yield was considered as the desired response, so the parameters were optimized to achieve a maximum yield of bio-jet. The three chosen parameters which were time, temperature, and catalyst loading were investigated and referred to as A, B, and C with each assigned with a coded factor as displayed in Table 8. The +1 and -1 were assigned as the higher and lower levels of the factors.

**Table 8: Table of parameters and their range values for central composition design for hydrocracking**

| Factors | code | Unit | Minimum values | Maximum value | Low coded | High coded |
|---|---|---|---|---|---|---|
| Time | A | Hours | 1 | 3 | -1 | +1 |
| Temperature | B | ˚C | 210 | 290 | -1 | +1 |
| Catalyst loading | C | mg | 100 | 160 | -1 | +1 |

The parameters experimental factors were then optimized using the CCD (Central composite design) under RSM. The CCD proposed 14 conducted experimental runs of which the RSM proposed the design points that fitted the experimental factors range mentioned in Table 8. The design points that RSM proposed can be observed in Table 9 with the obtained bio-jet yield after hydrocracking.

**Table 9: Table of the RSM central composition design reaction parameters with the obtained yields and predicted yields**

| | Parameters | | | Product yield | |
|---|---|---|---|---|---|
| No of runs | Time (Hours) | Temperature (◦C) | Catalyst loading(mg) | Actual yield (%) | Predicted yield (%) |
| 1 | 3 | 290 | 160 | 56,78 | 60,6713 |
| 2 | 2 | 182,728 | 130 | 42,85 | 37,8746 |
| 3 | 2 | 250 | 79,5462 | 30,54 | 34,8312 |
| 4 | 1 | 290 | 100 | 45,95 | 45,7089 |
| 5 | 1 | 210 | 160 | 35,56 | 32,9767 |
| 6 | 3 | 210 | 160 | 59,78 | 60,6743 |
| 7 | 3,68179 | 250 | 130 | 44,89 | 46,9169 |
| 8 | 0,318207 | 250 | 130 | 37,65 | 41,6989 |
| 9 | 1 | 290 | 160 | 39,78 | 45,4487 |
| 10 | 3 | 210 | 100 | 42,89 | 44,8065 |
| 11 | 2 | 317,272 | 130 | 55,23 | 43,8092 |
| 12 | 1 | 210 | 100 | 50,13 | 46,8919 |
| 13 | 2 | 250 | 180,454 | 57,3 | 53,7846 |
| 14 | 3 | 290 | 100 | 20,98 | 24,2165 |

### 5.3 Analysis of variance (ANOVA)

For the results optimization, the ANOVA (Analysis of variance) was used to analyse the obtained statistical variance influential values of parameters on bio-jet selectivity (Table 9) in order to evaluate the adequacy and consistency of the models. The 2FI model was the proposed model that related the selectivity to the independent variables. The ANOVA properties results from the designed experimental runs are presented in Table 10.

**Table 10: Table of ANOVA for 2FI (Factor investigation) selectivity response**

| Source | Sum of squares | df | Mean square | F-value | P-value | |
|---|---|---|---|---|---|---|
| Model | 1312,74 | 6 | 218,79 | 5,35 | 0,0223 | Significant |
| A-Time | 32,87 | 1 | 32,87 | 0,8031 | 0,3999 | |
| B-Temperature | 1,20 | 1 | 1,20 | 0,0293 | 0,8688 | |
| C-Catalyst ratio | 433,63 | 1 | 433,63 | 10,60 | 0,0140 | |
| AB | 77,81 | 1 | 77,81 | 1,90 | 0,2104 | |
| AC | 674,00 | 1 | 674,00 | 16,47 | 0,0048 | |
| BC | 93,23 | 1 | 93,23 | 2,28 | 0,1749 | |
| Residual | 286,46 | 7 | 40,92 | | | |
| Cor Total | 1599,20 | 13 | | | | |

From Table 10 the significance of each coefficient and the effective interaction of the independent variables between each other was depicted by the associate probability (P)-values and the F values. Generally, the statistical significance of the model and the model terms are demonstrated by a larger F-value and small P-value (Karami *et al.*, 2017). P values are expected to be less than 0. 005 for the factor to be considered significant (Goyal, Sharma and Jain, 2013; Kasim *et al.*, 2018). From Table 10 the results show that the model terms are statistically significant since the P-value is less than 0.0500. The terms C and AC are the only significant terms since their P-values are less than 0.05, while the model terms A, B, AB and BC are insignificant due to their P-values which are greater than 0.05. The C as the only significant factor with a larger F-value of 10.60 was considered to be the most affecting parameter in this research. From the ANOVA analysis of bio-jet selectivity, a regression coefficient ($R^2$) value of 0.8209 was obtained and it indicated a good model fitness since the fitted 2FI model accounted for above 82% of the variance in the experimental data. This suggests that the was a good relationship between the bio-jet yield as well as the utilised parameters and coded factors. The fit statistics of the data requires the precision value to be greater than 4, for the model to indicate an adequate signal and to also suggests that the model can be utilized for the navigation of the design space (Mohan, Viruthagiri and Arunkumar, 2014; Salam *et al.*, 2015). From the obtained data, an adequate precision of 8.0598 was obtained which shows that the model's signal is strong for it to be utilized for optimization.

The coded equation was useful for the relative impact of the factors identification by comparing the factor coefficients. The regression coded equation for the bio-jet selectivity is presented in equation 1,

$$\text{Selectivity} = +44.31 + 1.55\text{A} - 0.2965\text{B} + 5.63\text{B} - 3.12\text{AB} + 9.18\text{AC} + 3.41\text{BC}$$

Equation 1

Where:

A- time

B- Temperature

AC- time*catalyst loading

BC- temperature*catalyst loading

C- catalyst loading

**5.3 Validation of the models**

The obtained experimental bio-jet yield results and the predicted bio-jet fuel yield values from Table 10 can also be represented graphically in Figure 35, which ascertains the adequacy of the regression model. From the Figure, it can be observed that the residuals follow a normal distribution. The predicted values are quite close to the actual values.

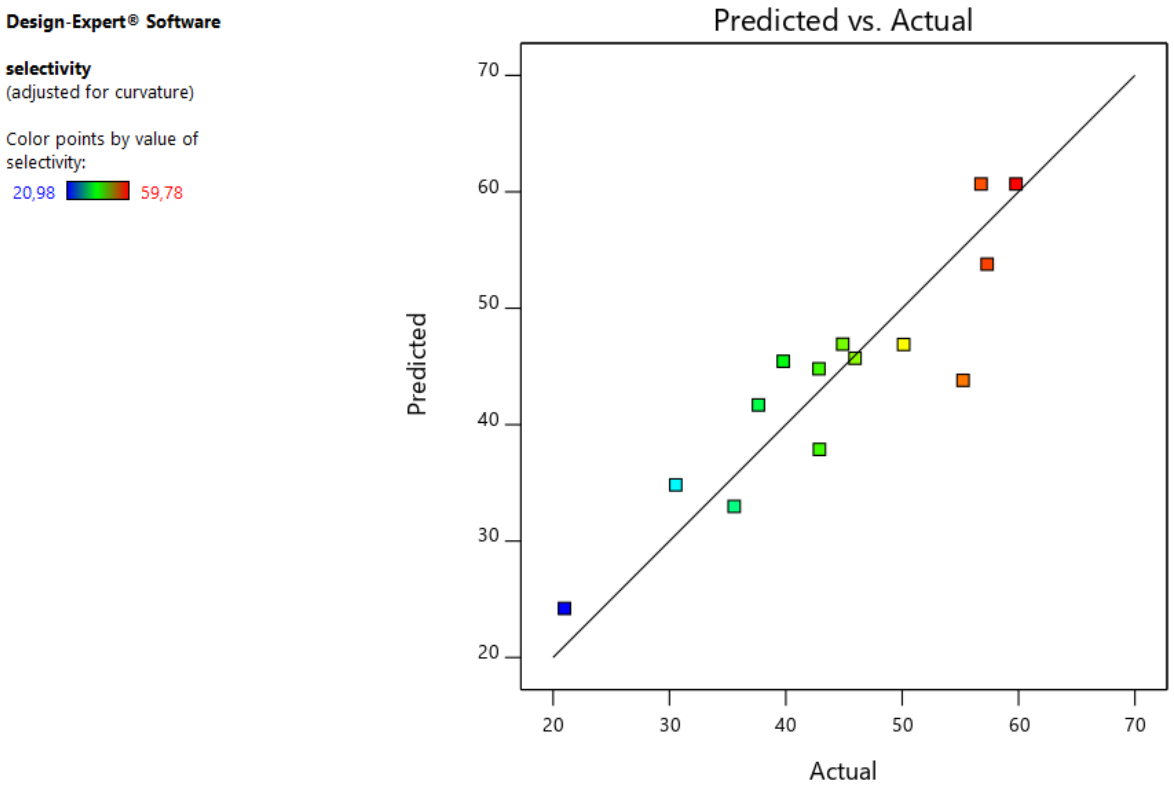


**Figure 35: Graph of the actual obtained yields vs the predicted yields**

Furthermore, 3D response surface plots as the most familiar forms to display the relationship/effect of multiple factors in the variable's response were plotted. When greater than two variables are considered in the model, two of them can be plotted, while the others are kept constant (Sánchez *et al.*, 2015). The parameters influence on the Bio-jets selectivity are represented in Figure 36(a, b and c) by the counter surface plots and 3D graphs. Figure 36(a) represents the effect that time and temperature interaction have on the bio-jet selectivity. From the Figure, the bio-jet selectivity is observed to be favoured at a higher time of 3 hours when the temperature is kept at its minimum of 210 °C. When time is kept at 3 hours and temperature is increased the selectivity decreases. Figure 36(b) shows the relationship of catalyst loading and time in relation to bio-jet selectivity. A higher reaction time of 3hours and a higher metal loading of 160 mg are observed to increase the bio-jet selectivity, this increase in bio-jet selectivity can also be observed at 1hour with metal loading of 100 mg. The bio-jet is observed to be at its lowest when the time is 3hours and the catalyst is at its minimum of 100 mg. Figure 36(c) relates the catalyst loading to temperature with bio-jet selectivity. In this Figure, both an increase in temperature and an increase in catalyst loading led to an increased bio-jet selectivity. This can be observed with an increase in temperature from 210 °C to 290 °C and catalyst loading from 100 to 160 mg. This trend was also observed by Suwannason *et*

*al.*, (2016), where bio-jet yield increased from the temperature of 350 to 418.87 °C producing 36%.

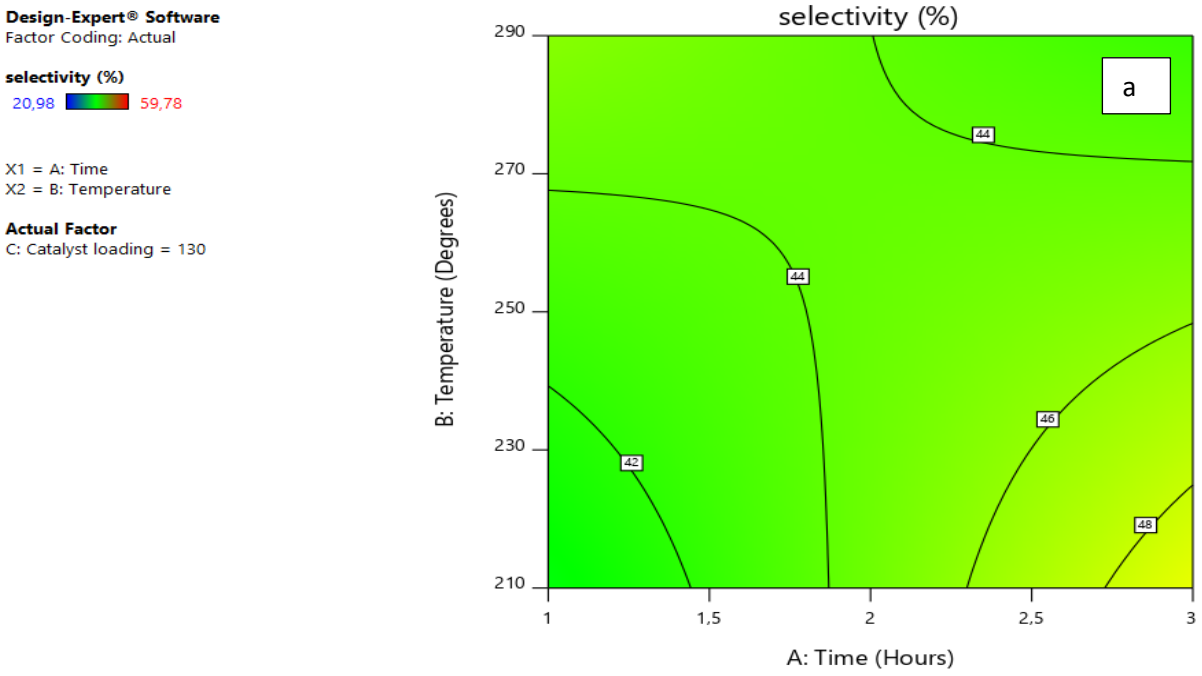


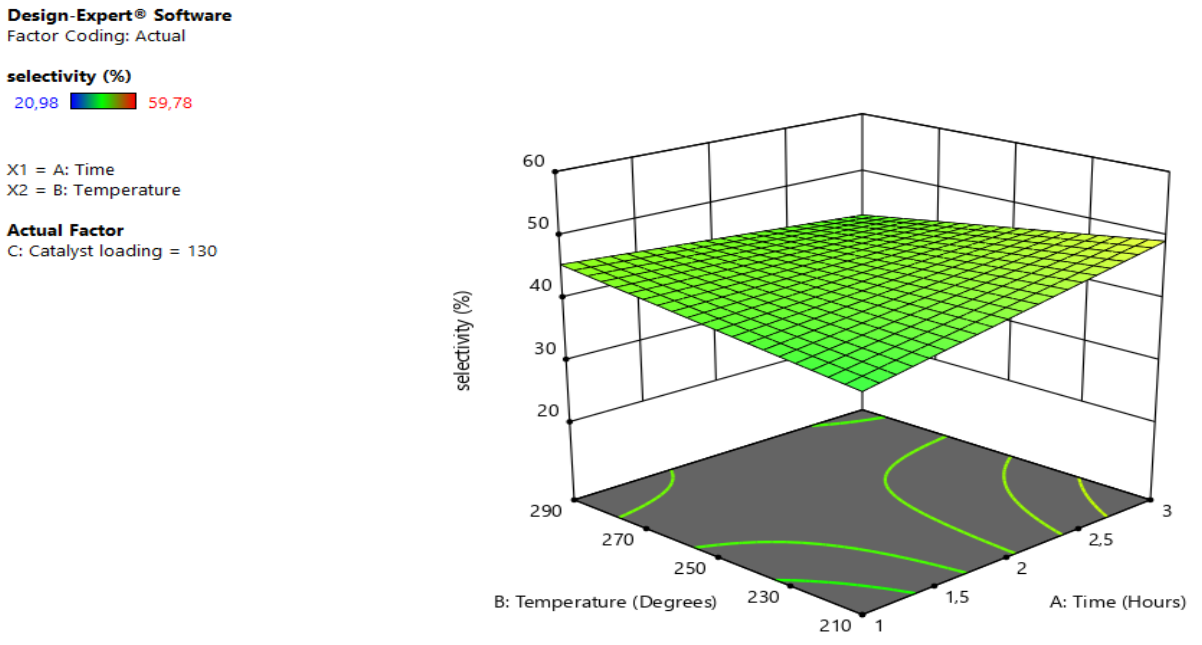

**Design-Expert® Software**
Factor Coding: Actual

**selectivity (%)**
20,98 59,78

X1 = A: Time
X2 = C: Catalyst loading

**Actual Factor**
B: Temperature = 250

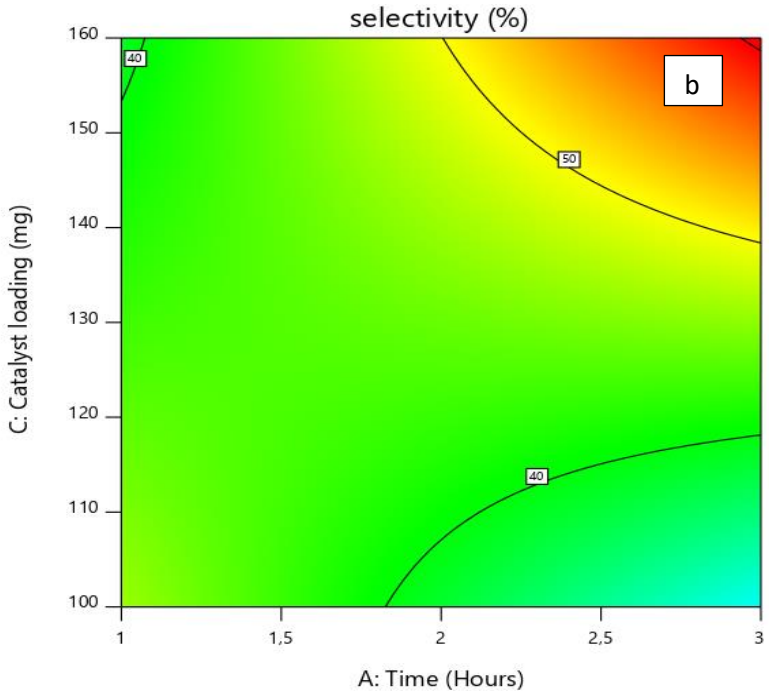


**Design-Expert® Software**
Factor Coding: Actual

**selectivity (%)**
20,98 59,78

X1 = A: Time
X2 = C: Catalyst loading

**Actual Factor**
B: Temperature = 250

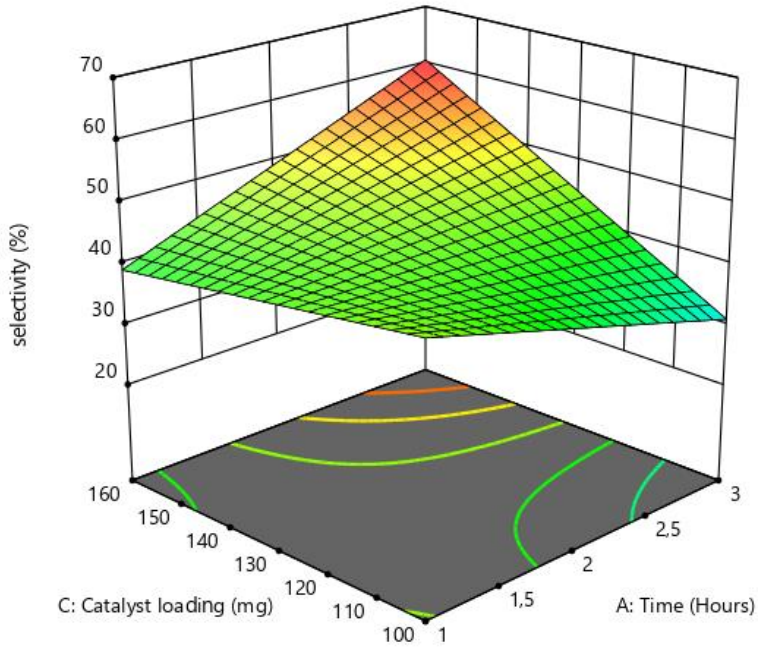

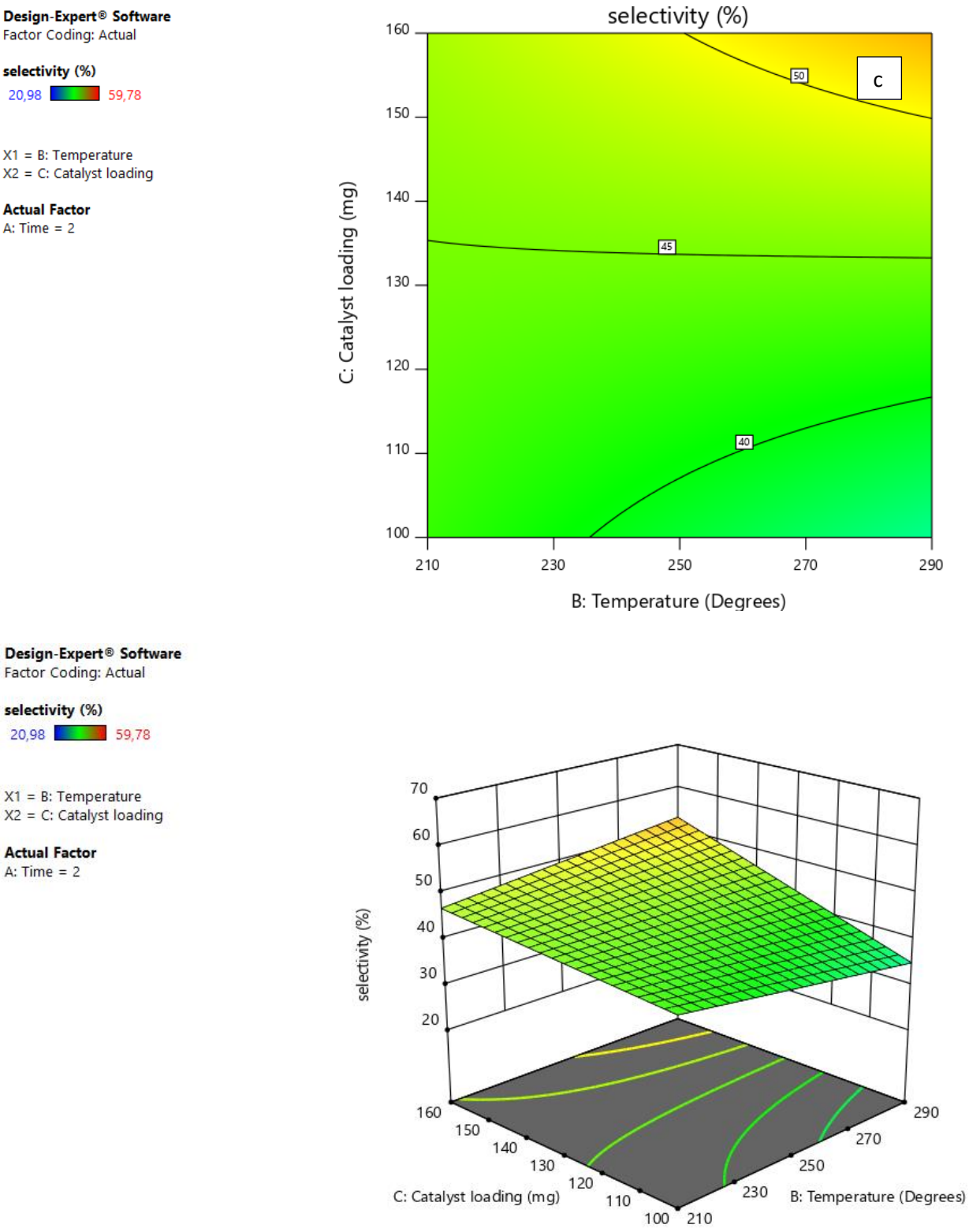


**Figure 36: Effect of temperature and time effect on the selectivity of bio-jet b) Effect of catalyst loading and time on the bio-jet selectivity and C) Effect of catalyst loading and temperature on the bio-jet selectivity**

### 5.4 Determination of the bio-jet fuel yield based on the predicted optimal conditions.

One experimental run was done in order to validate the generated model's accuracy. The model's aim was to predict the bio-jet maximum selectivity which must be reached in specific experimental conditions. The obtained optimum conditions were temperature of 280 °C, catalyst loading of 160 mg, and reaction time of 3 hours. These conditions were expected to produce 60% of bio-jet fuel but produced 55.62% which is close to the estimated production yield, so it can be assumed that the generated model was not 100% accurate. This might have been caused by the influence of other factors that were not investigated. In a study by Suwannason *et al.*, (2016) on bio-jet fuel production from palm oil optimum conditions for bio-jet production were obtained at 418.85 °C temperature, a catalyst of 3.16 wt%, and time of 119.37 min.

### 5.5 Conclusion and recommendations.

Design expert was successfully utilized to create the experimental design matrix and to analyse the data. The study postulated a regression coefficient ($R^2$) of 82% which indicates a good model fitness since the fitted 2FI model was used. The effect of different operating parameters on bio-jet was studied including time to temperature, catalyst loading to time, and catalyst loading to temperature. It was found that the required optimum conditions for maximizing the bio-jet selectivity were a time of 3 hours, catalyst loading of 160 mg, and temperature of 280°C, with the optimization, predicted results to be 60%. The optimum conditions were validated and the actual yield of 55.62% was obtained. It can be recommended that the optimum conditions experimental runs can be increased so that they can be done in duplicates in order to validate the first obtained results to reduce errors. When the CCD designed, experiments are compared to the first hydrocracking experimental runs it can be observed that the CCD designed experiments produced lower bio-jet yield.

**5.6 Reference's**

Abnisa, F., Wan Daud, W. M. A., and Sahu, J. N., (2010),Optimization and Modeling of Bio-oil Production from Palm Shell by Pyrolysis Using Response Surface Methodology, *ICAE*, 1465–1475.

Goyal, P., Sharma, M. P,. and Jain, S., (2013), Optimization of transesterification of Jatropha curcas Oil to Biodiesel using Response Surface Methodology and its Adulteration with Kerosene, *J. Mater. Environ. Sci.* 4(2), 277–284.

Kasim, N. N., Mohamed, A. R., Ishak, M. A. M., Ahmad, R., Nawawi, W. I., Ismail, K., and Salleh, N. H. M., (2018), Optimization of pyrolysis process parameters of torrefied demineralized palm empty fruit bunch (TDEFB) by response surface methodology, *ICoMEIA*, 1-13.

Karami, E., Sobati M. A., Khodaei, B., and Abdi, K., (2017), An experimental investigation on the ultrasound-assisted oxidation of benzothiophene in model fuel: Application of response surface methodology, *Applied Thermal Engineering*,118, 691–702.

Liu, J., and Wang, J., Leung, C., and Gao, F., (2018), A Multi-Parameter Optimization Model for the Evaluation of Shale Gas Recovery Enhancement, *Energies*, 11, 654,1-29.

Mohan, S.K., Viruthagiri, T., and Arunkumar, C., (2014), Statistical optimization of process parameters for the production of tannase by Aspergillus flavus under submerged fermentation, *Biotech*,4, 159–166

Salam, K. K., Agarry, S. E., Arinkoola, A.O and Shoremekun, I.O., (2015), Optimization of Operating Conditions Affecting Microbiologically Influenced Corrosion of Mild Steel Exposed to Crude Oil Environments Using Response Surface Methodology, *British Biotechnology Journal,* 7(2), 68–78.

Sánchez, N., Sánchez, R., Encinar, J. M., González, J. F., and Martínez, G., (2015), Complete analysis of castor oil methanolysis to obtain biodiesel Complete analysis of castor oil methanolysis to obtain biodiesel, *Fue*l ,147, 95–99

Suwannason, P., Kham-Or, P., and Ruangviriyachai C., (2016), Jet fuel production from palm oil by catalytic hydrocracking using a Ni-Mo/HY catalyst, Energy sources, 38 (23), 3549-3556.

# CHAPTER 6: CONCLUSIONS AND RECOMMENDATIONS

According to literature hydrocracking is a catalytic process in which heavy feedstocks are converted to saturated lighter products and is occasionally referred to as hydroprocessing or hydrogenation. Various feedstocks and various common catalysts such as Ni-Mo and Co-Mo are mostly used in hydrocracking to produces biofuels with a higher yield at high pressure and temperature. The selection of feedstock that is cheaper, available, and economically feasible is important for biofuel production as this will reduce production costs.

The results clearly showed that the employed catalysts preparation procedures and metals ratios strongly have different effects on the characteristics of the catalysts (Morphology, chemical composition etc)

All the co-impregnated catalysts had larger surface areas and the 1:2, 1:1 and 2:1 were observed to have increased surface areas when metal loadings were increased, with the 2:1 having the largest surface area. In the XRD patterns, an upshift was observed when the Zn metal was increased from the 1:1 to the 1:2 ratio. The lattice strain took place when the metal was increased of which changed the packing of the atoms. The FTIR bands that appeared to be in the same range, when the metal loadings were increased the bands appeared to be changing shapes appearing as narrow and wider.

In contrast to the co-impregnated catalysts, the sequential catalysts ratios of 1:2, 1:1 and 2:1 had their surface areas decreasing when the metal loadings were increasing. All the catalysts have lost a reasonable amount of their weight above 200◦C, this was because they were going under metal transition from $NiCl_2(OH)$ and Zn $(OH)_2$ to NiO and ZnO, respectively. The SEM and TEM images showed different sizes of cubic shapes of which the shapes were also present in XRD as cubic and hexagonal planes. These peaks in the XRD were also observed to be slightly disappearing. The FTIR displayed a pattern of bands moving towards higher and lower frequencies.

When only the two catalysts with the highest surface areas from the co-impregnated and sequential impregnated catalyst were compared, the results revealed that the 2:1(co-impregnation) had the highest surface area and the smallest pore size, while the 1:3 (sequential impregnation) had the smallest surface area and bigger pore size. The co-impregnated and sequential impregnated have the type IV isotherms and possess an H3 hysteric loop that

corresponds to the mesoporous regions. According to SEM and TEM, they revealed that both catalysts contain agglomerates, and the 1:3 have a cubic shape.

The catalyst's behaviour was mostly influenced by the preparation method(ratio), calcination temperature, operating conditions, etc. From the obtained trial runs results of hydrocracking of castor oil when the temperature was studied with both the 2:1 and 1:3 catalysts, it was observed that when the temperature was increased in both cases the bio-jet yield also increased until 250 °C then decreased. When the time was studied the catalyst showed that an increase in contact time also increased the bio-jet selectivity throughout until 2.5 hours of which the maximum bio-jet yield was obtained. Lastly, when the catalyst loading was varied, the catalyst increase was observed to decrease the bio-jet selectivity but increasing the biodiesel and long hydrocarbon yields. In general, the 1:3 catalyst showed higher selectivity of bio-jet in terms of the production yields. The Catalyst preparation method, metal used, and process temperature should be considered for the prediction of the catalyst activity, than predicting the catalyst activity based on the BET surface area. So, since the sequential impregnation catalyst gave better results than the co-impregnation, it can be said that it is a good catalyst.

The 1:3 catalyst was further used in the optimization of process parameters which was carried out using RSM in the design expert. The interaction of parameters was evaluated after the experimental design was done. A higher value of 82% for the regression coefficient was obtained and this indicated a good experimental data evaluation. The obtained optimum conditions were temperature of 280 °C, catalyst loading of 160 mg, and reaction time of 3 hours, these conditions produced the maximum yield of 55.62%. The first hydrocracking runs had the highest bio-jet selectivity compared to the experimental runs designed with design expert. The trial runs had the highest yields of bio-jet fuel with 72.33%, while the CCD designed reactions produced highest bio-jet fuel yield of 55.62% at their optimum conditions.

Recommendations.

- Employ the other techniques (e.g. functionalization/ doping techniques) for the dispersion of the CNO’s, since it is difficult to disperse them in water.
- More than one run of the RMS recommended optimization conditions must be conducted to solidly validate the model.
- Study the influence of other reaction parameters for optimization of bio-jet production, because other parameters that were not studied like $H_2$ flow rate might also affect the production yield without being aware of it.

# Appendices

Appendix A-GC-MS results for RAW castor oil

| R.Time | Area | Area% | Height | Height% | Name of compounds |
|---|---|---|---|---|---|
| **20.555** | 10102925 | 0.86 | 1679637 | 1.51 | 9-Octadecenoic acid, 1,2,3-propanetriyl |
| **20.597** | 11394006 | 0.97 | 1732441 | 1.56 | 9-Octadecenoic acid, 1,2,3-propanetriyl |
| **22.689** | 67855439 | 5.77 | 4431461 | 3.99 | Hexadecenoic acid, 2-hydroxyl-1,3-propar |
| **22.831** | 63080359 | 5.36 | 4537861 | 4.08 | Cis-Vaccenic acid |
| **23.235** | 27084250 | 2.30 | 2573743 | 2.32 | Undec-10-ynoic acid, decyl ester |
| **23.370** | 48996739 | 4.17 | 3040687 | 2.74 | Octadecanoic acid |
| **23.869** | 65154947 | 5.54 | 2216958 | 2.00 | Linoelaidic acid |
| **24.220** | 7546585 | 0.64 | 1341948 | 1.21 | Fumaric acid, 8-chlorooctyl dodecyl ester |
| **24.544** | 38051701 | 3.24 | 2888387 | 2.60 | Docosanoic acid, methyl ester (CAS) |
| **24.846** | 25558078 | 2.17 | 1410217 | 1.27 | (Z)-18-Octadec-9-enolide |
| **25.041** | 7254406 | 0.62 | 1149307 | 1.03 | DI-(9-OCTADECENOYL)-GLYCEROL |
| **25.150** | 7768830 | 0.66 | 1108753 | 1.00 | Hexadecanoic acid,1-(hydroxymethyl)-1 |
| **25.280** | 6054807 | 0.51 | 1151444 | 1.04 | Z-7-Hexadecenal |
| **25.480** | 19086773 | 1.62 | 1228808 | 1.11 | Tetracosanoic acid, methyl ester (CAS) |
| **25.822** | 15675118 | 1.33 | 1027164 | 0.92 | Debrisoquine |
| **26.178** | 39087792 | 3.32 | 2025221 | 1.82 | Glycidyl palmitate |
| **26.390** | 24003458 | 2.04 | 1635828 | 1.47 | Koiganal II |
| **26.584** | 12704178 | 1.08 | 1704387 | 1.53 | 1-Heptatriacotanol |
| **26.830** | 17074569 | 1.45 | 1650107 | 1.49 | Trichloroacetic acid, undec-2-enyl ester |
| **26.940** | 7041731 | 0.60 | 1728365 | 1.56 | Oxacyclopentadecan-2-one |
| **26.980** | 7293124 | 0.62 | 1749313 | 1.57 | 4-ethyl-1-thia-cyclohexane |
| **27.194** | 29743710 | 2.53 | 1944250 | 1.75 | Trichloroacetic acid,undec-2-enyl ester |
| **27.320** | 6144314 | 0.52 | 1752900 | 1.58 | 4,5-Decanediol,6-ethyl-(CAS) |
| **27.400** | 7954363 | 0.68 | 1702400 | 1.53 | Chloromethyl 5-chlorodecanoate |
| **27.485** | 9785144 | 0.83 | 1717412 | 1.55 | Petroselinic acid,TMS derivative |
| **27.658** | 16277143 | 1.38 | 1699202 | 1.53 | METHYL4-ACETYLHYDROXYPALM |
| **27.782** | 7360610 | 0.63 | 1564678 | 1.41 | Hexanoic acid, heptadecyl ester |
| **27.860** | 7309329 | 0.62 | 1524691 | 1.37 | 9exo-Methyl-anti(9,10)-tricyclo[4.2.1.1(2 |
| **27.960** | 7401705 | 0.63 | 1597978 | 1.44 | 2-((2R,4Ar,8As)-4a-Methyl-8-methylened |
| **28.030** | 5414100 | 0.46 | 1550024 | 1.40 | Oleoyl chloride |
| **28.110** | 13157975 | 1.12 | 1565016 | 1.41 | 9-Octadecenoic acid, 1,2,3-propanetriyl |
| **28.267** | 6085075 | 0.52 | 1484596 | 1.34 | 9-Octadecenoic acid(Z)-,2-hydroxy-1 |
| **28.410** | 13744502 | 1.17 | 1482862 | 1.33 | p-Menth-8(10)-en-9-ol,cis-(CAS) |
| **28.583** | 31338057 | 2.66 | 2235208 | 2.01 | Tetracosanoic acid, methyl ester (CAS) |
| **28.760** | 12021583 | 1.02 | 1608630 | 1.45 | Hexanoic acid, tridecyl ester |
| **29.080** | 27703703 | 2.36 | 1748915 | 1.57 | 9-Octadecenoic acid (Z)-, methyl ester (C |

| | | | | | |
|---|---|---|---|---|---|
| **29.332** | 24790724 | 2.11 | 1666283 | 1.50 | 9-Octadecenoic acid,1,2,3-propanetriyl |
| **29.460** | 10023118 | 0.85 | 1578755 | 1.42 | Urs-12-en-28-ol (CAS) |
| **29.680** | 20324205 | 1.73 | 1781169 | 1.60 | 9-Octadecenoic acid,1,2,3-propanetriyl |
| **29.800** | 12270865 | 1.04 | 1607567 | 1.45 | Adipic acid,.beta.-citronellyl butyl ester |
| **30.079** | 73839441 | 6.28 | 4191586 | 3.77 | Glycidyl oleate |
| **30.470** | 13343547 | 1.13 | 1633490 | 1.47 | 7,11-Hexadecadienal |
| **30.622** | 28779791 | 2.45 | 3139798 | 2.83 | Glycidyl palmitate |
| **30.740** | 6190898 | 0.53 | 1779663 | 1.60 | 4-Hexyl-1-(7-methoxycarbonnylheptyl)bic |
| **30.990** | 35932496 | 3.06 | 2023052 | 1.82 | 9,12-Octadecadienoyl chloride, (Z,Z)- |
| **31.120** | 7142402 | 0.61 | 1995840 | 1.80 | 1b,4a-Epoxy-2H-cyclopenta[3,4]cyclopro |
| **31.300** | 32802863 | 2.79 | 2288417 | 2.06 | Oleoyl chloride |
| **31.450** | 8023222 | 0.68 | 2276801 | 2.05 | 3-Hydroxypropyl palmite, TMS derivati |
| **31.530** | 9714578 | 0.83 | 2477173 | 2.23 | Petroselinic acid, TMS derivative |
| **31.620** | 18382859 | 1.56 | 2431051 | 2.19 | Undec-10-ynoic acid, undecyl ester |
| **31.690** | 18189212 | 1.55 | 2230996 | 2.01 | Cyclohexane, (heptylthio)- |
| **31.967** | 29870880 | 2.54 | 1999220 | 1.80 | (R) –(-)-14-Methyl-8-hexadecyn-1-ol |
| **32.197** | 10935359 | 0.93 | 1621087 | 1.46 | 2H-Pyran-4-ol,6(dimethoxymethyl)-2-(2 |

Table B: GC-MS raw data of hydrocracking using the 1:3 catalyst prepared using the sequential impregnation.

| R Time | Area | Area% | Height | Height% | Name of compounds |
|---|---|---|---|---|---|
| **5,170** | 3029377 | 10,19 | 231956 | 10,09 | HEXADECANE C16 |
| **5,208** | 261211 | 2,56 | 233364 | 10,15 | Tetradecane C14 |
| **5,254** | 4540618 | 15,28 | 233466 | 10,15 | Dodecane,2,7,10-trimethyl, C15 |
| **7,162** | 3568244 | 12,01 | 256926 | 11,17 | Heptadecane C17 |
| **7,202** | 3766405 | 12,68 | 258825 | 11,25 | Pentadecane (CAS) C8 |
| **8,168** | 61452 | 0,21 | 9741 | 0,42 | 1,25 –Dihydroxyvitamin D3,TMS derivati C23 |
| **8,285** | 45237 | 0,15 | 7961 | 0,35 | Benzane, 1,2-difluoro-4(4`propyl(1,1`bin |
| **8,385** | 48616 | 0,16 | 9524 | 0,41 | 4-Octanano (CAS) C8 |
| **8,623** | 118728 | 0,40 | 8409 | 0,37 | 5,5 Dibutylnonane C17 |
| **9,468** | 4745684 | 15,98 | 232010 | 10,09 | Hexadecane(CAS) C16 |
| **10,617** | 178454 | 0,60 | 8790 | 0,38 | Dodecane (CAS) C12 |
| **11.121** | 139202 | 0,47 | 6345 | 0,28 | Pentadecane,2-menthyl-(CAS) C16 |
| **11,983** | 1833963 | 6,17 | 126454 | 5,50 | Heptadecane C17 |
| **12,570** | 53097 | 0,18 | 4036 | 0,18 | Methyl trans-2-octadecanoate C19 |
| **12,670** | 74667 | 0,25 | 4146 | 0,18 | 1-(4[ACHLORO(DIFLUORO)METHOX |
| **12,970** | 54770 | 0,18 | 4536 | 0,20 | Decahydrobiscyclopenta[a,d]benzene-4,8 |
| **13,245** | 55364 | 0,19 | 5824 | 0,25 | Digitoxin |
| **13,469** | 135864 | 0,46 | 5692 | 0,25 | 16.deta-(Trimethylsioxy)-5,alpha-androx |
| **14,478** | 297909 | 1,00 | 29898 | 1,30 | Hexadecane(CAS) C16 |
| **15,068** | 45263 | 0,15 | 3171 | 0,14 | SILICONE OIL C16 |
| **16,245** | 38958 | 0,13 | 2571 | 0,11 | 2-PYRROLIDINECARBOXYLIC ACID C5 |

| | | | | | |
|---|---|---|---|---|---|
| **16.748** | 76606 | 0,26 | 6353 | 0,28 | 8-xa-1,3(2H)-diazaspiro[4,5]decane-2,4-dior C18 |
| **17,001** | 213713 | 0,72 | 11102 | 0,48 | Haptadecane C17 |
| **17,696** | 699621 | 2,35 | 105476 | 4,59 | Hexadecanoic acid, methyl ester C17 |
| **17,995** | 40374 | 0,14 | 5210 | 0,23 | Isoindone-1,3(2H)-dione,3a,4,7,7a-tetrahy |
| **18,245** | 57641 | 0,19 | 4797 | 0,21 | 1H-indene,(2,3-dihydro-1H-inden-1-yli C18 |
| **19,443** | 161895 | 0,34 | 5710 | 0,25 | 2-methyloctacosane C29 |
| **19,945** | 46211 | 0,16 | 3447 | 0,15 | 4-Methylpiperidine-1-thiocarboxylic acid 14 |
| **20,745** | 45147 | 0,15 | 4057 | 0,18 | 2,2,3,3.3-Pentafluoro-N-(5-methylisoxaza |
| **21,083** | 170360 | 0,57 | 12056 | 0.52 | 13-Hexyloxacyclotridec-10-en-2-one C18 |
| **22,945** | 2308921 | 7,77 | 277877 | 12,08 | 6-Octadecenoic acid,methyl ester,(Z) C19 |
| **22,545** | 209579 | 0,71 | 38869 | 1,69 | Methyl stearate C19 |
| **23,318** | 123085 | 0,41 | 4831 | 0,21 | 2,6-Pyridinedicarboxylic acid,decyl 3-me |
| **23,516** | 40837 | 0,14 | 3798 | 0,17 | 1H-Cyclopenta{c}furan-1-one,hexahydro C8 |
| **24,895** | 48788 | 0,16 | 2979 | 0,13 | 4-(2-Methoxyphenyl)piperidine C12 |
| **24,468** | 110687 | 0,37 | 5984 | 0,26 | Floroacctic acid, dodecyl ester C14 |
| **24,995** | 37888 | 0,13 | 3518 | 0,15 | 5,beta,-Coprostan-16,22-epoxy-3 alpha,2 |
| **25,302** | 39152 | 0,13 | 5095 | 0,22 | 1,4-BIS((P-CHLOROBENZYLIDENEAM |
| **25,395** | 38264 | 0,13 | 5152 | 0,22 | 2,5-Methano-1H-inden-6-ol,octahydro- C10 |
| **25,749** | 65986 | 0,22 | 5308 | 0,23 | OCTADECAMETHYLCYCLONONAST |
| **26,073** | 103969 | 0,35 | 5904 | 0,26 | 4-Amino-2.5-dimethoxy-N.N-abis[2-diethy |
| **26,336** | 66438 | 0,22 | 11408 | 0,50 | 9-Octadecenoic acid,12-hydroxy-methyl C19 |
| **26,502** | 49427 | 0,17 | 6404 | 0,28 | Cholestan-6,beta-ol(CAS) C27 |
| **27,139** | 42354 | 0,14 | 4365 | 0,19 | 1.alpha-(Acetoxymethyl)-7.alpha,8alpha C14 |
| **28,940** | 55561 | 0,19 | 5844 | 0,25 | 1.3-Benzodioxole,5-[[2-(2-butoxyethoxy) C19 |
| **30,337** | 59127 | 0,20 | 4415 | 0,19 | Pemtanedioic acid,3-ethyl-3 methyl C8 |
| **30,743** | 39962 | 0,13 | 4066 | 0,18 | Methyl cis-secopimarate C21 |
| **31,070** | 59557 | 0,20 | 5368 | 0,23 | Methyl 5-acetoxyhexadecanoate C19 |
| **31,245** | 85147 | 0,29 | 5816 | 0,25 | Octandecanoic acid,methyl ester(CAS) C19 |
| **31,992** | 114578 | 0,39 | 5751 | 0,25 | 1-Phenyl-1-(p-dimethylaminophenyl)-1-sil |
| **33,587** | 81074 | 0,27 | 3920 | 0,17 | 3-[4-(3-METHOXY-PHENYL)-3-METH C15 |
| **34,610** | 81074 | 0,15 | 3882 | 0,17 | Dimethyl 2,3-dihydro-2oxo-[5H-3a,5]ne C15 |
| **35,020** | 171558 | 0,58 | 3968 | 0,17 | Methyl 5-oxotridecanoate C15 |
| **35,714** | 56139 | 0,19 | 5106 | 0,22 | 6-[(5-Methoxy-3-nitrosalieylidene)amino] C15 |
| **35,920** | 96453 | 0,32 | 4192 | 0,18 | Cholest-4ene,3-methoxy-(3.beta)-C27 |
| **36,734** | 169729 | 0,57 | 3592 | 0,23 | 2,6 Lutidine 4methoxy-3nitro |

Table C: GC-MS raw data of hydrocracking using the 1:3 catalyst prepared using the sequential impregnation.

| R Time | Area | Area% | Height | Height% | Name |
|---|---|---|---|---|---|
| **4.244** | 52904 | 0.04 | 9835 | 0.11 | Tetradecaine (CAS) |
| **4.445** | 49588 | 0.04 | 9273 | 0.10 | 1-ACETYL-4-(2-BROMOETHYL)PIPER |
| **4.551** | 64834 | 0.05 | 13355 | 0.14 | 2,4-Decadienal,(E.E)-(CAS) |
| **5.130** | 5985373 | 4.24 | 552873 | 5.99 | Hexadecane(CAS) |
| **5.203** | 3028303 | 2.14 | 565697 | 6.13 | Hexadecane(CAS) |
| **5.240** | 11817276 | 8.36 | 563346 | 6.10 | Tetradecane (CAS) |
| **5.966** | 1464438 | 1.04 | 91996 | 1.00 | Nonanoic acid,9-oxo-,methyl ester(CAS) |
| **6.160** | 1650531 | 1.17 | 91943 | 1.00 | Nonanoic acid,9-oxo-,methyl ester |
| **7.160** | 18166724 | 12.86 | 623981 | 6.76 | Hexadecane |
| **8.399** | 553317 | 0.39 | 25670 | 0.28 | Hexadecane(CAS) |
| **8.651** | 344458 | 0.24 | 19143 | 0.21 | Pentadecane,3-methyl-(CAS) |
| **9.510** | 12415879 | 8.79 | 583208 | 6.32 | HENTRIACONTANE |
| **10.655** | 495511 | 0.35 | 16308 | 0.18 | Nonane,3,7-dimethyl- |
| **11.074** | 431855 | 0.31 | 15273 | 0.17 | Heptadecane |
| **11.993** | 4842266 | 3.43 | 337532 | 3.66 | Tetradecanoic acid, methyl ester (CAS) |
| **12.652** | 555313 | 0.39 | 42906 | 0.46 | Acetamide,2-(2-thiophenyl)-N-ethyl-N-de |
| **13.785** | 40737 | 0.03 | 4921 | 0.05 | Hexadecane (CAS) |
| **14.497** | 777135 | 0.55 | 82734 | 0.90 | 9-Octadecenoic acid (Z) -,methyl ester (C |
| **14.730** | 87657 | 0.06 | 7423 | 0.08 | Pentadecanoic acid, methyl ester |
| **15.178** | 208571 | 0.15 | 13638 | 0.15 | 2-MONOLINOLENIN |
| **15.980** | 51234 | 0.04 | 4385 | 0.05 | 9-Hexadecenoic acid, mythyl ester (Z) |
| **17.193** | 583202 | 0.41 | 45762 | 0.50 | Hexadecanoic acid ,mythyl ester (CAS) |
| **17.868** | 19351415 | 13.70 | 1558412 | 16.88 | Undec-10-ynoic acid, tridec-2-yn-1-y1 este |
| **18.803** | 516540 | 0.37 | 50101 | 0.54 | CIS-10-HEPTADECENOIC ACID ME |
| **19.571** | 524259 | 0.37 | 41061 | 0.44 | Androstane-11,17-dione,3-hydroxy,(3al |
| **19.830** | 46558 | 0.03 | 7221 | 0.08 | Heptadecanoic acid, methyl ester (CAS) |
| **20.187** | 270714 | 0.19 | 39209 | 0.42 | 9,12-Octadienoic acid(Z,Z), methyl |
| **20.505** | 45504 | 0.03 | 6820 | 0.07 | Methyl 2-octyleyelopropene-1-heptanoate |
| **21.268** | 1717791 | 1.22 | 185923 | 2.01 | 6-Octadecenoic acid, methyl ester |
| **22.250** | 43458360 | 30.76 | 1919214 | 20.79 | Methyl stearate |
| **22.663** | 6207775 | 4.39 | 956434 | 10.36 | Methyl 2-octylcyclopropene-1-octanoate |
| **23.573** | 565729 | 0.40 | 83493 | 0.90 | 9,12-Octadecadienoic acid (Z,Z) |
| **24.009** | 155415 | 0.11 | 17129 | 0.19 | Cis-10-Nonadecenoic acid,methyl ester |

| | | | | | |
|---|---|---|---|---|---|
| **24.225** | 160953 | 0.11 | 14605 | 0.16 | Cis-10-Nonadecenoic acid,methyl ester |
| **24.485** | 727813 | 0.52 | 158257 | 1.71 | Nonadecanoic acid, methyl ester |
| **24.855** | 106342 | 0.08 | 6754 | 0.07 | HAHNFETT |
| **25.279** | 170974 | 0.12 | 34048 | 0.37 | Tricyclo[20.8.0.0(7.16)triacontane |
| **25.555** | 71333 | 0.05 | 11566 | 0.13 | 1H-Purin-6-amine,[(2-fluoropherryl)methyl |
| **25.745** | 113490 | 0.08 | 13881 | 0.15 | Hexadecadicnoic acid, methyl ester |
| **25.997** | 222812 | 0.16 | 14725 | 0.16 | Cis-11-Eicosanoic acid, methyl ester |
| **26.501** | 478472 | 0.34 | 51038 | 0.55 | Eicosanoic acid,methyl ester (CAS) |
| **27.075** | 732455 | 0.52 | 125899 | 1.36 | 9-Octadecenoic acid,1,2,3-propanernyl es |
| **27.496** | 94250 | 0.07 | 14401 | 0.16 | 14-BETA-H-PREGNA |
| **27.708** | 121100 | 0.09 | 13422 | 0.10 | Tricyclo[20.8.0.0(7.16)]triacontane,1(22) |
| **28.002** | 77000 | 0.05 | 9642 | 0.28 | Tricyclo[20.8.0.0(7.16)] triacontane 1,(22) |
| **28.349** | 207858 | 0.15 | 25649 | 0.11 | Piperonyl butoxide |
| **28.937** | 144000 | 0.10 | 10441 | 0.02 | 1-Methionine, N-neopentyloxycarbonyl |
| **29.355** | 42564 | 0.03 | 2279 | 0.18 | Methyl 2-octyleyclopropene-1-octanoate |
| **29.651** | 148333 | 0.10 | 16190 | 0.04 | 1-Chloro-2-(methoxymethyl)-2-pentene |
| **30.754** | 57824 | 0.04 | 3299 | 0.63 | Decosanoic acid,methyl ester |
| **31.257** | 257439 | 0.18 | 58435 | 0.07 | 1,2-Benzenedicarboxylic acid, bis(2-ethyll |
| **31.674** | 111054 | 0.08 | 6777 | 0.05 | 4-(Benzothiazol-2-ylsulfanyl)-5-morpholir |
| **32.929** | 48355 | 0.03 | 4288 | 0.07 | Tricosanoic acid, mythyl ester (CAS) |
| **33.427** | 55876 | 0.04 | 6436 | 0.06 | Tetradecahydro-trimethyl-phenanthrene 1 |
| **33.580** | 132005 | 0.09 | 5526 | 0.05 | 9-Octadecenoic acid (Z),hexadecyl ester |
| **33.843** | 52277 | 0.04 | 4556 | 0.05 | 6-Bromo-3,4-butyl-6-(1-hydroxy-cyclohe9 |
| **33.455** | 143578 | 0.10 | 4745 | 0.05 | |
| **36.050** | 195297 | 0.14 | 21133 | 0.23 | Tetracosanoic acid, methyl ester(CAS) |